

R77-912887-3

AD A049312

# ASSESSMENT OF ADVANCED LASER MATERIALS PROCESSING TECHNOLOGY.

Final Report.

Summary of Work Performed:

1 Mar 1977 - 30 September 1977

30 November 1977

Prepared under Contract N00014-77-C-0418

Sponsored by

Advanced Research Projects Agency

✓ ARPA Order 3361

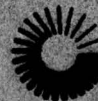
Monitored by Office of Naval Research

E. M. Breinan

DISTRIBUTION STATEMENT A

Approved for public release;  
Distribution Unlimited

**UNITED TECHNOLOGIES  
RESEARCH CENTER**



UNITED  
TECHNOLOGIES

EAST HARTFORD, CONNECTICUT 06108

Use or Disclosure of Report is Subject to the  
Restriction on the Title Page of this Report

409252

JB

✓ UNITED TECHNOLOGIES CORPORATION  
RESEARCH CENTER  
East Hartford, Connecticut

R77-912887-3

Final Report under Contract N00014-77-C-0418 *New*  
Summary of Work Performed for the Period  
1 March 1977 to 30 September 1977

ARPA Order No.:	3361
Program Cost Code:	000007L10K71
Contractor:	United Technologies Research Center
Effective Date of Contract:	1 March 1977
Contract Expiration Date:	30 November 1977
Contract Amount:	\$128,476
Contract Number:	N00014-77-C-0418
Principal Investigator:	Dr. E. M. Breinan (203) 565-8396
Scientific Officer:	Dr. Bruce A. MacDonald
Short Title:	Laser Materials Processing
Reported by:	E. M. Breinan, E. R. Thompson, C. M. Banas, B. H. Kear

Sponsored by Advanced Research Projects Agency  
ARPA Order No. 3361

The views and conclusions contained in this document are those of the authors and should not be interpreted as necessarily representing the official policies, either expressed or implied, of the Defense Advanced Research Projects Agency or the U.S. Government.

DISTRIBUTION STATEMENT A  
Approved for public release;  
Distribution Unlimited



Report R77-912887-3

Assessment of Advanced Laser Materials Processing Technology

ACCESSION for	
NTIS	White Section <input checked="" type="checkbox"/>
DIC	Buff Section <input type="checkbox"/>
UNANNOUNCED	<input type="checkbox"/>
JUSTIFICATION	
<i>File on file</i>	
BY	
DISTRIBUTION/AVAILABILITY CODES	
Dist.	AVAIL. and/or SPECIAL
<i>A</i>	

TABLE OF CONTENTS

SIGNIFICANT RESULTS AND CONCLUSIONS . . . . .	1
INTRODUCTION . . . . .	5
TASK 1 - PERFORMANCE AND COST BENEFITS/F-100(3) . . . . .	8
Weight . . . . .	8
Cost . . . . .	13
TASK 2 - PERFORMANCE AND COST BENEFITS/FEAT . . . . .	16
Weight . . . . .	16
Cost . . . . .	19
TASK 3 - PERFORMANCE AND COST BENEFITS/JT10D-4 . . . . .	21
Assumptions Made in These Analyses . . . . .	21
Results of Analyses Performed . . . . .	22
TASK 4 - LIFE CYCLE COST STUDIES/F-100(3), FEAT . . . . .	34
General . . . . .	34
LCC LAYERGLAZE/F-100(3), Designed for Maximum Weight Savings . . . . .	35
LCC-LAYERGLAZE/F-100(3) with a Design Partially Optimized for LCC Reduction . . . . .	36
LCC-LAYERGLAZE/FEAT Engine . . . . .	41
TASK 5 - DEVELOPMENT PLAN . . . . .	44
First Year (1978) . . . . .	44
Second Year (1979) . . . . .	45
Third Year (1980) . . . . .	46

TABLE OF CONTENTS (Cont'd)

TASK 6 - TECHNICAL FEASIBILITY DEMONSTRATION . . . . .	48
A. Physical Process . . . . .	48
B. Thermal Analysis . . . . .	60
TASK 7 - ALLOY DESIGN AND EVALUATION . . . . .	70
Background . . . . .	70
Experimental Procedure . . . . .	71
Results . . . . .	71
REFERENCES . . . . .	96



# LIST OF TABLES

<u>Table No.</u>		<u>Page</u>
1-I	LAYERGLAZE Titanium Alloy Design Values Used	9
1-II	LAYERGLAZE Nickel Alloy Design Values Used	10
1-III	F-100(3) B/M vs LAYERGLAZE/F-100(3) Weights	12
1-IV	F-100(3)/LAYERGLAZE Cost Study Summary	15
2-I	FEAT/PED vs LAYERGLAZE/FEAT/PED Weights	18
2-II	PED/FEAT - LAYERGLAZE Cost Study Summary	20
3-I	Potential Weight Saving with LAYERGLAZE Process	23
3-II	Estimated JT10D HPC Benefits with LAYERGLAZE Process	32
3-III	Estimated Weight and/or Cost Savings Achievable by Using LAYERGLAZED Alloys on the JT10D-4	31
4-I	Ground Rules for F-100(3) Life Cycle Cost Studies	35
4-II	Langley 2000 Hr Air Combat Mission Duty Cycle	37
4-III	Life Cycle Cost Study - LAYERGLAZE/F-100(3) Designed for Maximum Weight Savings	38
4-IV	Life Cycle Cost Study - LAYERGLAZE/F-100(3) with Design Partially Optimized for LCC Reduction	42
4-V	Ground Rules for FEAT Life Cycle Cost Studies	43
4-VI	Life Cycle Cost Study - LAYERGLAZE/FEAT Engine	43
6-I	LAYERGLAZE Energy Deposition Estimates	53
7-I	Alloy Compositions	70
7-II	Strength and Approximate Plastic Strain at Fracture for FeTiB Alloys	76
7-III	Yield Strength of Incrementally Processed Alloys	81

# LIST OF FIGURES

<u>Fig. No.</u>		<u>Page</u>
1-1	Composite Engine Cross Section, F100-3	11
2-1	Composite Engine Cross Section, FEAT	17
3-1	Modifications of JT10D-4 HPC Rotor Stages 4-13 Using LAYERGLAZE Processed Alloys	24
3-2	Modifications of JT10D-4 HPT R-1 Disl Using LAYERGLAZE Processed Alloys	25
3-3	Weight vs Ultimate Strength	27
3-4	Weight vs Ultimate Strength	28
3-5	Weight vs Ultimate Strength	29
3-6	Weight vs Ultimate Strength	30
4-1	1st Fan Disl Cost vs Life for F100(3)	39
4-2	1st HPT Disk Cost vs Life for F100(3)	40
5-1	Development Plan for LAYERGLAZE Component Part Fabrication	47
6-1	The LAYERGLAZE Process	49
6-2	Effect of Melt Depth and Power on Average Cooling Rate	51
6-3	Cooling Rate and Dwell Time as a Function of Absorbed Power Density for Two Melt Thicknesses	52
6-4	LAYERGLAZE Apparatus (Phase II)	55
6-5	Preliminary LAYERGLAZE Model Parts	56
6-6	0.2 Inch LAYERGLAZE Buildup	58
6-7	0.2 Inch LAYERGLAZE Buildup	59



# LIST OF FIGURES (Cont'd)

<u>Fig. No.</u>		<u>Page</u>
6-8	Two-Dimensional Finite-Element Heat-Balance Model	61
6-9	Effect of Power Density on Substrate Temperature Profile	63
6-10	Effect of Dwell Time on Substrate Surface Temperature	64
6-11	Operating Map for LAYERGLAZE	65
6-12	Operating Map for LAYERGLAZE	66
6-13	Operating Map for LAYERGLAZE	67
6-14	Optimum Operating Conditions	68
6-15	Surface Temperature as a Function of Power Density and Melt Depth	69
7-1	Structure of LASERGLAZED CoTaC	72
7-2	Structure of LASERGLAZED NiTiC	73
7-3	Structure of LASERGLAZED FeTiB	74
7-4	Electron Micrograph of As Received FeTiB Alloy	77
7-5	Transmission Electron Micrograph of FeTiB Alloy After 800°C Thermal Treatment	79
7-6	Structure of Incrementally Melted Ni-Mo-Al Eutectic Alloy	80
7-7	Structures and Properties of Co-TaC Alloys	82
7-8	Microstructure of Sputtered Deposits	84
7-9	Structure and Electron Diffraction Pattern from Sputtered CoTaC Deposit	85
7-10	Structure and Electron Diffraction Pattern from Sputtered NiTiC Deposit	86

# LIST OF FIGURES (Cont'd)

<u>Fig. No.</u>		<u>Page</u>
7-11	Structure and Electron Diffraction Pattern from Sputtered FeTiB Deposit	87
7-12	Hardness of CoTaC Alloy as a Function of Thermal Treatment	88
7-13	Hardness of NiTiC Alloy as a Function of Thermal Treatment	89
7-14	Hardness of FeTiB Alloy as a Function of Thermal Treatment	90
7-15	Hardness of Sputtered Deposits as a Function of Nucleation Temperature	91
7-16	Structure and Electron Diffraction Pattern from Sputtered CoTaC Deposit after 538°C/4 hr and 649°C/4 hr Thermal Treatment	93
7-17	Structure and Electron Diffraction Pattern from Sputtered NiTiC Deposit After 538°C/4 hr and 649°C/4 hr Thermal Treatment	94
7-18	Structure and Electron Diffraction Pattern from Sputtered FeTiB Deposit After 538°C/4 hr and 649°C/4 hr Thermal Treatment	95



## SIGNIFICANT RESULTS AND CONCLUSIONS

Major conclusions are specified in Section A. Additional significant results and conclusions are listed in Section B. These supplementary conclusions are numbered consecutively, with the first digit indicating the number of the task from which they were derived.

### A. Major Conclusions

#### 1. Performance

A 50% reduction in the live (load carrying profile) disk weights of the JT10D-4 can be realized for the high pressure compressor, high pressure turbine and low pressure turbine rotors, when designed using LAYERGLAZED alloys with assumed properties. This amounts to a minimum of 400 lbs (181.8 kg)/engine.

#### 2. Cost

The total estimated Life Cycle Cost (LCC) reduction due to the use of LAYERGLAZED alloys in the F-100(3) engine for the F-15 aircraft, when designed for optimum LCC in the high pressure compressor and maximum weight savings in the remaining components, is \$222.4 million.

#### 3. Process Feasibility

The LAYERGLAZE process for sequential, in-situ buildup of dense, high cooling rate structures appears to be feasible at rates of 0.5 cu in/min (8.2 cc/min) at the -6.0 kW laser power level, with deposition rates of 1.0 cu in/min (16.4 cc/min) anticipated in the 10.0-15.0 kW power range. Thermal calculations indicate that the part can be cooled and rapid cooling rates can be maintained in large parts.

#### 4. Alloy Design Concept

High yield strength alloys were produced from eutectic starting materials; the results from the NiMoAl alloy which displayed a yield strength of 1755 MPa at 760°C suggest a fruitful path for further alloy optimization.

B. Additional Results and Conclusions

Task 1 - Performance and Cost Benefits/F-100(3)

1.1 Design evaluations of the F-100(3) and FEAT engines indicated that yield strength was less important than LCF and fracture toughness, pointing the way for emphasis in the areas of microstructural perfection and in-situ inspectability during future process development work.

1.2 A composite engine layout depicting the present B/M F-100(3) as compared to the redesigned engine using LAYERGLAZE processing was shown, Fig. 1-1.

1.3 The total expected weight savings from using LAYERGLAZE processed PDS alloys in the F-100(3) is 111.3 lbs (51.4 kg).

1.4 A manufacturing cost reduction of \$27,900/unit (17% of cost of parts studied) is projected for the F-100(3) engine by using LAYERGLAZE processed PDS alloys.

Task 2 - Performance and Cost Benefits/FEAT

2.1 A composite engine layout depicting the present B/M FEAT as compared to the redesigned engine using LAYERGLAZE processing was shown, Fig. 2-1.

2.2 The total expected weight savings from using LAYERGLAZE processed PDS alloys in the FEAT is 71.8 lbs (32.6 kg).

2.3 A manufacturing cost reduction of \$9,600/unit (16% of cost of parts studied) is projected for the FEAT engine by using LAYERGLAZE processed PDS alloys.

Task 3 - Performance and Cost Benefits/JT10D-4

3.1 Although strengths of 200,000 psi (1380 MPa) and 300,000 psi (2070 MPa) were assumed for Ti and Ni base alloys respectively, substantial fractions of the total predicted weight savings can still be realized at much lower strength levels, i.e. ~80% of weight savings could be realized with alloy strengths as much as 30% below those sought.

3.2 Total weight savings for the engine parts analyzed is predicted to be no less than 400 lbs (181.8 kg) which is equivalent to a reduction of 0.40% in Direct Operating Cost + Interest. By optimizing the way in which improved material properties are utilized, weight savings could potentially be increased by approximately 100 additional pounds (45.4 kg) (equivalent to 0.478% DOC + INT).



3.3 Because the rotor weights can be reduced with LAYERGLAZE process it is possible to also save weight at the bearing supports. Maneuver loads will be reduced due to smaller rotor weight thus possibly reducing case thicknesses. However, where static structures are limited for deflection requirements, no weight savings would be realized.

3.4 Cases fabricated by the LAYERGLAZE process could result in some weight savings where the design is limited by containment or LCF. Wall thickness could be reduced with a high ultimate and fatigue strength material.

3.5 Manufacturing cost estimates indicated that there would be no predictable difference in the manufacturing costs for commercial engines with LAYERGLAZED parts, so that predicted performance/weight/DOC+INT gains would be obtained without initial cost increases.

#### Task 4 - Life Cycle Cost Studies/F-100(3), FEAT

4.1 Maximum impact on life cycle cost savings was not coincident with maximum weight reduction in all cases. Extension of part life to the cycle limit, and acquisition cost reduction are the most potent factors.

4.2 According to design personnel, the ability to tailor structures for added life with LAYERGLAZE processing is potentially the most important benefit of the technology. The flexibility to adjust the structure, and to opt for specific properties is not available to the same degree in presently utilized materials systems.

4.3 The total estimated Life Cycle Cost reduction due to the use of LAYERGLAZE/PDS alloys for the F-100(3) engine in the F-15 aircraft, when redesigned for maximum weight savings, is \$141.7 million. When optimized from the LCC standpoint, rather than weight savings, the total estimated Life Cycle Cost reduction was \$222.4 million.

4.4 The total estimated Life Cycle reduction due to use of LAYERGLAZE/PDS alloys for the FEAT engine in the ATS aircraft due to initial cost and weight reduction is \$103.4 million. (Since the FEAT is designed based on presently unobtainable advanced material properties, should its construction be made possible by LAYERGLAZE technology, this technology should "get credit" for the much larger performance and cost benefits inherent in the FEAT design.)

Task 6 - Technical Feasibility Demonstration

6.1 Cooling rates of  $10^5$ - $10^6$ °C/sec can be produced at power densities in the range of  $10^4$ - $10^5$  watts/sq cm, a level comfortably within the equipment capability. (It has been shown under Task 7 that alloys produced at these cooling rates have exhibited significant properties.)

6.2 Process efficiency increases with increased cooling rate, with less specific energy being required for unit deposition of new material. Increased power densities and higher processing speeds (shorter dwell times) are required to obtain higher cooling rates.

6.3 Thermal analysis modeling the LAYERGLAZING process indicated that a 1 in. wide, 0.001 in. strip on the surface of a disk could achieve a cooling rate in excess of  $10^6$ °C/sec.

6.4 Observations of the deposition process to date indicate that substantial progress in LAYERGLAZE processing will result from further development effort.

6.5 A 0.200 in. (0.508 cm) deep flange of type 304 stainless steel was fabricated using a small scale LAYERGLAZE apparatus which applied material by a wire feed technique. Flange material was fully dense and free of flaws as inspected by radiography.

Task 7 - Alloy Design and Evaluation

7.1 In order to obtain high strength coupled with ductility, the best approach appears to be through the preparation of metastable, single phase alloys which are hardened by phase decomposition in the solid state.

## INTRODUCTION

↓  
Since the initial development of continuous high power CO<sub>2</sub> lasers, there has been rapid progress in their application to materials processing. With less than five years having elapsed since their development, these continuous lasers have been applied successfully in production areas of welding (Refs. 1-22), cutting (Refs. 10,18,23-28), and heat treatment (Refs. 10,18,29,30).

↪ Within the past year the laser has strongly impacted the technology for controlled rapid solidification and solid state cooling of metals and alloys. (Refs. 31-35). The initial means for achieving rapid cooling was the LASERGLAZE<sup>TM</sup> process, which involves the melting of thin surface layers at high melting efficiencies so that they remain in intimate contact with the cold, solid substrate material, producing rapid solidification and cooling. Laser-glazing has produced a variety of novel, nonequilibrium structures generally characteristic of rapid cooling.

Within the past few months, the LASERGLAZE concept has been evolved into a new process for production of rapidly cooled alloys in bulk form. This process was named LAYERGLAZE, since it involves the sequential deposition and "glazing-into-place" of thin layers of material in order to build up a dense, bulk part with the structure and properties characteristic of rapidly-cooled alloys. Since the structure is consolidated in-situ, the problem of subsequent consolidation is absent. An important element of the LAYERGLAZE concept is the development of alloys with structures and properties which are ideally suited for specific applications, and which derive these structures and properties as a direct result of the rapid solidification processing inherent in the process. ↪ The alloy design approach has been termed phase decomposition strengthening (PDS). Initial concepts are aimed at improving material properties for aircraft gas turbine parts, and the potential for parts processed in this manner is being evaluated in depth.

This final report documents an assessment of the performance and cost benefits which could be realized by developing and incorporating LAYERGLAZE technology in the production of gas turbine disks for a currently important military engine, (F-100(3)), an advanced future version of the F-100, (the "FEAT" engine) and a proposed commercial engine of the 1980's (JT10D-4). ↪ The tasks relating to this performance and cost benefit analysis which were addressed in this study are summarized below:



Task 1 - Performance and Cost Benefits/F-100(3)

Evaluation of the performance and cost benefits expected to be derived from applying phase-decomposition strengthened alloys in disks of the F-100(3) engine on a substitutional basis.

Task 2 - Performance and Cost Benefits/FEAT

Evaluation of the performance and cost benefits expected to be derived from applying phase-decomposition strengthened alloys in drum rotors and disks of an advanced military engine for the mid 1980's (the FEAT engine).

Task 3 - Performance and Cost Benefits/JT10D-4

Evaluation of the performance and cost benefits expected to be derived from applying phase-decomposition strengthened alloys in disks and drum rotors of an advanced commercial engine for the mid 1980's (the JT10D-4).

Task 4 - Life Cycle Cost Studies/F-100(3), FEAT

Performance of a detailed evaluation of the actual return on investment (Life Cycle Cost Study) which would result from development and application of phase-decomposition strengthened alloys and sequential structural buildup using lasers to produce turbine disks and/or drum rotors for the F-100(3) and FEAT engines.

Task 5 - Formation of Development Plan

Formation of a specific plan for the orderly development of the above-mentioned advanced laser materials processing technology through the component demonstration phase.

In addition to the above five tasks, which are primarily aimed at assessment of potential performance and cost benefits, studies performed under this contract also included a significant Technical Feasibility Demonstration phase. Two major tasks were addressed under the technical feasibility demonstration phase, as follows:

Task 6 - Technical Feasibility/Physical Process

- a. Construction of a small scale buildup machine with the goal of producing a small model shape in order to demonstrate process feasibility.
- b. Thermal analysis of the LAYERGLAZE process.

Task 7 - Technical Feasibility/Alloy Design

Fabrication, heat treatment, and mechanical testing of rapidly-quenched materials, melt-quenched ribbons and sputtered deposits of candidate alloys selected by UTRC in an effort to establish the capability of producing the required mechanical properties in phase-decomposition strengthened alloys.

All of the proposed tasks were successfully completed within the period of performance of the contract. The procedures and results are presented in the following sections, grouped by task number as indicated above. This task by task form of reporting is believed to be the most effective form for this particular program, since some tasks are experimental and require substantial reporting of procedures, whereas other tasks are primarily analytical, and thus are reported primarily as ground rules or assumptions, and results.

## TASK 1 - PERFORMANCE AND COST BENEFITS/F-100(3)

This task involved the evaluation of the Performance and Cost Benefits expected to be derived from applying phase-decomposition strengthened alloys in disks of the F-100(3) engine, an engine currently employed in F-15 and F-16 aircraft. The analysis was performed by the Preliminary Design Group (F-100 Derivatives) of the Pratt and Whitney Aircraft Government Products Division by Messrs. A. Kalb, J. Sandy, D. Garcia, and D. Turner.

## Weight

In order to assess the potential benefits to be derived from application of LAYERGLAZE processing and use of Phase Decomposition Strengthened (PDS) alloys in the F-100(3) engine, design studies were conducted with the object of determining the weight savings which could be generated by use of LAYERGLAZE and PDS in the rotating parts of these engines. The engine parts analyzed included the fan, high pressure compressor (HPC), high pressure turbine (HPT), and low pressure turbine (LPT) rotors, including disks, some aspects of blades, spacers, seals, bolts, and hub. The estimated weight savings for the F-100(3) reflects savings both due to reducing the sizes of some disks, and substitution of drum rotors for disks as a result of using PDS alloys with improved properties.

Initial evaluations indicated that yield strength was less important than low cycle fatigue (LCF) and fracture toughness, since LCF limits the life of most parts in the present B/M F-100(3).

Tables 1-I and 1-II respectively present the mechanical property data assumed for LAYERGLAZE fabricated PDS titanium and nickel-base alloys respectively. Although the ultimate properties of these alloys will be known only after full development of both the alloys and the process and an adequate period of testing, the assumptions made for the design studies are represented as a conservative estimate of what might be achieved with the LAYERGLAZE process as it is presently conceived. Due to the fact that the design studies point to a relative deemphasis on strength, with the emphasis to be placed on LCF and fracture toughness, it is considered that there will be expanded emphasis in future development programs on creation of microstructural perfection and in-situ inspectability to insure the smallest possible maximum flaw size for the structure.

The composite engine layout in Fig. 1-1 depicts the profiles of the parts analyzed in the present bill-of-material (B/M) F-100(3) and in the redesigned LAYERGLAZE/PDS version. The present B/M engine profile lies above the engine center line in this figure, with the redesigned profile below. Table 1-III is



Table 1-I

## LAYERGLAZE Titanium Alloy Design Values Used

<u>Temperature</u>		<u>Strength</u>				<u>Elongation (%)</u>
		<u>Yield</u>		<u>Ultimate</u>		
<u>°F</u>	<u>°C</u>	<u>psi</u>	<u>MPa</u>	<u>psi</u>	<u>MPa</u>	
75	24	150,000	1035	180,000	1240	>5
400	204	140,000	965	165,000	1135	↓
800	427	130,000	895	150,000	1035	
1000	538	120,000	825	140,000	965	

75°F Strain Range - LCF Life (0 Mean Stress)

<u>Smooth Section</u>		<u>Notched Section</u>	
<u>Nf1 Cycles</u>	<u>Δt in./in.</u>	<u>Nf Cycles</u>	<u>Δf in./in.</u>
100	.031	100	.0315
1,000	.019	1,000	.020
10,000	.012	10,000	.014
100,000	.0093	100,000	.0095

Creep and Rupture

<u>Temperature</u>		<u>Stress for .2% Creep, 100 Hrs</u>		<u>Stress Rupture for 100 Hrs</u>	
<u>°F</u>	<u>°C</u>	<u>psi</u>	<u>MPa</u>	<u>psi</u>	<u>MPa</u>
800	427	85,000	585	130,000	895
900	482	50,000	345	110,000	760
1000	538	20,000	140	65,000	450

Fracture Mechanics

Used four times the present titanium alloy cycle value at a given stress and temperature.

Other Properties

Density, elastic modulus, thermal expansion coefficient, thermal conductivity, and specific heat are same as base titanium alloy.

Table 1-II

## LAYERGLAZE Nickel Alloy Design Values Used

		<u>Strength</u>				<u>Elongation (%)</u>
<u>Temperature</u>		<u>Yield</u>		<u>Ultimate</u>		
<u>°F</u>	<u>°C</u>	<u>psi</u>	<u>MPa</u>	<u>psi</u>	<u>MPa</u>	
75	24	250,000	1720	300,000	2065	>5 ↓
800	427	230,000	1585	275,000	1895	
1100	593	230,000	1585	275,000	1895	
1400	760	165,000	1135	200,000	1380	

75°F Strain Range - LCF Life (0 Mean Stress)

<u>Smooth Section</u>		<u>Notched Section</u>	
<u>Nf1 Cycles</u>	<u>Δt in./in.</u>	<u>Nf Cycles</u>	<u>Δf in./in.</u>
100	.030	100	.0197
1,000	.018	1,000	.0176
10,000	.012	10,000	.0159
100,000	.0088	100,000	.0143

Creep and Rupture

<u>Temperature</u>		<u>Stress for .2% Creep, 100 Hrs</u>		<u>Stress Rupture for 100 Hrs</u>	
<u>°F</u>	<u>°C</u>	<u>psi</u>	<u>MPa</u>	<u>psi</u>	<u>MPa</u>
1200	649	135,000	930	150,000	1035
1300	704	95,000	655	110,000	760
1400	760	15,000	105	55,000	380
1500	816	-	-	25,000	170

Fracture Mechanics

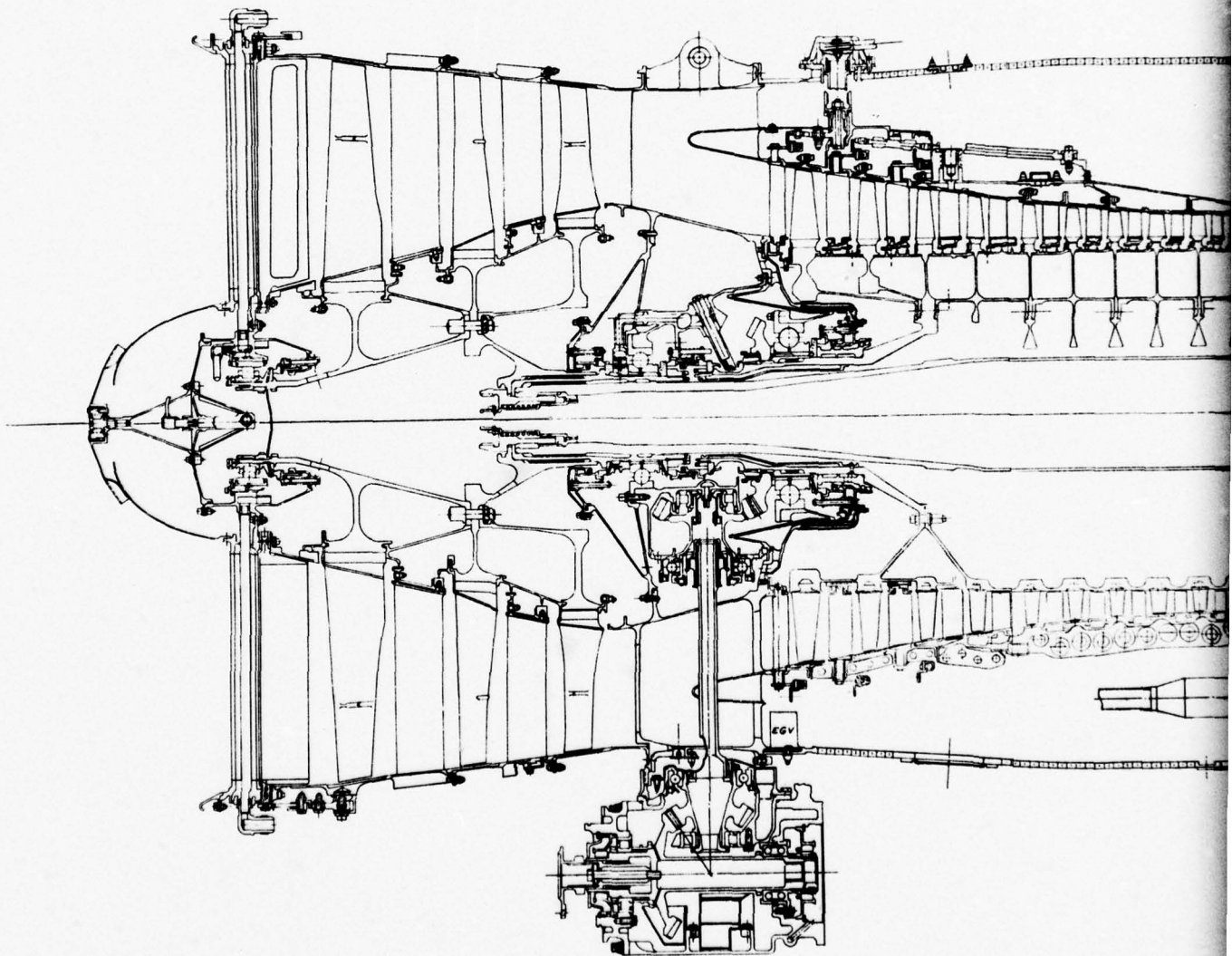
Used four times the present nickel alloy cycle value at a given stress and temperature.

Other Properties

Density, elastic modulus, thermal expansion coefficient, thermal conductivity, and specific heat same as base nickel alloy.

**COMPOSITE ENGINE**  
**F100**

(PRESENT B/M -  
(USING LAYERGLAZ





# COMPOSITE ENGINE CROSS SECTION F100-3

(PRESENT B/M - ABOVE  $\phi$ )  
(USING LAYERGLAZE - BELOW  $\phi$ )

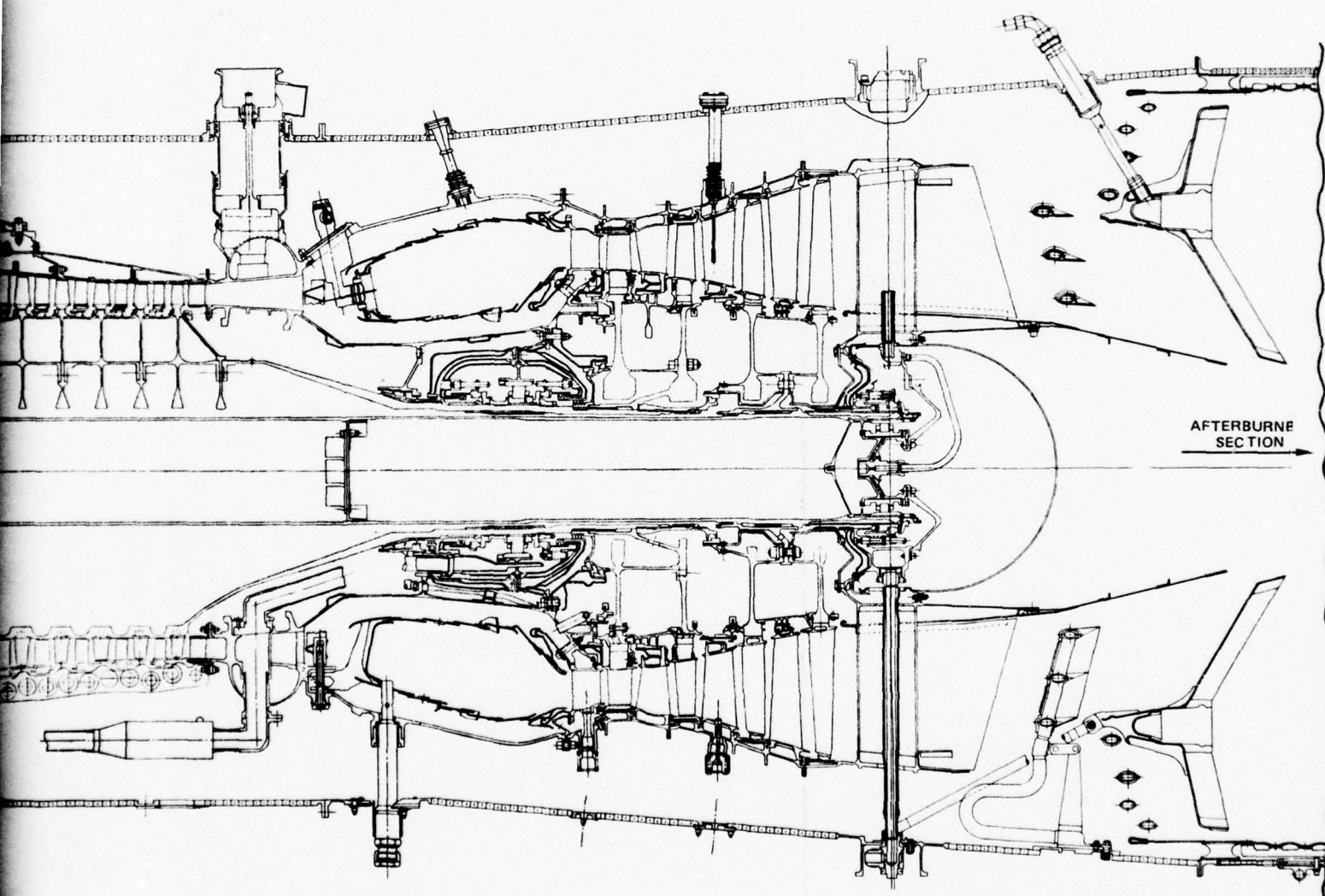


Table 1-III

F-100(3) B/M vs LAYERGLAZE/F-100(3) Weights

High Compressor Rotor		LAYERGLAZE Weights		F-100(3) B/M Weights		$\Delta$ Weight		% Wt Change from B/M
		lbs	kg	lbs	kg	lbs	kg	
<u>Disks</u>	4th Disk	9.2	4.18	16.9	7.68	-7.7	-3.50	-45.5
	5th Disk	6.4	2.91	11.0	5.00	-4.6	-2.09	-41.9
	6th Disk	5.3	2.41	11.6	5.27	-6.3	-2.86	-54.4
	7th Disk	5.9	2.68	10.0	4.55	-4.1	-1.87	-41.0
	8th Disk	6.4	2.91	10.6	4.82	-4.2	-1.91	-39.6
	9th Disk	6.9	3.14	7.5	3.41	-0.6	-0.27	- 8.0
	10th Disk	6.6	3.00	10.3	4.68	-3.7	-1.68	-35.9
	11th Disk	7.0	3.18	8.5	3.86	-1.5	-0.68	-17.6
	12th Disk	6.7	3.05	10.5	4.77	-3.8	-1.72	-36.1
	13th Disk	6.9	3.14	10.2	4.64	-3.3	-1.50	-32.3
Spacers & Seals (4-13)		43.0	19.55	66.6	30.27	-23.6	-10.72	-35.5
Bolts & Nuts		2.0	0.91	13.6	6.18	-11.6	-5.27	-85.3
Rear Hub		47.2	21.45	43.3	19.68	+3.9	+1.77	+ 9.0
Blades (4-13)		<u>27.8</u>	<u>12.64</u>	<u>29.9</u>	<u>13.59</u>	<u>-2.1</u>	<u>-0.95</u>	- 7.0
		187.3	85.14	260.5	118.41	-73.2	-33.27	
<u>High Turbine Rotor</u>								
1st Live Disk		21.4	9.73	36.3	16.50	-14.9	-6.77	-41.0
2nd Live Disk		14.6	6.64	25.2	11.45	-10.6	-4.81	-42.1
1-2 Spacer		10.0	4.55	13.0	5.91	-3.0	-1.36	-23.1
Remaining Hdw.		<u>68.2</u>	<u>31.00</u>	<u>68.2</u>	<u>31.00</u>	-	-	
		114.2	51.91	142.7	64.86	-28.5	-12.95	
<u>Low Turbine Rotor</u>								
3rd Live Disk		13.7	6.23	19.2	8.73	-5.5	-2.50	-28.6
4th Live Disk		12.5	5.68	15.4	7.00	-2.9	-1.32	-18.8
Remaining LPT Hdw.		74.9	34.04	74.9	34.04	-	-	
W/O Shaft		<u>101.1</u>	<u>45.95</u>	<u>109.5</u>	<u>49.77</u>	<u>-8.4</u>	<u>-3.82</u>	
<u>Fan Rotor</u>								
Disks (1-3)						-1.2	-0.55	
Total wt. change =						-111.3	-50.59	
						lbs	kgs	

a detailed breakdown of F-100(3) B/M rotor weights and comparable design weights assuming use of LAYERGLAZE and PDS alloys. Percentage weight reductions are also detailed in Table 1-III. The total weight savings from the combined use of LAYERGLAZE processing and the ability to produce the engine with a drum rotor, is 111.3 lbs (50.59 kg) of which 76 lbs (34.5 kg) savings is directly attributable to the use of LAYERGLAZE processing and the remaining 35 lbs (15.9 kg) is saved by configuring the engine as a drum rotor rather than the present double backbone design as used in the B/M.

#### Cost

A manufacturing cost analysis was performed on the F-100(3) engine as follows: Ground rules were applied as indicated below. A ribbon feed process, as detailed schematically in Fig. 6-1, was assumed, since ribbon feed cost can be most realistically estimated at present. Figure 6-1 depicts the sequential deposition of feedstock material on a rotating mandrel. For purposes of cost analysis, the following important features of the production process were anticipated.

- Mandrel rotates and translates
- Helium atmosphere environment
- Mandrel convection cooled by gas jets (helium)
- Feedstock is special ribbon or rod deposited in .002 in. (.0008 cm) layers at .5-1.0 in<sup>3</sup>/min (8.2-10.4 cc/min)
- Laser is 15 kW continuous beam CO<sub>2</sub> type
- Material candidates are Ti, Fe, Ni and Co base
- Continuous Q.C. monitoring in process expected to result in a cross-section more nearly net shape than conventional sonic configuration due to visibility of lay-up in .002 in. (0.005/cm) thick increments, and in process repair capability
- Mandrel removed by machining or chemical action.



In addition, the following factors were assumed in the analysis for the purpose of estimating manufacturing costs.

- Raw material cost was derived by taking the current base cost and adding processing expense as supplied by Allied Chemical Co. for conversion to ribbon feed material.
- Material volume was based on near net shape outline plus machining allowance and mandrel contamination zone.
- Disposable mandrels made from centrifugally cast iron.
- Machining time was based on machineability of IN-100 with the selective use of Borazon.
- Current F-100 labor rates and overhead used.
- 20% contingency factor included.
- Material deposition was assumed to be  $.5 \text{ in}^3/\text{min}$  (8.2 cc/min).

Table 1-IV presents a cost comparison of the present B/M F-100(3) with the same engine utilizing the properties of LAYERGLAZE processed alloys as shown in the composite engine cross section (Fig. 1-1). Engine speeds and physical envelope remain the same, but a split case and drum rotor are substituted in the compressor and all turbine disks are substantially reduced in cross-section. Deletion of the disk bores in the drum result in major cost savings of \$27,900 (17% of cost of parts considered) per engine, even though the split case, which would be presently required with the drum rotor, is more expensive than current B/M design. It is anticipated that due to expected progress in split case design and manufacture, use of a split case may not carry current weight and cost penalties by the time the LAYERGLAZE process would be ready for application.

Table 1-IV

## F-100(3)/LAYERGLAZE Cost Study Summary

L-233613	F-100 Baseline <u>B/M Cost</u>	LAYERGLAZE Cost <u>Estimate</u>	Cost Δ <u>from B/M</u>
<u>Compressor</u>			
Rotor 4-6 stg.	16,755	15,514	\$ - 1,241
Rotor 7-13 stg.	69,764	37,649	-32,115
Stator 4-6 stg.	14,741	19,371	+ 4,630
Stator 7-13 stg.	31,603	45,029	<u>+13,426</u>
	Compressor Δ Cost		\$ -15,300
<u>Turbine</u>			
Hi Turbine Rotor	30,365	21,890	\$ - 8,475
Lo Turbine Rotor	12,767	8,634	<u>- 4,133</u>
	Turbine Δ Cost		\$ -12,608
	Total Engine Δ Cost		\$ -27,908

The figures in the above B & P estimate do not reflect complete engine sections - only the cost of parts directly affected.

## TASK 2 - PERFORMANCE AND COST BENEFITS/FEAT

This task involved the evaluation of the Performance and Cost Benefits expected to be derived from applying phase-decomposition strengthened alloys in disks and drum rotors of the FEAT engine, an advanced military engine for the mid 1980's. The analysis was performed by the Preliminary Design Group (F-100 derivatives) of the Pratt and Whitney Aircraft Government Products Division by Messrs. A. Kalb, J. Sandy, D. Garcia and D. Turner.

## Weight

The initial performance and cost benefit analyses performed on the FEAT (Florida-East Hartford Advanced Technology) derivative of the F-100 engine consisted of weight and manufacturing cost studies which closely paralleled the weight and cost studies performed on the F-100(3) and detailed under Task 1 in section 1, above.

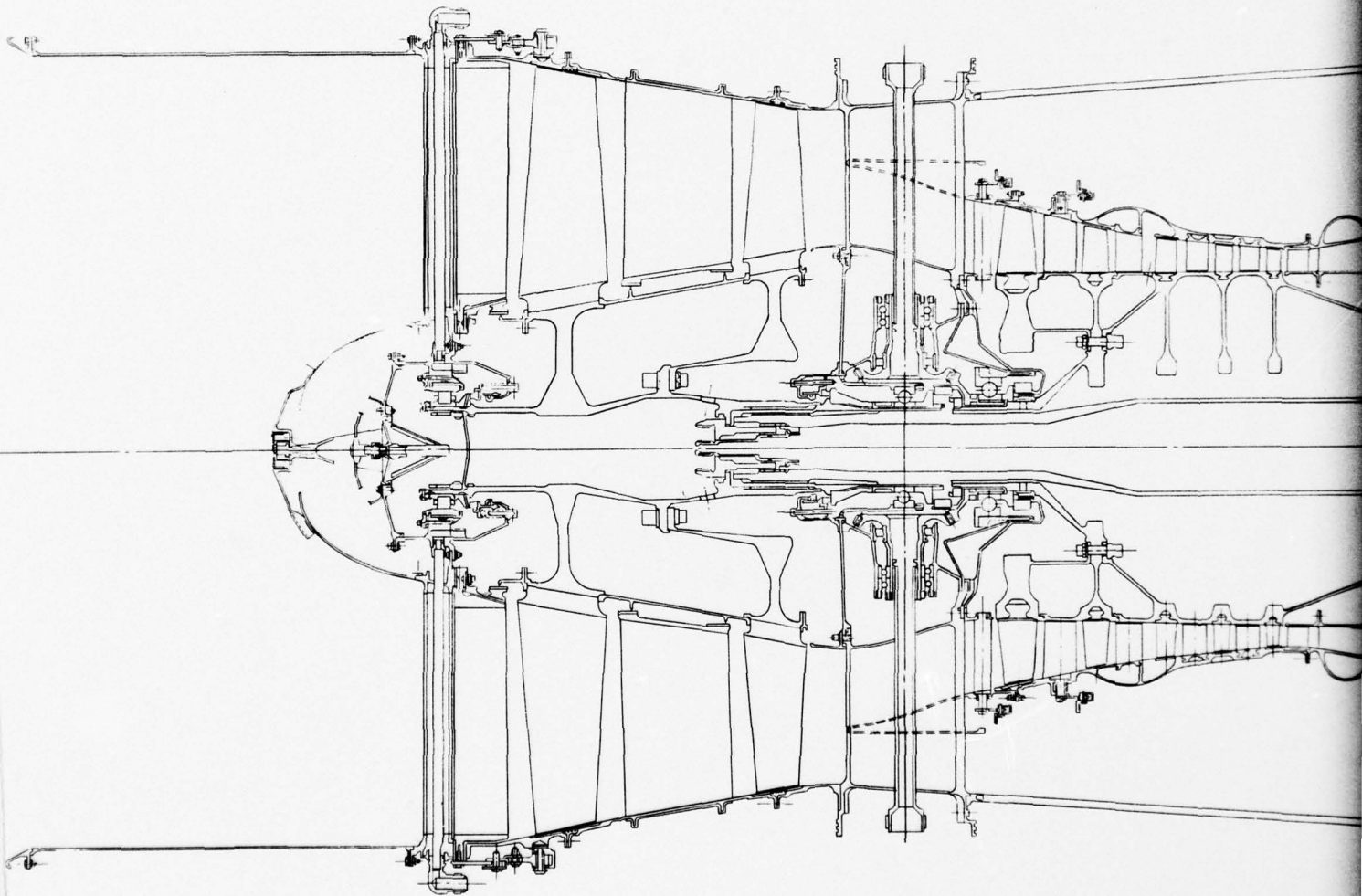
The FEAT engine is an advanced engine designed for the ATS (Advanced Tactical System) mission and is a very lightweight, high specific thrust, low cost derivative of the F-100. This derivative engine, with only nine stages (vs 17 for the F-100(3)) obtains its thrust from very high speed operation and its design requires the use of advanced materials technology wherein 10% better material properties than present B/M IN-100 and titanium alloys are assumed, as is a substantially reduced maximum flaw size, 0.005 in. (0.013 cm) for the purpose of predicting fatigue and fracture mechanics behavior. No increase in LCF, however, was assumed over present LCF limits. In these studies, the potential for weight and cost savings through eventual use of LAYERGLAZE technology and PDS alloys was estimated. In the FEAT studies, this lightweight turbofan's fan, HPC, HPT, and LPT rotors, were considered. Weight savings projected for the FEAT do not require a major change in configuration, as was the case with the F-100(3). LCF and fracture toughness again proved to be more important criteria than yield strength. The mechanical property data assumed for the FEAT studies was identical to that used for the F-100(3) estimates, and was detailed for titanium base alloys in Table 1-I and for nickel base alloys in Table 1-II, in the previous section.

The composite engine layout in Fig. 2-1 depicts the profiles of the parts analyzed in the present B/M FEAT engine above the engine center line, and of the redesigned LAYERGLAZE/PDS version, below the engine center line. Table 2-I is a detailed breakdown of FEAT B/M rotor weights and comparable design weights assuming use of LAYERGLAZE and PDS alloys. Percentage weight reductions are also identified in Table 2-I. The total weight savings from the use of LAYERGLAZE processing is 71.8 lbs (32.64 kg).



COMPOSITE ENGINE CR  
FEAT

(PRESENT B/M - BASED ON ASSUMED ADVANC  
(USING LAYERGLAZE - BEL



ASSUMED ADVANCED PROPERTIES – ABOVE  $\zeta$  )  
LAYERGLAZE – BELOW  $\zeta$  )

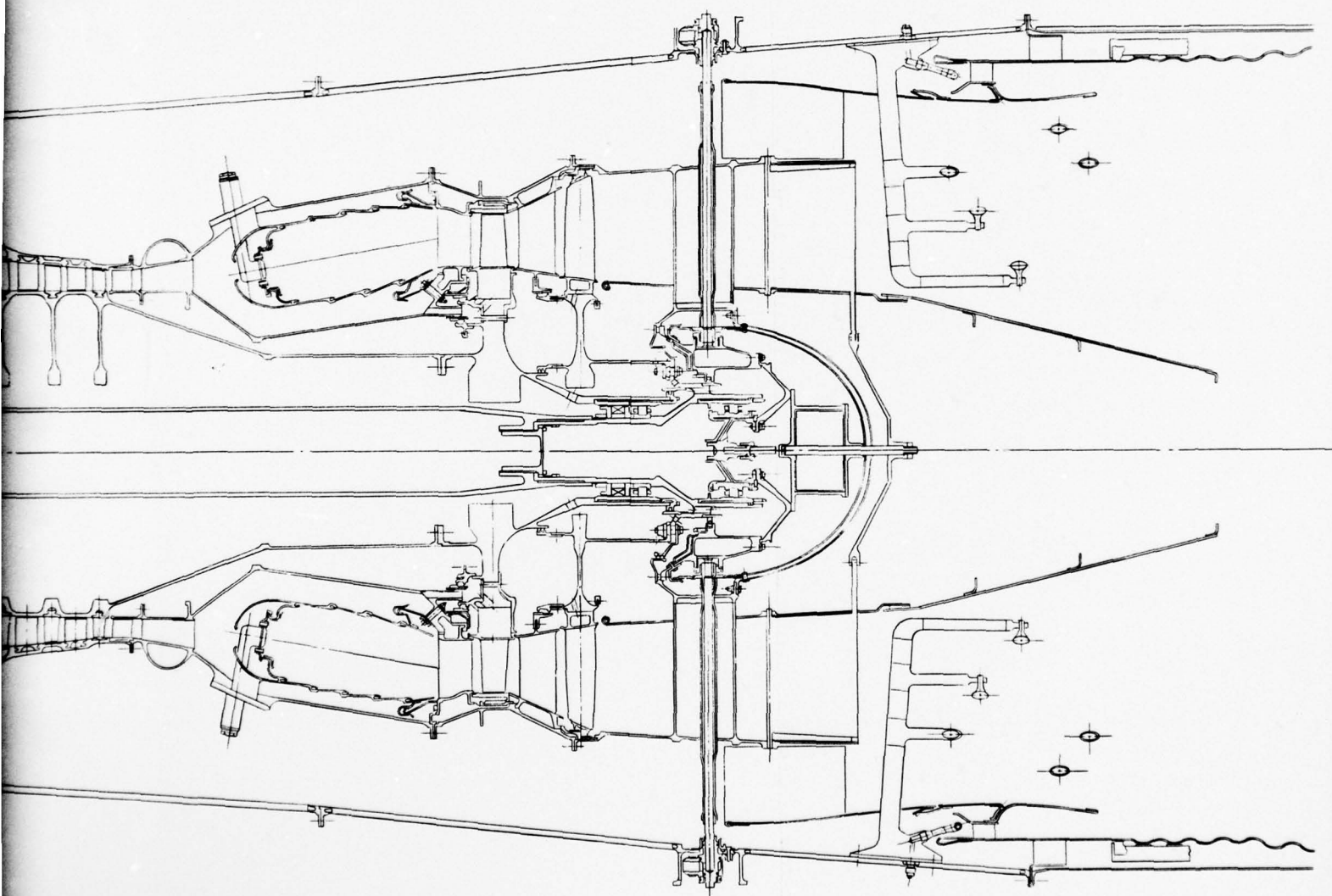


Table 2-I

## FEAT/PED vs LAYERGLAZE/FEAT/PED Weights

High Compressor	LAYERGLAZE		FEAT/PED				% Wt Change
<u>Rotor</u>	<u>Weights</u>		<u>Weights</u>		<u>Δ Weight</u>		<u>from B/M</u>
	lbs	kg	lbs	kg	lbs	kg	
<u>Live Disks</u>							
3rd Disk	20.6	9.36	28.8	13.09	- 8.2	-3.73	-28.5
4th Disk	13.3	6.05	17.6	8.00	- 4.3	-1.95	-24.4
5th Disk	7.6	3.45	15.7	7.14	- 8.1	-3.68	-51.6
6th Disk	6.6	3.00	13.5	6.14	- 6.9	-3.14	-51.1
7th Disk	<u>7.2</u>	<u>3.27</u>	<u>13.0</u>	<u>5.91</u>	<u>- 5.8</u>	<u>-2.64</u>	-44.4
	55.3	25.14	88.6	40.27	-33.3	-15.14	
<u>High Turbine Rotor</u>							
Live Disk	49.5	22.50	68.0	30.91	-18.5	-8.41	-27.2
<u>Low Turbine Rotor</u>							
Live Disk	20.5	9.32	27.7	12.59	- 7.2	-3.27	-26.0
<u>Fan Rotor</u>							
1st	19.0	8.64	24.9	11.32	- 5.9	-2.68	-23.7
2nd	19.5	8.86	24.4	11.00	- 6.9	-3.14	-26.1
Total wt. change =					-71.8	-32.64	
					lbs	kgs	



## Cost

A manufacturing cost analysis identical to that for the F-100(3) was performed for the FEAT engine. The assumptions and ground rules were listed on page 13. Table 2-II presents a cost comparison of the B/M FEAT engine with the same engine utilizing the properties of LAYERGLAZE processed alloys as shown in the composite engine cross section, (Fig. 2-1). Since the PED/FEAT configuration already features a more advanced design concept than the F-100(3), the acquisition cost savings are not projected to be as great, but material properties include the 120%  $N_2$  speed increase which is an integral part of the FEAT engine. Due to the higher projected cost (although uncertain, conservatively estimated) of titanium alloys in feedstock form, titanium alloys offer less attractive payoffs than nickel base alloys. This is apparent both in Table 2-I and in Table 1-IV in the previous sections. Compressor stator cases were not included in the results of the FEAT analysis, since no changes would occur whether LAYERGLAZE is included or not. The results in Table 2-I project a manufacturing cost savings of \$9,600/engine (16% cost savings on the parts studied).

Table 2-II

## PED/FEAT - LAYERGLAZE Cost Study Summary

L-233614	PED Base <u>B/M Cost</u>	LAYERGLAZE Cost <u>Estimate</u>	Cost $\Delta$ <u>from B/M</u>
<u>Fan</u>			
First Disk & Hub	6992	7962	\$ + 970
Second Disk	4201	5142	<u>+ 941</u>
	Fan Cost		\$ +1911
<u>Compressor</u>			
First Disk	3316	3943	\$ + 627
Second Disk & Hub	5900	6535	+ 635
3-5 Drum Rotor	19,482	12,060	<u>-7422</u>
	Compressor $\Delta$ Cost		\$ -6160
<u>Turbine</u>			
Hi Turbine Disk	13,468	9539	\$ -3929
Lo Turbine Disk	6,707	5254	<u>-1453</u>
	Turbine $\Delta$ Cost		\$ -5382
	Total Engine $\Delta$ Cost		\$ -9631

The figures in the above B & P estimate do not reflect complete engine sections - only the cost of those parts directly affected.

## TASK 3 - PERFORMANCE AND COST BENEFITS/JT10D-4

This task involved the evaluation of the Performance and Cost Benefits expected to be derived from applying phase-decomposition strengthened alloys in disks and drum rotors of the JT10D-4, an advanced commercial engine for the mid 1980's. The analysis was performed by the Preliminary Engine Design Group of the Pratt and Whitney Aircraft Commercial Products Division by Messrs. F. J. Mike, R. J. Comeau and R. F. Brodell.

## Assumptions Made in These Analyses

The performance and cost benefit analyses comprising this task made use of the following assumptions:

1. The JT10D-4 high compressor drum and first stage high turbine disks were selected for this study because of the availability of information for comparison and the fact that a follow-on engine is assumed to be a potential high production engine in the future.
2. It was assumed that the yield, fatigue, creep and stress rupture strengths and the bore fracture mechanics capability of the material fabricated by the LAYERGLAZE process are adequate to achieve the optimum savings possible with materials of 300,000 psi (2070 MPa) and 200,000 psi (1380 MPa) ultimate strengths for nickel and titanium alloys respectively.
3. Maintenance cost (material plus labor) calculated for this study was based on a model that evaluates the 15 year cumulative M.C. for a number (block feed) of mature engines using the JT10D-4 flight mission (1.25 hr/flight). Fully burdened labor rates and 1977 dollars were used.
4. Direct Operating Cost (DOC + Interest) and the performance, cost, weight and maintenance cost trade factors used in this study are based on a JT10D-4 29,000 pound (13,182 Kg) thrust engine for application on a twin-160 passenger one stop transcontinental aircraft.
5. Material Utilization Factor (MUF) and Average Tangential Stress: The MUF or geometry factors used for the materials to determine the allowable average tangential stresses for a given ultimate strength are from the P&WA Design Manual Page 9.2.5.

$$\text{Stress Tangential Average} = \frac{\text{MUF} \cdot (\text{Ultimate Stress})}{(\text{Burst Margin})^2}$$



The MUF for a cylindrical drum analyzed for the HPC was considered to be .75 because insufficient data exist for a blade carrying disk that has no bore and web.

6. A red line speed of 11,625 RPM and burst margins of 22% for the HPC and 24% for the turbine disks were used for the analyses.

In the evaluation of the potential of the LAYERGLAZE process, it is noted that materials so produced result in disk designs that are burst limited in all cases studied. It is observed, however, that other factors could limit a disk fabricated by this process at the final engine design. Because a high strength disk has smaller mass and higher stresses than those of a conventional disk, the disk could become vibration or deflection limited where additional mass would have to be added to relieve the problem. This would result in less weight savings than concluded in these burst limited designs.

#### Results of Analyses Performed

The JT10D-4 high compressor drum and first high turbine disks were studied in detail. The fan disk was not analyzed for this study, as fan disks are usually limited by vibration rather than burst. By redesigning the disk with higher strength material, and tailoring the profile (hollow disk) a potential 20-30% weight savings could be realized.

Table 3-I summarizes the weight savings (which can be traded off as desired for other factors) for the disks studied. The results indicate that a 50% weight savings in the live (load carrying profile) disk weights can be realized for the high pressure compressor, the high pressure turbine, and also, the low pressure compressor. For the purposes of the above estimate it was assumed that the yield, fatigue, creep, and bore fracture mechanics capability of the LAYERGLAZE alloys were proportional to their ultimate strengths, as detailed under assumptions, above. Figure 3-1a shows the high pressure compressor disk profiles achievable with LAYERGLAZE quality alloys compared to the base JT10D-4 rotor designed with presently utilized materials. Figure 3-2 shows the high pressure turbine disk profiles for the JT10D-4 first stage as currently designed, a LAYERGLAZED disk with a 300,000 psi (2070 MPa) ultimate strength, and a reduced rim diameter disk for a rotor designed for a 10% speed increase, which is also an option, as discussed below.

Table 3-I  
Potential Weight Saving with LAYERGLAZE Process  
(JT10D-4 HPC and HPT Rotor Disk Study)

Rotor Disk	Material	Live Disk Weight Base lbs (kg)	Burst Limited Disk Weight (Layerglaze) lbs (kg)	Potential Max Weight Savings lbs (kg)	% Weight Saving	Avg. Tang. Stress Burst Limited @ 11625 rpm psi (MPa)	Required psi (MPa)	Disk Mat. Utilization Factor (MUF)
HPC R-4 thru R-10	AMS 4928	114.0 (51.2)	66.0 (30)	48.0 (21.8)	42	95,000 (654)	180,000 (1240)	.75
	PWA 1209 Ti							
HPC R-11	PWA 1214 Ti	20.8 (9.5)	8.0 (3.6)	12.8 (5.8)	61	126,000 (868)	195,000 (1344)	.93
HPC R-12,13	PWA 1007 Wasp.	117.8 (53.5)	40.0 (18.2)	77.8 (35.4)	66	140,000 (965)	243,000 (1674)	.83
HPT R-1	PWA 1057 Wasp.	167.0 (75.9)	85.0 (38.6)	82.0 (37.2)	49	162,000 (1116)	300,000 (2067)	.83
Total for Disks Studied		419.6 (190.7)	199.0 (90.4)	220.6 (100.3)	52			

Conclusion: 50% live disk weight can be saved for all rotor stages (compressor and turbine).  
Expected total HPC, HPT, and LPT weight saved = 400 lbs (181.8 Kg) (Equivalent to 0.40% DOC + INT)

## MODIFICATIONS OF JT10D-4 HPC ROTOR STAGES 4-13 USING LAYERGLAZE PROCESSED ALLOYS

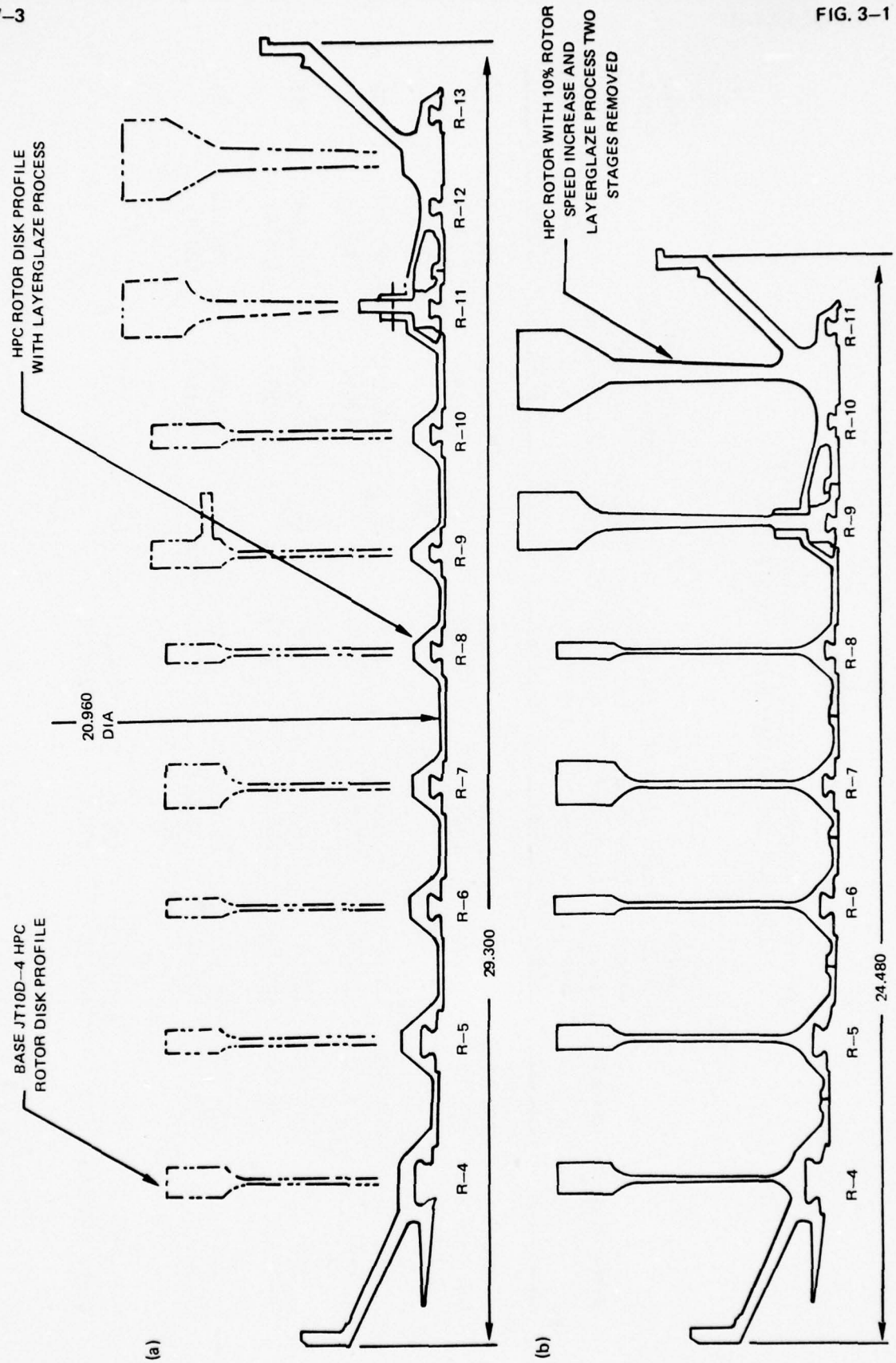
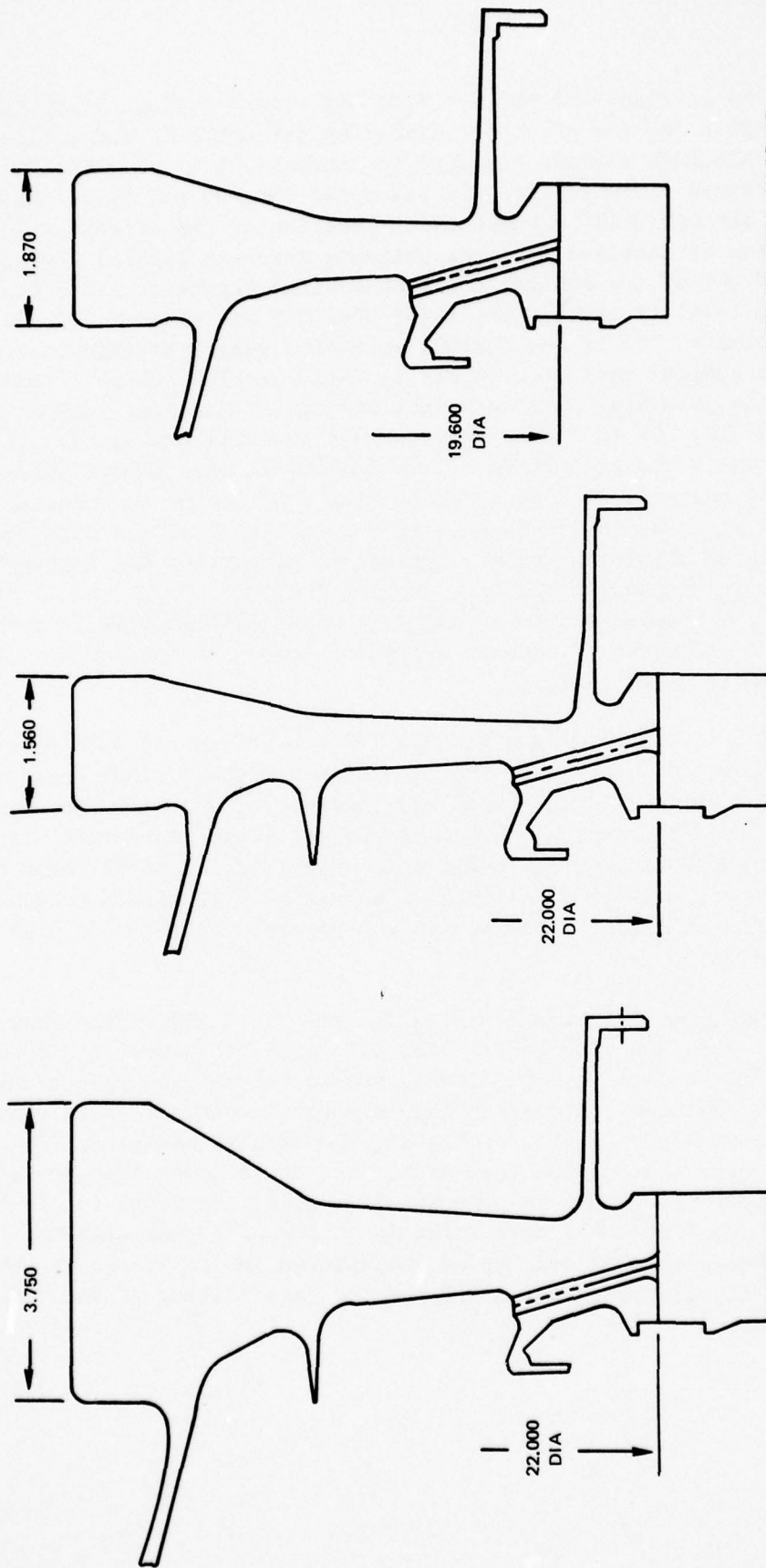


FIG. 3-1



MODIFICATIONS OF JT10D-4 HPT R-1 DISK USING LAYERGLAZE PROCESSED ALLOYS

ENGINE Q



BASE

LIVE DISK WEIGHT = 167 LB  
= 75.9 kg

300ksi (2.1x10<sup>9</sup> N/m<sup>2</sup>) ULTIMATE STRENGTH

LIVE DISK WEIGHT = 85 LB  
= 38.6 kg

10% ROTOR SPEED INCREASE

300ksi (2.1x10<sup>9</sup> N/m<sup>2</sup>) ULTIMATE STRENGTH

LIVE DISK WEIGHT = 80 LB  
= 36.4 kg

The curves in Figs. 3-3 and 3-4 show the weight savings at different ultimate tensile strengths for the HPC rotor disks R-4 through R-10 and R-11. It is obvious that although savings continue to increase up to the 200,000 psi (1380 MPa) assumed ultimate for R-11 and up to 180,000 psi (1240 MPa) ultimate for R-4 through R-10, a substantial fraction of the weight savings in these disks can be achieved at lower ultimate strength levels. For example in R-4 - R-10 96% of the available weight savings can be obtained at an ultimate strength level of 160,000 psi (1102 MPa) UTS and even at 140,000 psi (965 MPa) ultimate, 79% of the maximum potential weight savings is still available. A similar condition exists at R-11. At 160,000 psi (1102 MPa) UTS, 86% of the potential maximum weight savings is obtained, and at 140,000 psi (965 MPa) UTS, 68% of the maximum savings is still available. It is thus clear that even if the properties of LAYERGLAZED Ti base alloys should fall short of the present goals by 20-30%, a substantial fraction of the available weight savings could still be realized, primarily as a result of the fact that weight savings increases slowly as maximum mechanical properties are approached. As of now, however, preliminary properties suggest that goals will be met or exceeded. Alternatively, a greater factor of safety could be designed in if mechanical property goals are achieved, and if designers choose to opt for less than the maximum available weight savings.

Figure 3-5 shows the weight savings for the HPC 12 and 13th stage disk. These are usually nickel base alloys. The base disk for the JT10D-4 present design is LCF limited and weighs 111 lbs (50.5 kg); however, a burst limited disk would weigh only 79 lbs (35.9 kg). Because of the potential improvement in fatigue strength of a LAYERGLAZED disk, additional weight can be saved for a burst limited disk up to a 243,000 psi (1674 MPa) ultimate tensile strength. Further weight reduction at higher strengths is not possible because the disk shape becomes cylindrical.

Figure 3-6 shows the weight saving for the first HPT disk. Large weight savings can be realized with LAYERGLAZED alloys at UTS levels to 300,000 psi (2067 MPa). Beyond that strength level, additional smaller percentage gains could be realized. Because higher strength materials could allow reduced disk profiles with less elastic restraint, the elastic radial growth at the rim will increase over that of the base disk. The curve shows that the radial deflection is 0.026 in. (0.066 cm) for the base disk, and 0.042 in. (0.106 cm) for a 300,000 psi (2067 MPa) disk which is 82 lbs (37.3 kg) lighter. The growth differences can, of course, be compensated for in design to achieve the desired blade tip clearances by modifying the case cooling of the active clearance control system.

# WEIGHT VS ULTIMATE STRENGTH

JT10D-4 HPC DRUM ROTOR R-4 MRD R-10  
 LAYER GLAZE PROCESS FOR TITANIUM ALLOYS  
 ROTOR SPEED = 11625 RPM

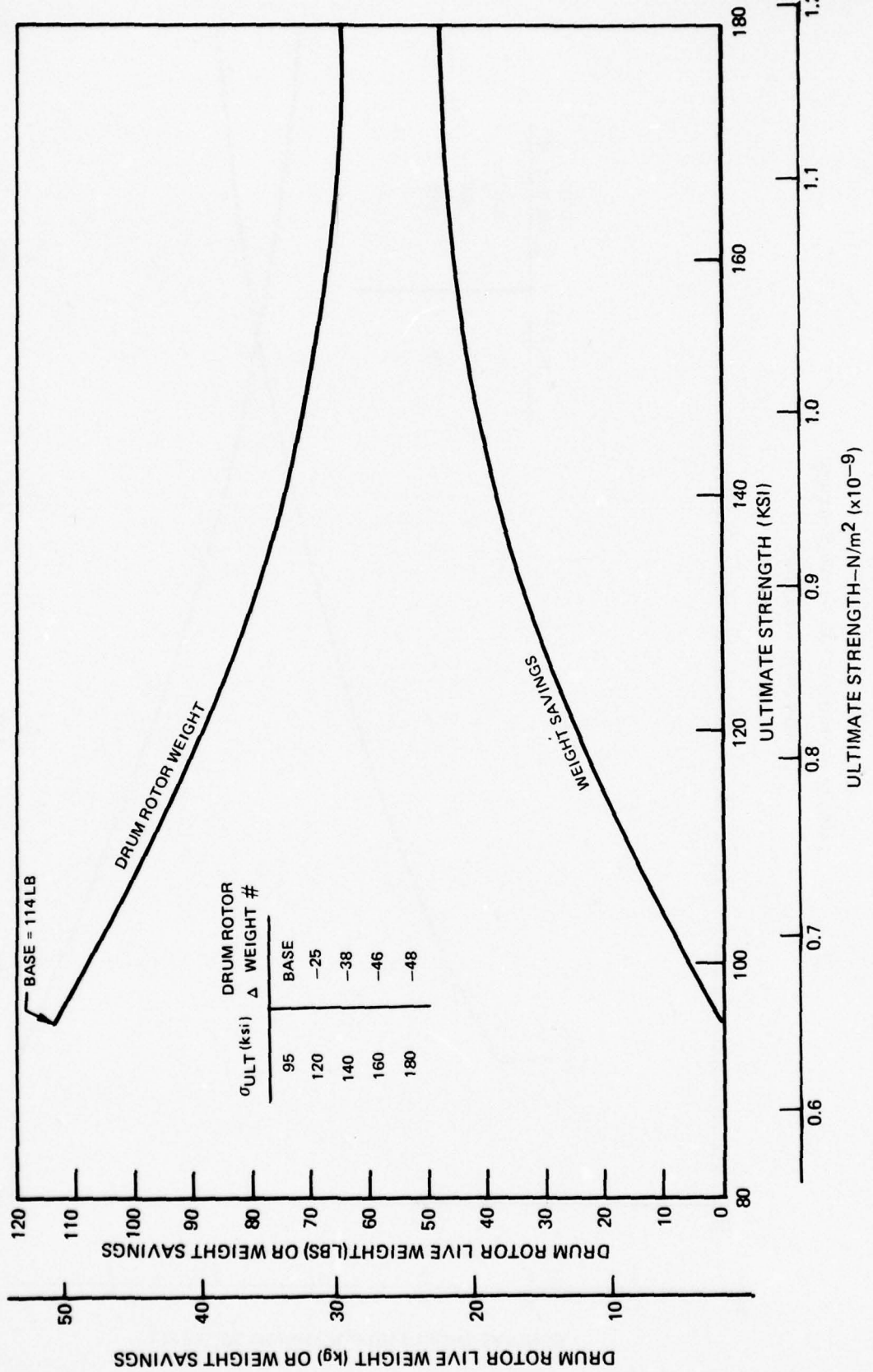
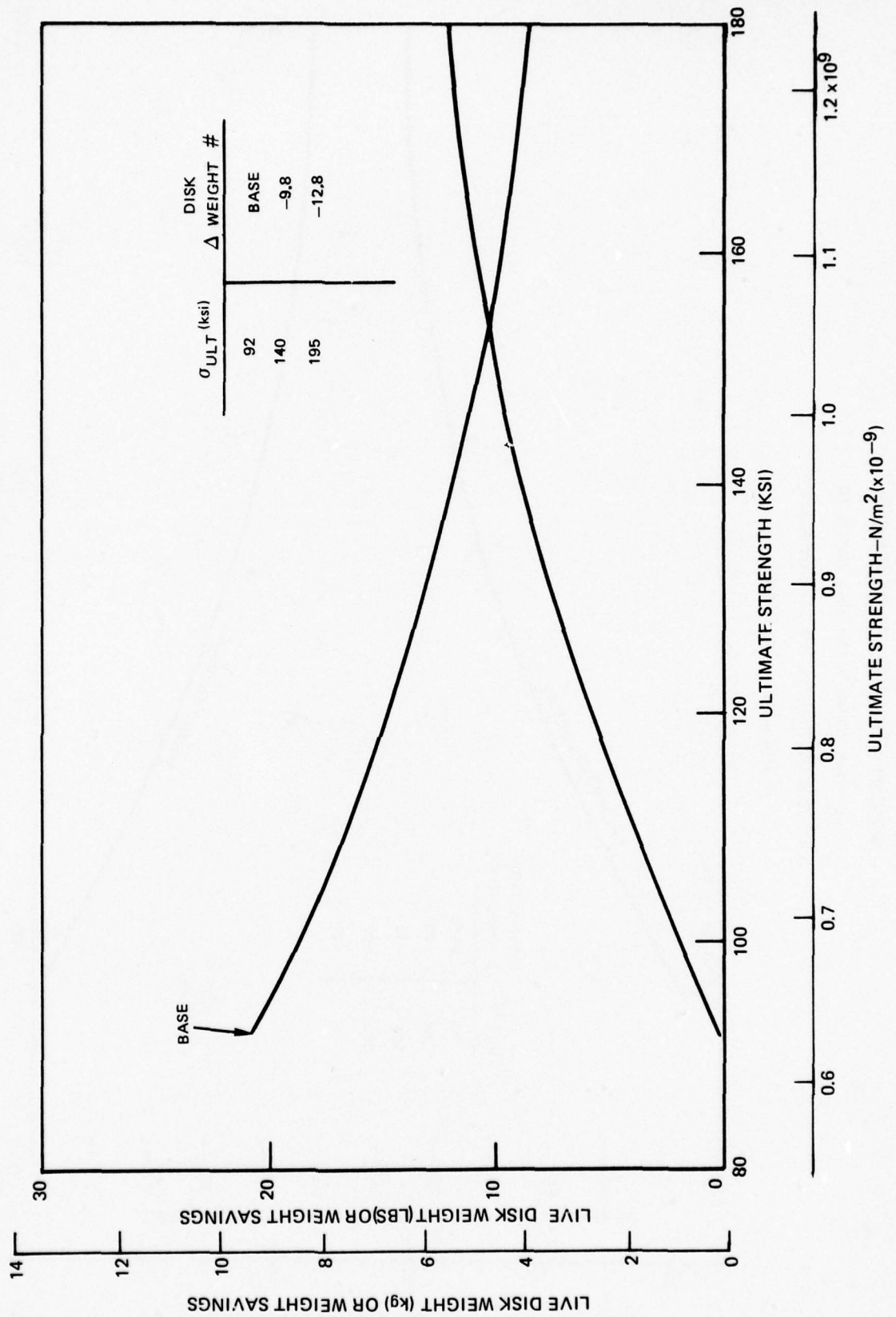


FIG. 3-3



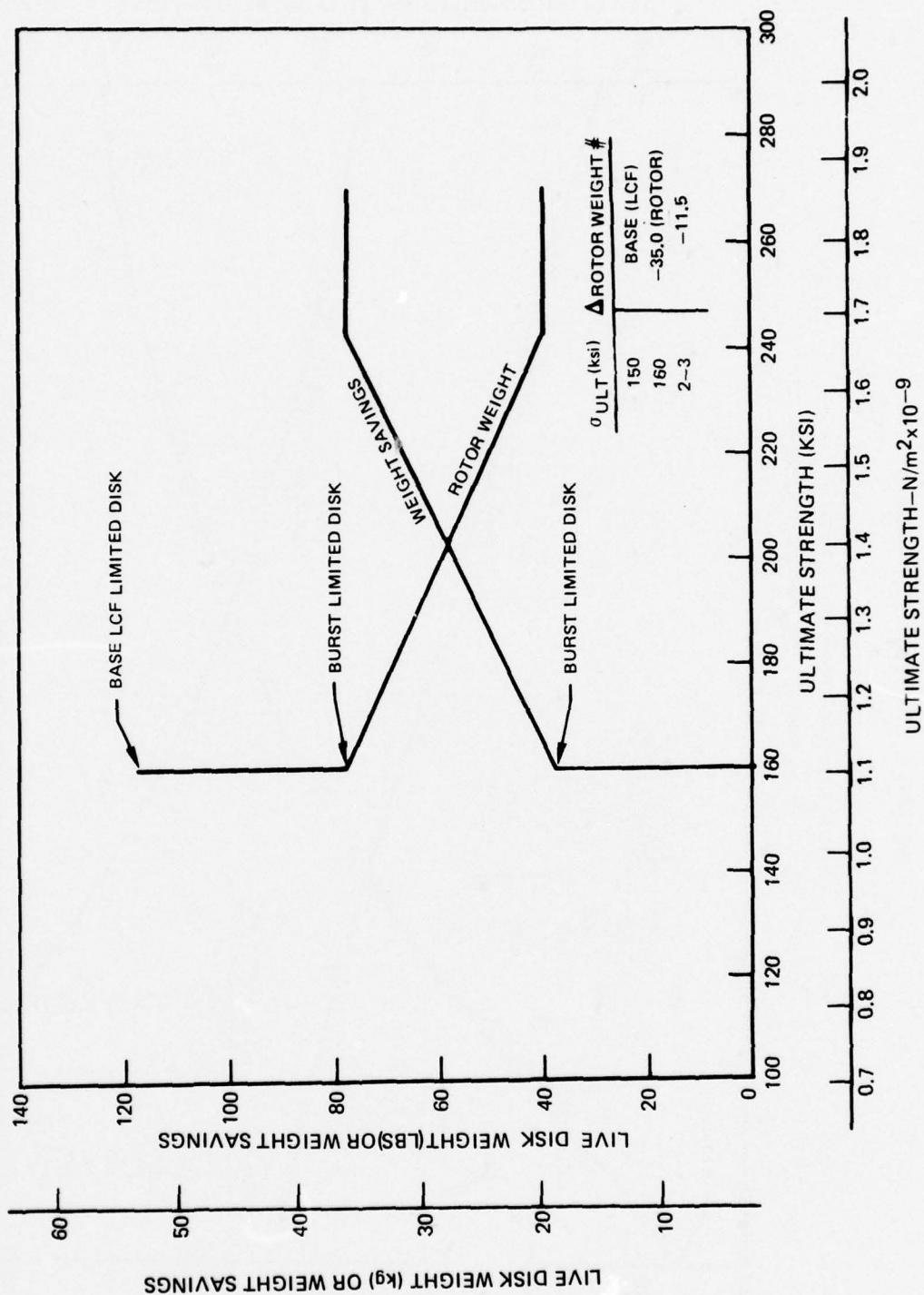
**WEIGHT VS ULTIMATE STRENGTH**  
 JT10D-4 HPC R-11  
 LAYERGLAZE PROCESS FOR TITANIUM ALLOYS  
 ROTOR SPEED = 11625 RPM



77-08-266-12

## WEIGHT VS ULTIMATE STRENGTH

JT10D-4 HPC STAGES R-12, R-13  
 LAYERGLAZE PROCESS FOR NICKEL ALLOYS  
 ROTOR SPEED = 11625 RPM



## WEIGHT VS ULTIMATE STRENGTH

JT10D-4 1st HPT DISK  
 LAYERGLAZE PROCESS FOR NICKEL BASE ALLOY  
 DEFLECTION AT REDLINE ROTOR SPEED = 11625 RPM

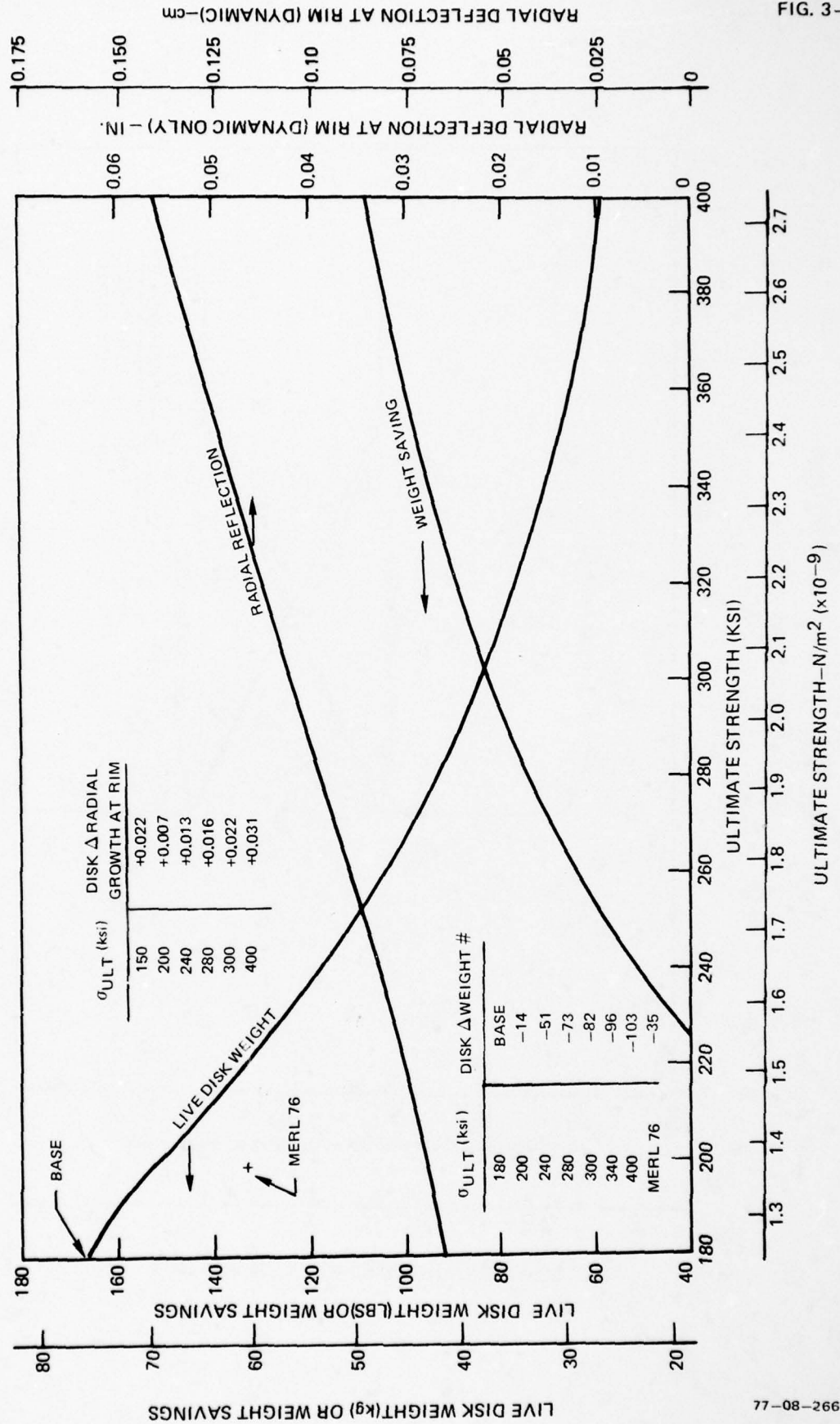




Table 3-II summarizes three possible options for the high pressure compressor when the rotor speed can be increased by 10% due to stronger material produced by the LAYERGLAZE process. Further rotor speed increases are limited by the high pressure turbine blade attachments.

- Option I - Increases HPC Performance
- Option II - Removes Two HPC Stages (rotor is shown in Fig. 3-1b)
- Option III - Reduces HPC Airfoils by 10%.

In the case of the high pressure compressor, Option II obviously offers the greatest performance/cost improvement, and is considered to be close to the optimum utilization of LAYERGLAZE processing to improve the HPC. This would add an additional equivalent of 93 lbs (42.3 kg) weight savings to the total estimated for the HPC in Table 3-I which was constructed based on component size reduction alone.

Although other sections of the JT10D-4 were not analyzed in as much detail as the HPC, designers were able to estimate these weight savings based on their experience and the results on the HPC and HPT analyses described above. Table 3-III indicates potential weight savings and DOC + INT benefits as estimated for the JT10D-4.

Table 3-III

Estimated Weight and/or Cost Savings Achievable by  
Using LAYERGLAZED Alloys on the JT10D-4

<u>Part</u>	<u>Δ Weight (lbs)</u>	<u>Δ Weight, kg</u>
HPC (Option II)(R4-R11)	-231 (involves 10% speed increase and stage removal)	-105.0
HPC (R1-3)	- 10	- 4.5
HPT (R-1)	- 82	- 37.3
HPT (Additional Stages)	<u>- 77</u>	<u>- 35.0</u>
	-400 + possible additional on HPT (R-2) depending on effects of speed increase	-181.8

400 lbs (181.8 kg) Direct Weight Savings = -0.40% DOC + INT.

Table 3-II

## Estimated JT10D HPC Benefits with LAYERGLAZE Process

Allows increase of hi-rotor speed by 10%  
Results in three optional benefits to JT10D HPC

<u>Option</u>	<u>Remarks</u>	<u>JT10D-4 HPC Compressor</u>				
		<u>Δ Weight</u> lbs (kg) <u>from Base</u>	<u>Δ Cost</u> lbs (kg) <u>from Base</u>	<u>Performance</u> Improvement % TSFC <u>from Base</u>	<u>Δ Material</u> Maintenance Cost <u>from Base</u>	<u>DOC + INT</u> <u>Equivalent</u>
1	HPC efficiency gain = .75% HPC flowpath dia. decreases	-	-	-.6% TSFC	+1.20\$/hr	-0.16%
2	Remove two HPC stages Rotors & Stators 9 & 10 HPC case & low shaft shorter ACC plumbing removed for 2 stages	-80.0 (-36.4)	-4.2% of HPC modular cost	-	-1.20\$/hr	-0.22%
3	Remove 10% airfoils Rotors & Stators	-9.0 (-4.1)	-	-	-	-0.01%

Concerning the information in Table 3-III, it can be seen that the equivalent of 231 lbs (105 kg) can be saved on the HPC (R4-R11) using a 10% speed increase and removal of two stages. An additional 82 lbs (37.3 kg) can still be saved on the HPT (R-1) and it was estimated that another 80 lbs (36.4 kg) might be saved on the HPT (R-2), although this additional savings was not included because there is uncertainty concerning the compressor-turbine matchup with the 10% speed increase in the compressor. Since some of the weight saved might have to be added back to match the redesigned compressor and turbine, the 80 lb (36.4 kg) estimate for HPT (R-2) was not included in the analysis. An additional savings of at least 10 lbs (4.5 kg) can be realized on HPC R-1 to R-3, and approximately 77 lbs (35.0 kg) should be saved in the remainder of the HPT. This totals to at least 400 lbs (181.8 kg) equivalent weight savings which can be traded off for direct operating cost + interest reduction of 0.40%.

Manufacturing cost estimates indicated that there would be no predictable difference in direct manufacturing cost for engines with LAYERGLAZED parts. This amounts to obtaining either increased performance or decreased operating cost (as explained by the trade-off factors) for the same manufacturing cost, making the full performance or operating cost benefits come through to the user. It is anticipated that eventually, when the process is fully developed, some manufacturing cost benefits would also accrue, but there is not sufficient information at present to document this. It was thus deemed conservative and prudent at this time not to anticipate substantial manufacturing cost savings.

The performance/operating cost benefits, however, are substantial, and in fact, there are substantial additional benefits to be gained in this category. The decreases in disk weight will be magnified through the entire engine, and substantial weight savings in shafts, bearing, and supporting structures can be anticipated. With substantially reduced engine weight, other savings within the aircraft may be possible. Although it was not possible, within the scope and funding of this program to analyze the total weight picture, the direct weight savings on disks is so substantial that LAYERGLAZE technology, if successfully developed, will produce revolutionary engine designs and improvements.



## TASK 4 - LIFE CYCLE COST STUDIES/F-100(3), FEAT

This task involved a detailed evaluation of the actual return on investment (Life Cycle Cost Study) which would result from development and application of phase-decomposition strengthened alloys and sequential structural buildup using lasers to produce turbine disks and/or drum rotors for the F-100(3) and FEAT engines. The analysis was performed by the Life Cycle Cost/Systems Effectiveness group of the Pratt & Whitney Aircraft Government Products Division by Messrs. J. Sandy, E. Reed and J. Isiminger.

## General

Clearly, from the standpoint of DOD, one of the most important considerations in the funding of research and development must be the potential payoff to DOD, should the research be successful and the development effort eventually deliver the promised end product. Initially, weight and cost studies were performed on a current military engine (F-100(3), section 1), an advanced military engine, (FEAT, section 2), and an advanced commercial engine (JT10D-4, section 3). Since the responsibility for commercial and military work is divided between divisions within the Pratt & Whitney Aircraft Group, these studies took slightly different approaches. In all cases, however, substantial potential weight savings were projected, the proportionately largest contribution arising in the commercial engine. Large cost savings were projected for the military engines, with the commercial engine projecting a "break-even" on cost. This is generally due to the fact that military engines, which stress performance, are currently more expensive to produce.

Life cycle cost (LCC) studies were performed on the military engines only. For these engines, particularly for the case of the F-100(3) as utilized in the F-15 aircraft, there was sufficient fleet size and mission data to do meaningful LCC analyses. It became apparent during the LCC studies that the maximum impact from the LCC standpoint was not coincident with the maximum weight reduction in all cases. While reduction of weight always results in savings, extension of part life is a more influential contributor to LCC savings, especially where part life can be extended out to the total life cycle goal. Acquisition cost reduction is another significant factor.

As a result of these realizations, although a first LCC estimate on the F-15 fleet F-100(3) was made based on already generated design data for maximum weight savings as reported below, a second LCC calculation was also made with the designers optimizing only HPC parts from the LCC standpoint. These optimizations primarily were accomplished by adding back in a portion of the maximum

weight savings in order to increase expected life. As the results will show, the LCC savings was significantly increased. It was not possible within the time and fiscal constraints of the program to fully optimize the engine design from the LCC standpoint; however, it is the strong aggregate opinion of the designers and cost estimators involved that such optimization could further significantly increase the projected LCC benefits of LAYERGLAZE processing as applied to the F-100(3) for the F-15.

In the course of their initial attempts to optimize the F-100 designs from the LCC standpoint, the designers realized and pointed out an additional potential of LAYERGLAZE which is absent from conventional B/M. Since LAYERGLAZED alloys may be used in parts with substantially reduced weights, initially weight may be traded back into the design of a part for added life. In addition, since LAYERGLAZE structures are built up in small increments, and in theory, may be accurately designed, there should be increased flexibility in determining the exact microstructures of parts in order to extend the useful lives of these parts by combating their specific design limitations possibly even within localized failure-prone regions. With parts produced by conventional alloys, such flexibility usually does not exist; even the simple trading of added weight for longer life has been optimized in design to the point of not being a fruitful avenue for further increase in useful life. According to our design personnel, the ability to tailor structures for added life may be one of the most important benefits offered by the LAYERGLAZE process.

#### LCC LAYERGLAZE/F-100(3), Designed for Maximum Weight Savings

The ground rules established for the LCC study of the application of LAYERGLAZE technology to the F-100(3) engine in the F-15 aircraft are summarized in Table 4-I below.

Table 4-I

#### Ground Rules for F-100(3) Life Cycle Cost Studies

1. Only USAF F-15 program considered
2. Total number of aircraft - 729
3. Number of operational aircraft - 540
4. Total number of engines - 1674
5. Flight hours/operational aircraft - 300 hr/year for 20 years
6. Lives based on Langley mission (Table 4-II)
7. A "rubber aircraft" is assumed so that engine weight savings also produce LCC savings due to reduction of aircraft size

The above ground rules indicate engine life predictions based on the "Langley Mission". This mission is detailed in Table 4-II.

The LCC studies of the LAYERGLAZE F-100(3) were first conducted on the engine designed for maximum weight savings. As indicated above, these weight savings were not consistent with optimal LCC reduction. The results of the study are presented in Table 4-III.

The most significant item in Table 4-III is that by fully minimizing the weight of the high pressure compressor, the life of the parts was halved. Although a net LCC savings of \$22.7M was obtained for the HPC, this small savings was not commensurate with effective use of the material property gains projected for the LAYERGLAZE process. As a result, attempts were made to optimize the designs of the HPC for a combination of life, and weight. Those results are reported in the next section.

The total projected life cycle cost reduction for the F-100(3) when designed for maximum weight savings is \$141.7 million.

#### LCC-LAYERGLAZE/F-100(3) with a Design Partially Optimized for LCC Reduction

Based on the observed life decrease which accompanied the maximum weight reduction in the HPC stage, a further optimization was attempted in order to determine its effect on the total F-100(3) LCC picture. Essentially, 20 lbs (9.1 kg) were added back into the design of the 4th through 13th HPC rotor stages to increase their life to 6000 engine flight hours.

The tradeoffs between part cost, life, and weight, are illustrated in Figs. 4-1 and 4-2 for a fan disk and HPT disk. Figure 4-1 indicates how the first fan disk was analyzed for LCC. The line indicates constant LCC for no change in weight. The current part, with a 3000 hr life and a cost of 100%, could tolerate a cost of 200% (point 1) in the LAYERGLAZED form with its 6000 hr life. Instead, the part actually comes in at point 2 with a 120% cost (20%) increase. The remaining 80% produces a savings in life cycle costs of \$9.7M over the engine production schedule.

For the first HPT disk (Fig. 4-2) the nearly adequate 8000 hr life was extended to greater than 10,000 hrs (the total cycle life) by using a LAYERGLAZED part. Since this is the maximum life required, and was obtained along with a 15 lb (6.8 kg) weight reduction, the weight savings could still be realized. At 10,000 cycles and a 15 lb (6.8 kg) weight reduction, a 50% increase in



Table 4-II

## Langley 2000 Hr Air Combat Mission Duty Cycle

FTIT Trim: Nominal (8 Clicks)

Altitude: Base

	<u>MN/ALT</u>	<u>Installation</u>	<u>Hot Time ~ Hrs</u>		<u>Takeoff Cycles</u>
			<u>MIL</u>	<u>MAX</u>	
1.	0/0	Uninstalled	12.3	2.0	35
2.	Trim (0/0)	Installed	24.0		
3.	SLTO (0/0)	Installed	31.4		
4.	0.6/15K	Installed		7.1	
5.	0.7/15K	Installed	10.7		
6.	0.7/20K	Installed	51.2		
7.	0.9/20K	Installed	11.9	14.3	917
8.	0.6/25K	Installed		9.5	
9.	0.9/25K	Installed		<u>10.7</u>	
Total Hr			141.5	+ 43.6 = 185.1	952
% of 2000 Hr			7.08	+ 2.18 = 9.26	

<u>Cycles</u>	<u>Takeoff Cycles</u>	<u>Partial Cycles</u>	<u>A/B Lights</u>
M-37 and Ground Runs	95	694	95
ACM Missions	<u>857</u>	<u>5142</u>	<u>7713</u>
	952	5836	7808

Average Mission Length =  $\frac{2000}{952} = 2.10$  Hr/Average No. of Partial Cycles per

Mission =  $\frac{5836}{952} = 6.13$

- Note: 1 185 hrs hot time included in 2000 hr total  
 2 Remainder of time is idle/cruise  
 3 Ratio engine flight hours to total operating = 0.63

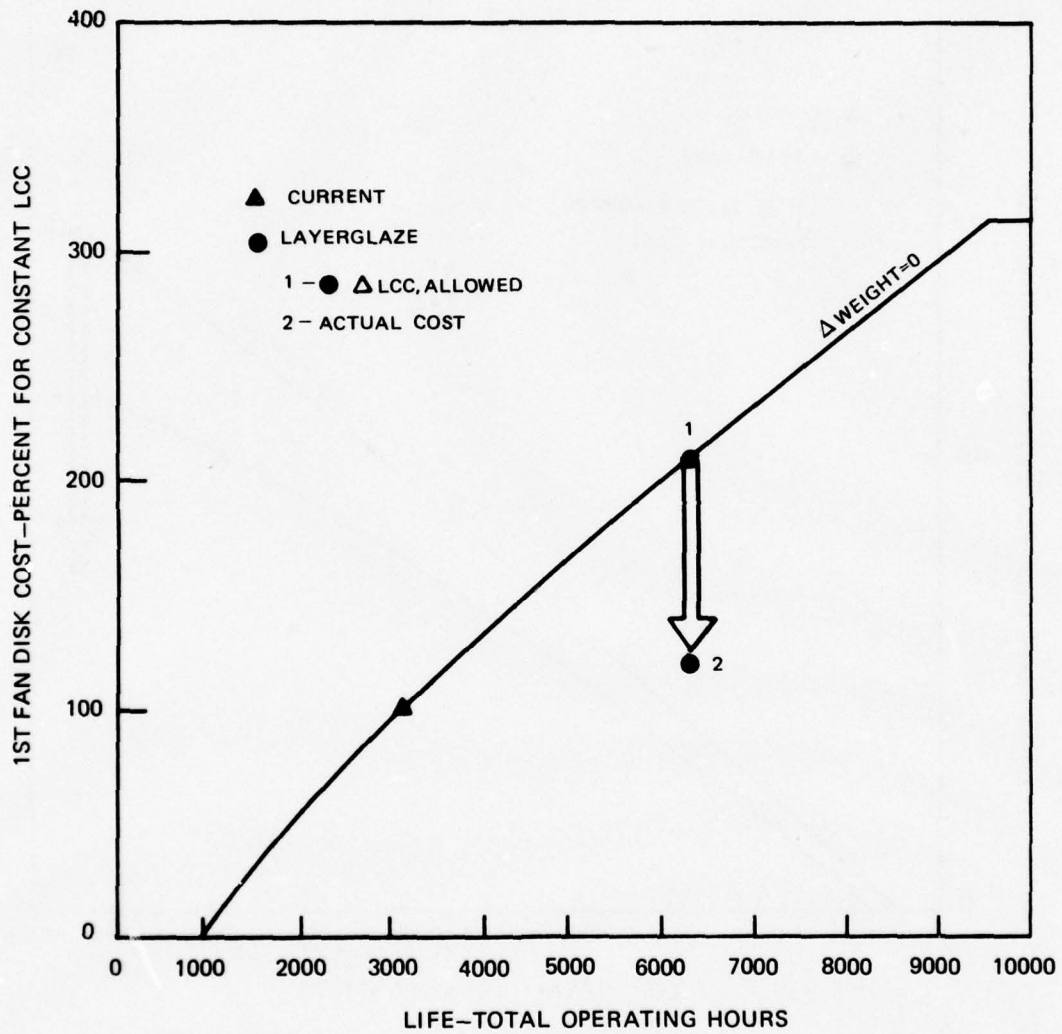
Table 4-III

Life Cycle Cost Study - LAYERGLAZE/F-100(3)  
Designed for Maximum Weight Savings

<u>Part</u>	<u>Δ Life</u>	<u>Δ Cost</u>	<u>Δ Weight</u>		<u>Δ LCC (\$)</u>
			lb	kg	
<u>Fan</u>					
1st disk	+100%	+20%	0	0	-9.7M
2nd disk	+100%	+20%	0	0	-6.7M
					<u>-16.4M</u>
<u>HPC</u>					
4-6 Rotor (Ti)	-50%	- 7%	-20	- 9.1	+11.3M
7-13 Rotor (Ni)	-50%	-45%	-54	-24.6	-87.3M
Stator	-	+40%	+25	+11.4	+53.3M
					<u>-22.7M</u>
<u>HPT</u>					
1st disk	+50%	-25%	-15	- 6.8	-18.8M
1-2 spacer	-	-30%	- 3	- 1.4	-10.2M
2nd disk	+50%	-25%	-10	- 4.5	-12.1M
					<u>-41.1M</u>
<u>LPT</u>					
3rd disk	+300%	-25%	- 5	- 2.3	-39.3M
4th disk	+300%	-40%	- 3	- 1.4	-22.2M
			-85	-38.6	<u>-61.5M</u>

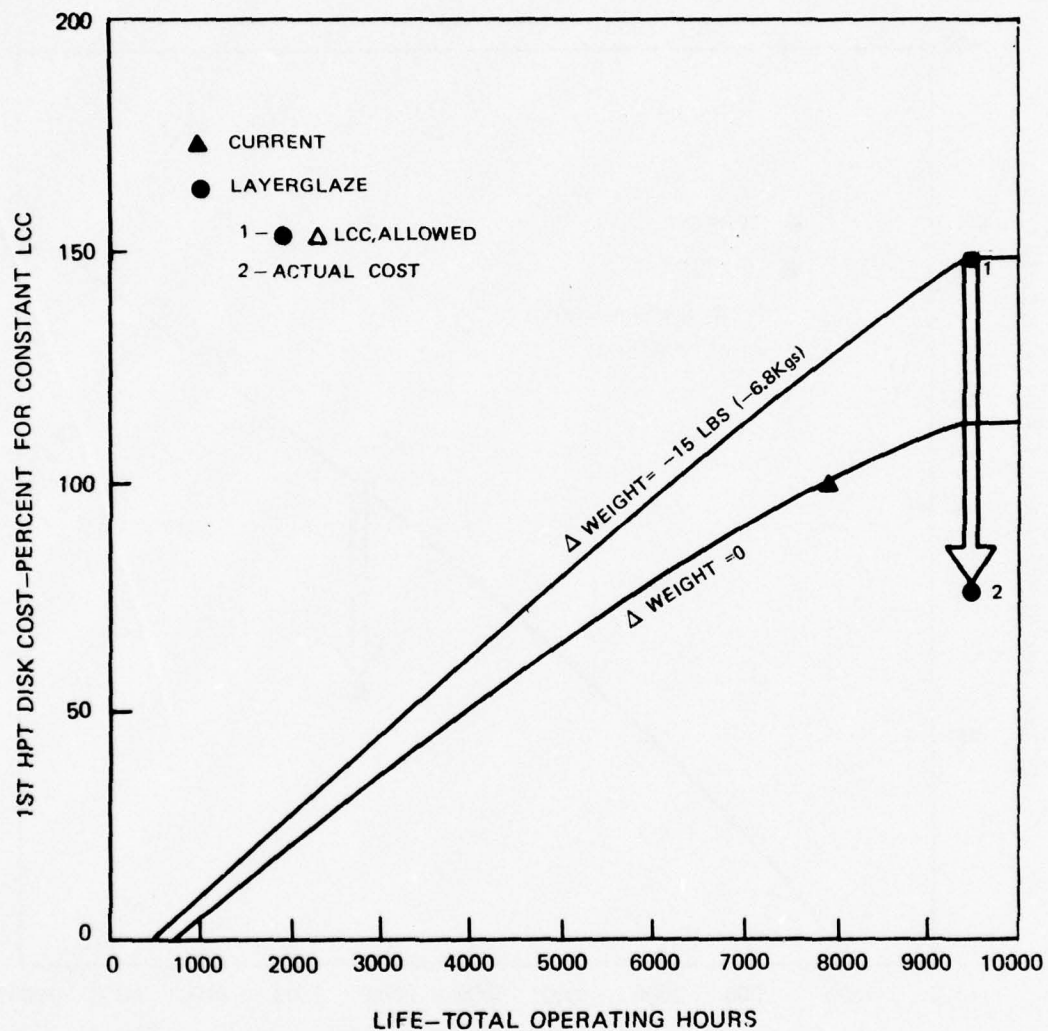
Total LAYERGLAZE F-100(3) ΔLCC = -\$141.7M

## 1ST FAN DISK COST VS LIFE FOR F100(3)





## 1ST HPT DISK COST VS LIFE FOR F100(3)



acquisition cost could be tolerated for a constant life cycle cost (point 1). Instead, a 25% reduction (75% net difference) in acquisition cost is projected (point 2) for a net \$18.8M life cycle cost reduction for this part.

Results of this second iteration LCC analysis are indicated in Table 4-IV and show a total of \$103.4M LCC savings for the optimized HPC stage as compared to the \$22.7M savings projected for the HPC designed for maximum weight savings. The total projected life cycle cost reduction for the F-100(3) with the HPC design optimized from the LCC standpoint is \$222.4M.

The above optimization of the HPC for life cycle is a clear example of the fact that the available benefits of a process such as LAYERGLAZE may be used in different ways which produce differing results. With the benefit of additional iterations of design and LCC analysis, further optimization of LCC is possible.

#### LCC-LAYERGLAZE/FEAT Engine

In the design of the FEAT engine, advanced material properties have been assumed. The projected property improvements apply to the same properties as those projected for the LAYERGLAZE process, and it is these properties which allow the design and eventual manufacture of the low cost, high performance FEAT engine. Essentially, many of the performance-related benefits projected for LAYERGLAZE were already in the FEAT design, leaving less "room for improvement" when the properties of the LAYERGLAZE processed, PDS alloys were input to the design. Nonetheless, in excess of \$100M savings due to initial cost reduction and some weight effects were projected. Operating and support cost on the parts affected were assumed to be zero for both the B/M FEAT and LAYERGLAZE FEAT, since all disks are designed to exceed their life cycles in both cases.

The ground rules for the LAYERGLAZE/FEAT LCC analysis are summarized in Table 4-V.

The projected LCC savings from applying LAYERGLAZE processing to the FEAT engine is summarized by components in Table 4-VI. The total projected LCC reduction for the FEAT engine is \$103.2M. It is indicated, however, that materials technology to produce the FEAT engine is not currently available, and if the engine could be produced with LAYERGLAZE processed parts, the LAYERGLAZE process should be given credit for the substantial performance improvements and cost savings already inherent in the FEAT design.

Table 4-IV

Life Cycle Cost Study - LAYERGLAZE/F-100(3) with  
Design Partially Optimized for LCC Reduction

<u>Part</u>	<u>Δ Life</u>	<u>Δ Cost</u>	<u>Δ Weight</u>		<u>Δ LCC \$</u>
			lb	kg	
<u>Fan</u>					
1st disk	+100%	+20%	0	0	- 9.7M
2nd disk	+100%	+20%	0	0	<u>- 6.7M</u>
					-16.4M
<u>HPC</u>					
4-6 Rotor	-	- 5%	-12	- 5.5	8.4M
7-13 Rotor	-	-45%	-42	-19.1	-148.3M
Stator	-	+40%	+25	+11.4	<u>+ 53.3M</u>
					-103.4M
<u>HPT</u>					
1st disk	+ 50%	-25%	-15	- 6.8	-18.8M
1-2 spacer	-	-30%	- 3	- 1.4	-10.2M
2nd disk	+ 50%	-25%	-10	- 4.5	<u>-12.1M</u>
					-41.1M
<u>LPT</u>					
3rd disk	+300%	-25%	- 5	- 2.3	-39.3M
4th disk	+300%	-40%	<u>- 3</u>	<u>- 1.4</u>	<u>-22.2M</u>
			-65	-29.5	-61.5M
			lb	kg	

Total LAYERGLAZE F-100(3) ΔLCC = \$222.4M



Table 4-V

## Ground Rules for FEAT Life Cycle Cost Studies

1. Advanced Tactical System - Twin Engine Aircraft
2. Total Number of Aircraft - 876
3. Total Number of Operational Aircraft - 720
4. Total Number of Engines - 2000
5. Flight Hours/Operational Aircraft - 300 hr/year for 12 years
6. A "rubber aircraft" is assumed so that engine weight savings also product LCC savings due to reduction of aircraft size

Table 4-VI

## Life Cycle Cost Study - LAYERGLAZE/FEAT Engine

<u>Part</u>	<u>Δ Life*</u>	<u>Δ Cost</u>	<u>Δ Weight</u>		<u>Δ LCC \$</u>
			lb	kg	
FAN	-	+15%	-13	- 5.9	- 5.3M
HPC	-	-20%	-33	-15.0	-59.9M
HPT	-	-30%	-18	- 8.2	-25.0M
LPT	-	-20%	- 7	- 3.2	-13.0M
			-71	-32.3	-103.2M

Total LAYERGLAZE FEAT ΔLCC = \$-103.2M

\*All parts meet life in both B/M and LAYERGLAZE designs

## TASK 5 - DEVELOPMENT PLAN

This task involved formulation of a specific plan for the orderly development of the LAYERGLAZE concept for advanced laser materials processing technology through the component development phase.

Before attempting to form a development plan, it seems useful to provide an estimate of the expected total development cost and time to bring the LAYERGLAZE process through the actual production and application phase. As a base line parameter, layerglazing will be compared to another sophisticated materials processing development which was successfully applied within United Technologies Corporation, the directional solidification of turbine blades. The production of LAYERGLAZE fabricated gas turbine parts would represent a materials-processing accomplishment of somewhat greater sophistication and difficulty than directional solidification of gas turbine blades. The investment made in the directional solidification program through the initial application of directionally solidified turbine blades was multi-millions of dollars. This project was conducted over the time span of 10 years. A reasonable estimate for LAYERGLAZE development and application would be a similar period of time and the research and development investment would require many millions of dollars.

Development of a full-scale demonstration component by LAYERGLAZE appears to be at least a 3 year effort. What is indicated herein is an *ambitious* program which is geared to producing a demonstration LAYERGLAZE component; goals for the envisioned 3-year effort are specified below.

## First Year (1978)

There appears, based on results to date and included in this report, to be little doubt that the physical LAYERGLAZE process can be accomplished, given sufficient dedication of effort and financial support. There is a question concerning which of the alternative choices for deposition of feedstock material would ultimately lead to the most optimum final process. In addition, given that the process can be successfully accomplished, the most important question is whether the alloys so produced would meet projected property goals. The first year's program would attempt to achieve the following goals:

- Obtain tensile, fatigue, and creep data on one alloy produced by an incremental rapid chilling process and which is suggestive of the potential of layerglazing.
- Convert a feedstock material into a bulk rapidly-chilled disk-shaped part, with a structure representative of a LAYERGLAZE fabricated material.

Alloy formation for the mechanical property studies would be accomplished by one of the following three means:

- 1 - Incremental Epitaxial Solidification (Laser or EB)
- 2 - Layerglazing (Laser-Melted)
- 3 - Layerglazing (EB-Melted).

It is anticipated that the first alloy studied in depth would be from the Ni-Al-Mo system.

Processing would involve use of a liquid feed in the form of a "melt-drag" from a liquid drop (vertical meniscus or pendant drop) with the addition of laser or EB energy at or near the interaction point so that LAYERGLAZE buildup rather than filament production would result. Although there may be added difficulty in working directly from a liquid drop, the fact that the feedstock could be a simple cast bar, not even requiring ductility would result in substantial advantage in that sources of feedstock would cease to be a problem. Since the disk shape produced for demonstration purposes would not actually be used as a finished part, thermomechanical treatment (TMT) processing could be applied to the as-fabricated part in order to assess the importance of TMT in producing LAYERGLAZE alloys with specific properties. Eventually, as the LAYERGLAZE process is used to produce bulk parts to finished dimensions, TMT would have to be accomplished sequentially, in-situ, so as not to change the final part shape.

The goals for the first year are ambitious and could require somewhat more than a year. By meeting these goals, however, the program will be in an excellent position to grow rapidly in the direction of application, as follows.

#### Second Year (1979)

From the time of completion of the first year's goals, a relatively straightforward route to LAYERGLAZE component development is probable. The second year's effort would include:



Alloy Development

- Further optimization of the selected alloy family.
- Initial development of titanium base alloys, and techniques for their fabrication.

Processing

- Development and construction of suitable size processing equipment to provide the capability for fabrication of full scale size parts.

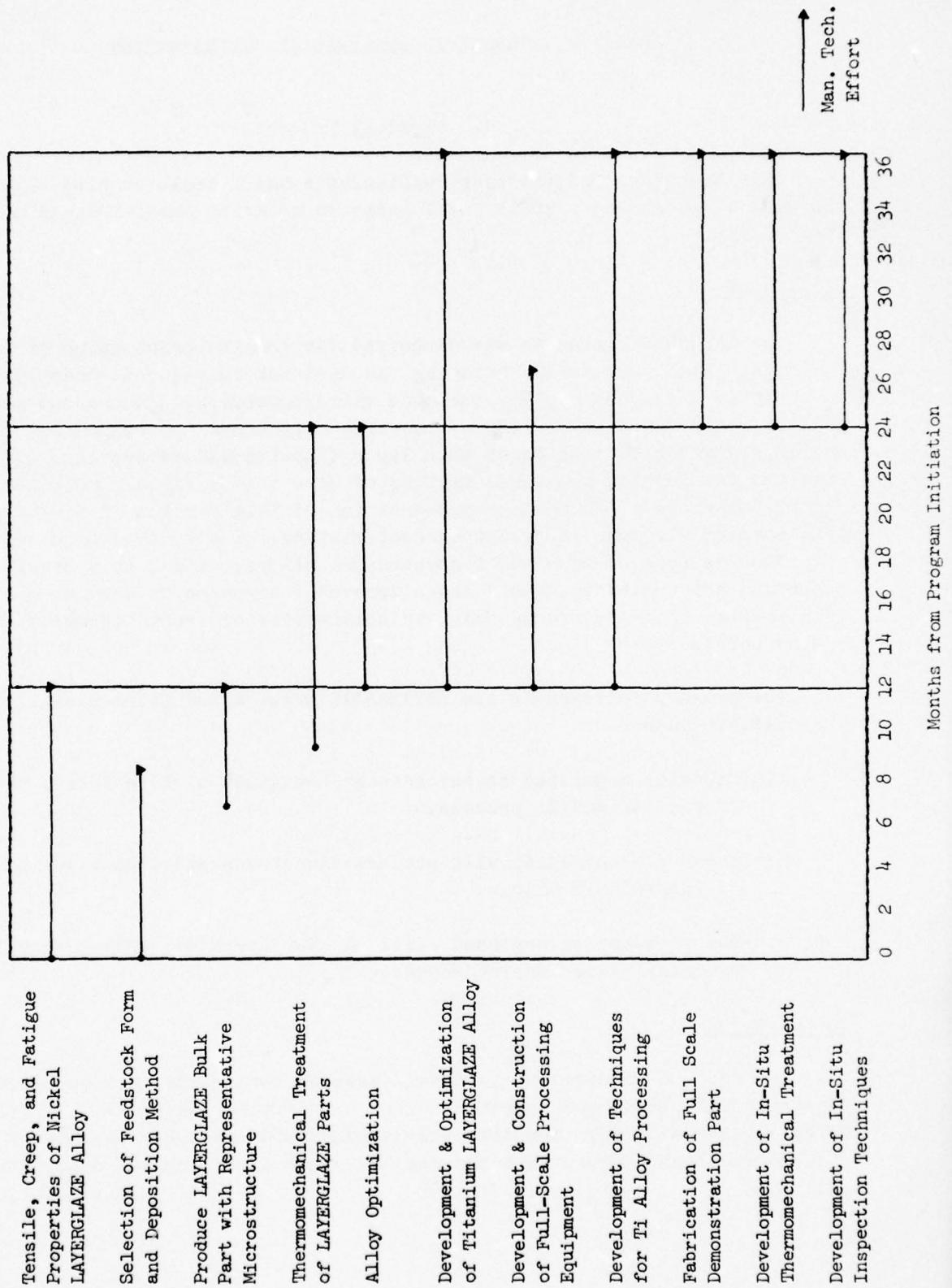
Third Year (1980)

By the third year, alloys will have been selected, and the capability of producing full scale parts will have been developed. The task will be to fabricate a full scale part as a demonstration component. During this year, it will also be appropriate to begin considering the actual techniques of fabrication, including in situ thermomechanical treatment, and inspection.

The milestones for the projected 3-year effort are indicated in Fig. 5-1. It is anticipated that the successful completion of this component demonstration program should lead directly into a Manufacturing Technology Effort, considering the magnitude of the potential cost savings.

## DEVELOPMENT PLAN FOR LAYERGLAZE COMPONENT PART FABRICATION

## MILESTONES



## TASK 6 - TECHNICAL FEASIBILITY DEMONSTRATION

## A. Physical Process

This task involved the construction of a small scale buildup machine with the goal of producing a small model shape in order to demonstrate process feasibility.

Background

The LAYERGLAZE process was conceived for in-situ fabrication of bulk rapidly-chilled structures obviating the need for subsequent consolidation steps which could influence rapidly quenched microstructures. In the course of this program, only one of a variety of possible approaches for sequential deposition and laserglazing into place of thin layer deposits was attempted. This concept involved the feeding and laser melting of wire onto a rapidly rotating mandrel. Figure 6-1 shows a schematic representation of this version of the process along with some of its more important characteristics. The process should be capable of producing more homogeneous high-strength alloys, which, as a result of their refined microstructures, would have improved fatigue resistance at high strength levels so as to allow nearly complete utilization of these strengths in rotating engine parts.

The primary features of the LAYERGLAZE process, as schematically depicted in Fig. 6-1, include:

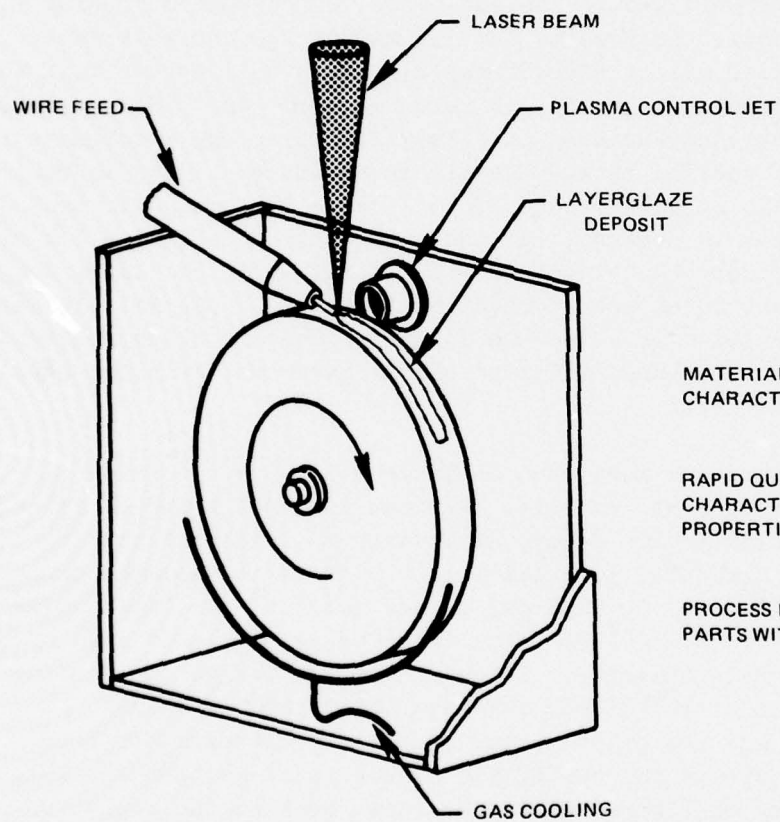
1. Material deposited in thicknesses (and with cooling rates) characteristic of the LASERGLAZE process.
2. The rapid quenching will produce structures and properties characteristic of LASERGLAZED alloys.
3. The process, as depicted, is ideal for rotating parts with cylindrical symmetry, i.e. turbine disks.

Calculations

In order to predict the important process parameters such as laser power density, dwell time, and specific energy required for deposition, a series of calculations was made. The data base used was for the case of surface melting, with corrections made so that the results would apply for the case of material additions.



## THE LAYERGLAZE PROCESS



MATERIAL DEPOSITED IN THICKNESS  
CHARACTERISTICS OF LASER GLAZING

RAPID QUENCHING PRODUCES  
CHARACTERISTIC STRUCTURE/  
PROPERTIES OF LASER GLAZED ALLOYS

PROCESS IDEAL FOR ROTATING  
PARTS WITH CYLINDRICAL SYMMETRY

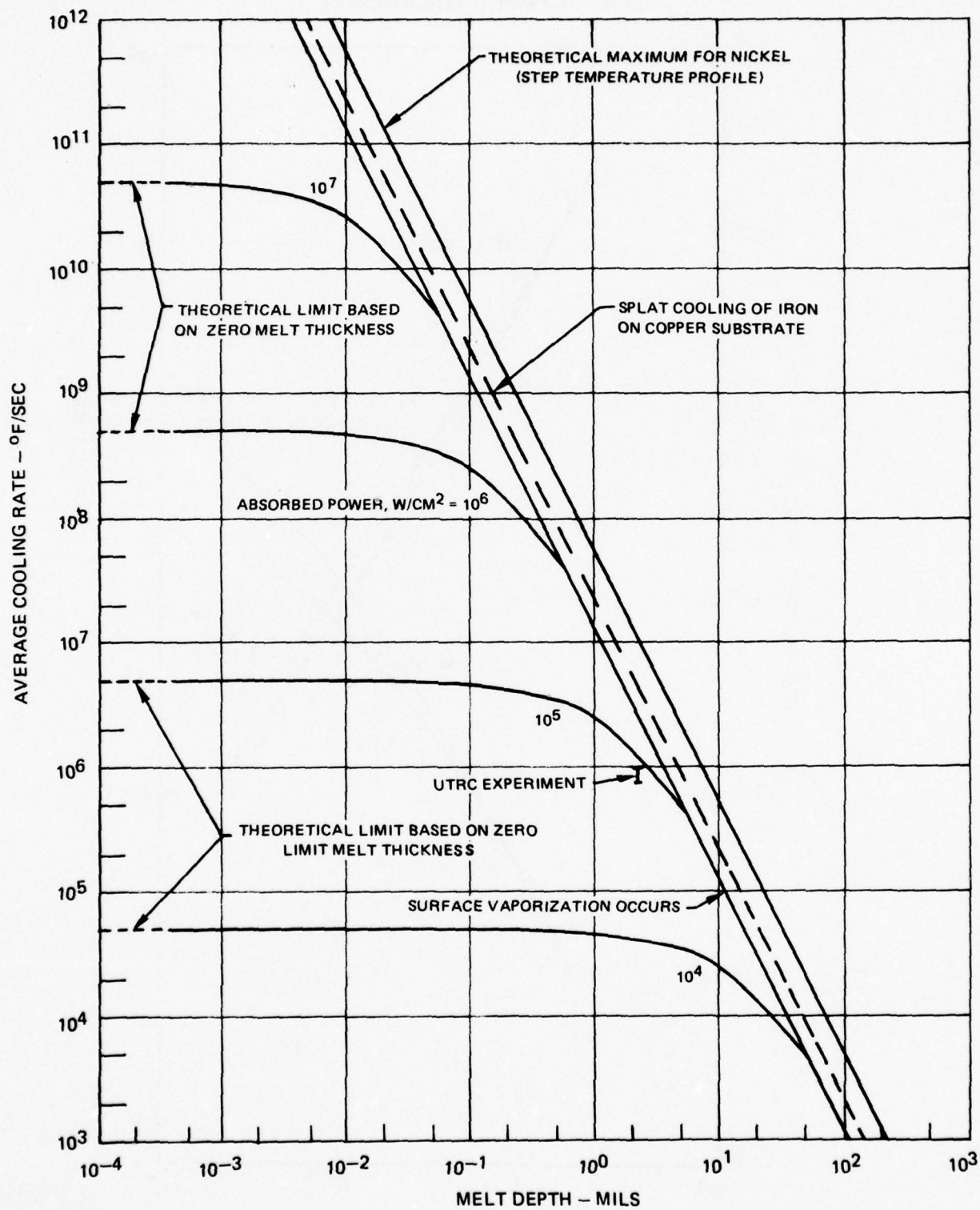
First, from the curves of Fig. 6-2 (Ref. 36), values of cooling rate and power density corresponding to melt depths of 1.1 and 2.2 mils were obtained. These data are shown plotted on Fig. 6-3 (the ascending curves). Note the presence of limiting cooling rates, corresponding to the surface vaporization which occurs at high power densities. A similar set of curves was used to determine the dwell time as a function of power density corresponding to melt depths of 1.1 and 2.2 mils. These data are also shown on Fig. 6-3.

From the curves of Fig. 6-3, the power density required to obtain a given cooling rate can be read. At this power density, the required dwell time can also be read on Fig. 6-3 for the corresponding (1.1 or 2.2 mil) melt depth. Such data for various cooling rates are shown in Table 6-I. Knowing the power density and the dwell time, the required energy density ( $\text{j}/\text{cm}^2$ ) is easily calculated. Since these results are for surface melting, it was assumed that 10% of the melt was in the substrate, with remainder being in the added material. Thus, the results for 1.1 mil of surface melt were assumed equivalent to 1.0 mil of added material. With this assumption, the volume of melt corresponding to a unit of material  $1 \text{ cm}^2$  and 1.0 mils or 2.0 mils in depth was calculated and used to determine the energy requirement in  $\text{j}/\text{in}^3$  as a function of cooling rate. The final results are shown in Table 6-I. Note that the melt energy for the 2.2 mil cases is about half that of the 1.1 mil cases. This is because, for the same cooling rate, the 2.2 mil melt requires higher power densities than the 1.1 mil melt, but lower dwell times. As a result, the total energy required for the 2.2 mil melt is only slightly more than for 1.1 mil, while the volume of melt is twice as great. Thus the melting energy, measured in  $\text{j}/\text{in}^3$  of new material, is about half as much for the greater depth.

The results obtained are indicated in Table 6-I. Power densities, dwell times, and total absorbed energies required to deposit two different layer thicknesses of nickel base alloys at a variety of assumed cooling rates are indicated. Essentially, a 1.1 mil (0.0028 cm) total melt depth means a deposition of 1.0 mil (0.0025 cm) of new material per layer while melting an additional 0.1 mil (0.00025 cm) into the already-deposited structure to insure structural integrity. It should be noted that for cooling rates of  $10^5$  °C/sec, and of  $10^6$  °C/sec, absorbed laser power need not exceed  $10^5$  watts/ $\text{cm}^2$ , and are often as low as  $5 \times 10^4$  watts/ $\text{cm}^2$  or even less. These are well within the capability of our laser systems and will provide some leeway for configuration of the focal spot at the region of energy transfer. Work in the alloy design portion of the program (Task 7) has already indicated that significant properties can be achieved at cooling rates in the range of  $10^5$ - $10^6$  °C/sec, that range being characteristic of most of the alloys prepared to date and discussed in Section 7.

## EFFECT OF MELT DEPTH AND POWER ON AVERAGE COOLING RATE

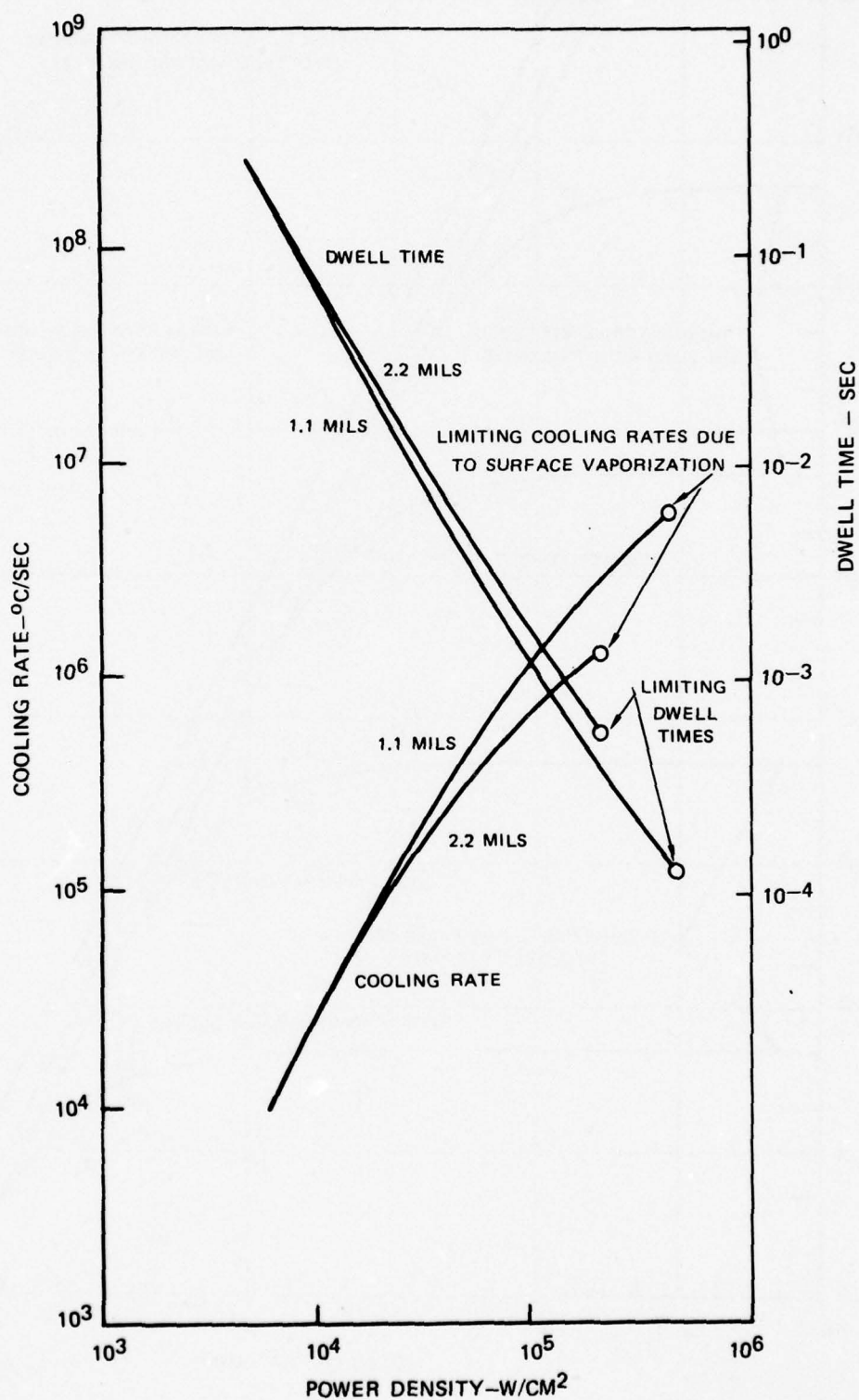
MATERIAL: NICKEL



77-11-214-2



COOLING RATE AND DWELL TIME AS A FUNCTION OF ABSORBED POWER DENSITY  
FOR TWO MELT THICKNESSES



77-11-214-1

Table 6-I  
 LAYERGLAZE Energy Deposition Estimates  
 (Nickel Alloys)

Cooling Rate °C/sec	1.1 mil Total Melt			2.2 mil Total Melt		
	Power Density w/cm <sup>2</sup>	Dwell Time sec	Energy J/in. <sup>3</sup>	Power Density w/cm <sup>2</sup>	Dwell Time sec	Energy J/in. <sup>3</sup>
10 <sup>4</sup>	6 x 10 <sup>3</sup>	1.7 x 10 <sup>-1</sup>	6.58 x 10 <sup>6</sup>	6.4 x 10 <sup>3</sup>	1.7 x 10 <sup>-1</sup>	3.51 x 10 <sup>6</sup>
5 x 10 <sup>4</sup>	1.4 x 10 <sup>4</sup>	3.5 x 10 <sup>-2</sup>	3.16 x 10 <sup>6</sup>	1.5 x 10 <sup>4</sup>	3.55 x 10 <sup>-2</sup>	1.72 x 10 <sup>6</sup>
10 <sup>5</sup>	2 x 10 <sup>4</sup>	1.83 x 10 <sup>-2</sup>	2.36 x 10 <sup>6</sup>	2.28 x 10 <sup>4</sup>	1.68 x 10 <sup>-2</sup>	1.24 x 10 <sup>6</sup>
5 x 10 <sup>5</sup>	5.1 x 10 <sup>4</sup>	3.4 x 10 <sup>-3</sup>	1.12 x 10 <sup>6</sup>	7.0 x 10 <sup>4</sup>	2.4 x 10 <sup>-3</sup>	5.58 x 10 <sup>5</sup>
10 <sup>6</sup>	8.4 x 10 <sup>4</sup>	1.45 x 10 <sup>-3</sup>	7.87 x 10 <sup>5</sup>	1.5 x 10 <sup>5</sup>	8.2 x 10 <sup>-4</sup>	3.97 x 10 <sup>5</sup>
5 x 10 <sup>6</sup>	3.9 x 10 <sup>5</sup>	1.50 x 10 <sup>-4</sup>	3.77 x 10 <sup>5</sup>	-	-	-
5.56 x 10 <sup>6</sup>	447,200	1.28 x 10 <sup>-4</sup>	3.69	-	-	-
1.28 x 10 <sup>6</sup>	-	-	-	2 x 10 <sup>5</sup>	5.5 x 10 <sup>-4</sup>	3.55 x 10 <sup>5</sup>

It is also notable in Table 6-I that the process efficiency increases with increased cooling rate, less specific energy being required for unit deposition of new material as the cooling rate is increased. Increased power density and higher processing speeds (shorter dwell times) are, however, required to obtain higher cooling rates.

#### Experimental Evaluation of LAYERGLAZE Process

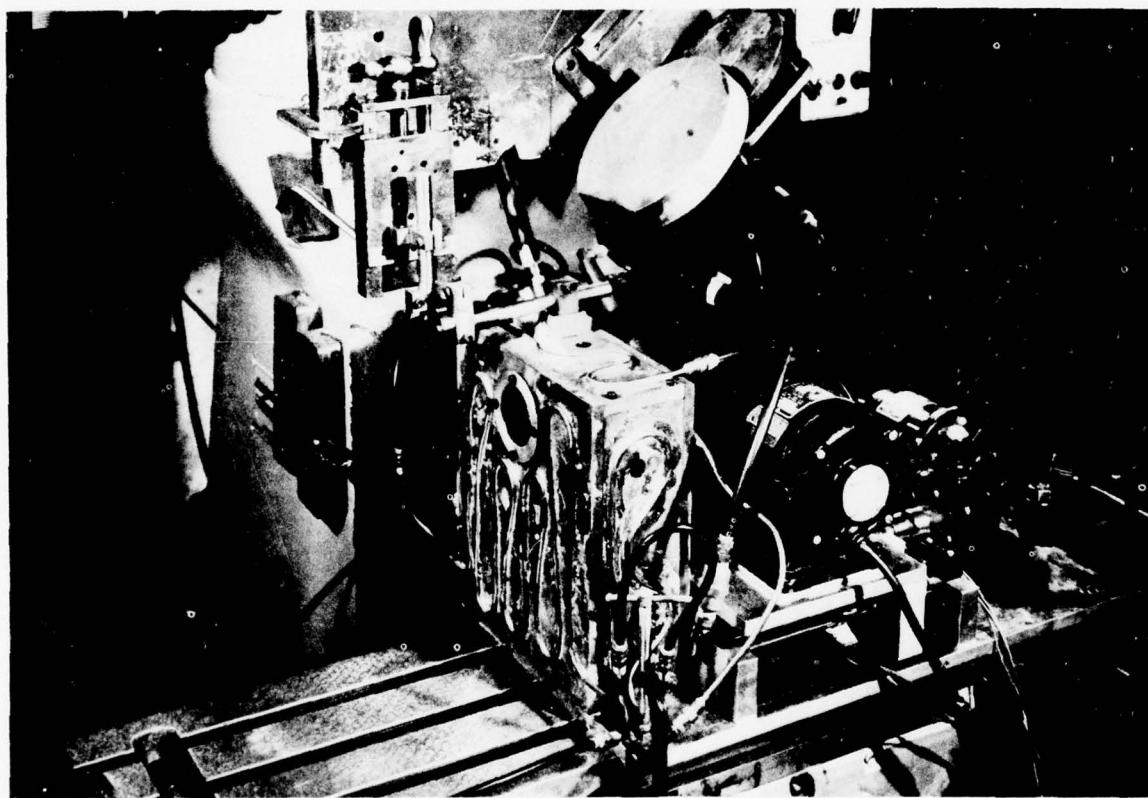
A small scale, model LAYERGLAZE apparatus was initially constructed and, eventually modified to improve its operating characteristics. The second, most advanced iteration of this apparatus is pictured in Fig. 6-4. This apparatus was capable of rotating and traversing a 6.0 in. (15.2 cm) diameter x 0.5 in. (1.3 cm) wide precursor mandrel in a controlled helium atmosphere and continually feeding wire to the laser beam interaction point in order to deposit material on the circumference of the mandrel. Type 304 stainless steel was chosen as a convenient material to model the deposition process. In the first phase (I) of the apparatus (not shown), the wire feed nozzle was located rigidly on the upper surface of the chamber, making it impossible to compensate for the increase in diameter of the mandrel as material was deposited. In addition, as the mandrel grew in diameter, the outer surface was no longer located at the exact focal point of the laser beam.

Using the phase I apparatus, subject to the constraints described above, deposits of up to 0.090 in. (0.228 cm) thickness were built up at rates of 0.2 cu in/min (3.28 cc/min). These disks are shown in Fig. 6-5, along with a macrograph cross section of a three layer deposit with a depth of 0.090 in. (0.228 cm). In deposition experiments accomplished with the initial apparatus, linear speeds were lower than those which are eventually anticipated, with thicker deposits per layer and excessive laser penetration and meltback into the precursor mandrel and already-deposited layers. Solid state cooling rates in these experiments were determined by observation of microstructures to be approximately  $10^5$ °C/sec, although ultimately, cooling rates of up to  $10^8$ °C/sec will be sought in this process.

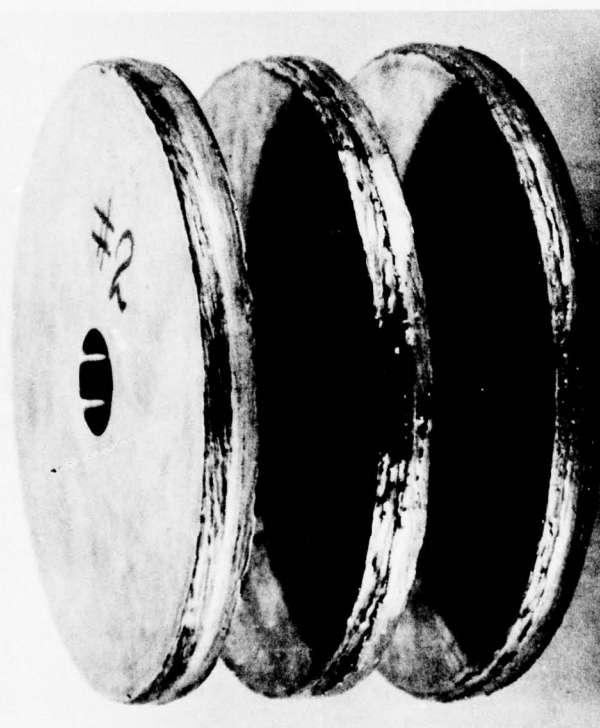
Since the rigid position of the wire feed nozzle and lack of a third axis of motion to compensate for focal point motion in relation to the growing diameter precluded the deposition of more than approximately 0.090 in. (0.228 cm) of new material, a third axis of motion was added and the wire feed nozzle was suspended independently of the chamber so that the wire feed distance remained approximately constant providing the apparatus was indexed to maintain the growing diameter at the original focal point location. By lowering the Bridgeport milling machine base on which the apparatus was carried, adjustments for diameter increase were easily made.



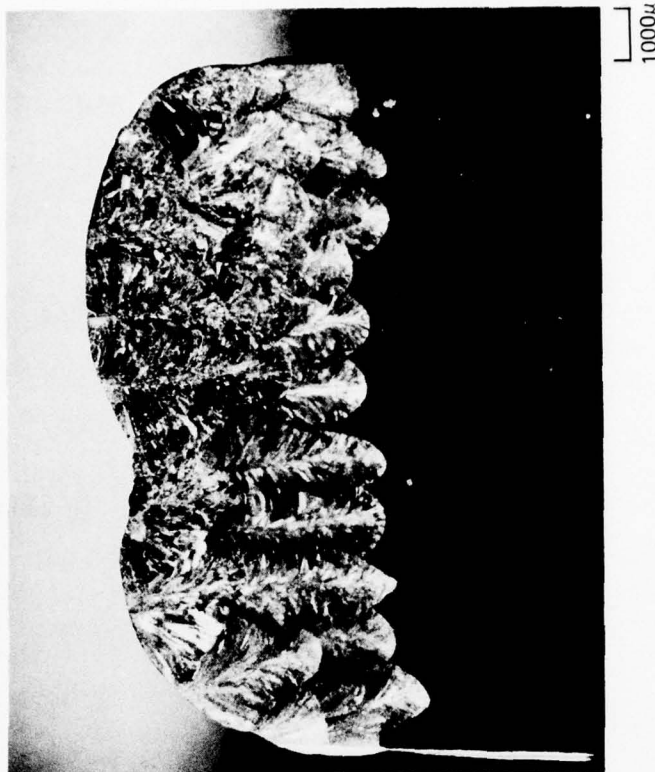
LAYERGLAZE APPARATUS (PHASE II)



PRELIMINARY LAYERGLAZE MODEL PARTS



DISKS



TRANSVERSE CROSS SECTION OF DEPOSIT

Using this apparatus as pictured in Fig. 6-4, a 0.200 in. (0.508 cm) thick deposit was built up on the disk shown in Fig. 6-6. This built-up region was subsequently machined on the sides only to make a flange on the original disk. The machined shape is shown in Fig. 6-7. The outside diameter, however, remains as-deposited. Inspection of the machining chips, and X-ray of the machined flange showed the deposited material to be fully dense - a result which was not anticipated so early in the experimental feasibility stage.

Based on the results achieved to date and described above, it appears that the physical process for in-situ buildup of dense, high cooling rate structures using laser energy should be feasible at rates of 0.5 cu in/min (8.2 cc/min) at the 6 kW power level, with deposition rates of 1.0 cu in/min (16.4 cc/min) possible in the 10-15 kW range. The deposition process, as observed by high-speed photography, appeared to be quite controllable, even in the relatively simple phase I and II apparatus. Consequently, it is expected that substantial progress can be made with the application of adequate further development time and effort.

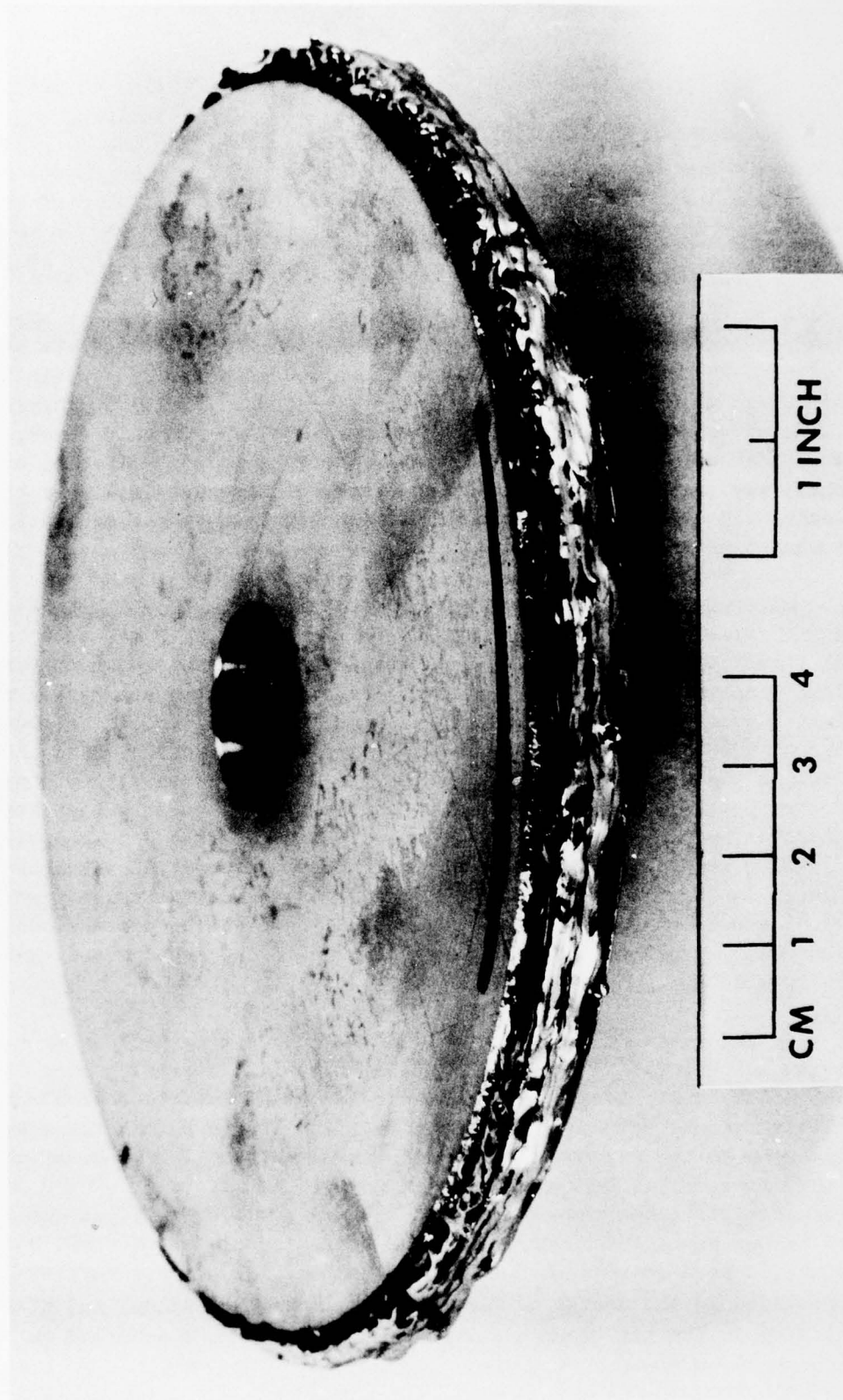
The main apparent problem to be solved, which will result in smoother deposition with fewer perturbations in the outer surface, is to make possible continuous liquid transfer by a "meniscus drag" type interaction, as opposed to the "drop transfer" which occurred often during our tests, apparently as a result of imperfect matching between the wire feed speed and the circumferential velocity of the workpiece surface. This transfer mode was observed in the high speed motion pictures taken of the process as it was operated. By converting to a molten metal or meniscus drag technique or to a tape or ribbon feed, meniscus drag transfer should be easier to accomplish, and smoother deposits will be obtained. As a result of the effects of mechanical deformation which have been encountered during the early stages of the alloy-design feasibility work (see Task 7), the possibility of using a mechanical deformation process such as a roller or peening hammers to simultaneously smooth and mechanically work the deposit is also under consideration.

A very important aspect of the LAYERGLAZE deposition process promises to be in-situ inspectability on a layer-by-layer basis. A primary conclusion of the preliminary design analyses (see Tasks 1-3) was that enhanced strength alone is of little if any value. Improved fatigue and fracture toughness, which are usually keyed to the maximum flaw size in the structure, are primary goals. Since the structure is being built up in individual layers of ~0.002 in. (0.005 cm) thickness, it seems reasonable that the maximum flaw size can ultimately be limited to the deposited layer thickness, a size nearly an order of magnitude lower than is used in present designs, and which will allow substantial benefits to be realized in the design of parts using layerglazed alloys and structures, as concluded in the performance and cost benefit analyses detailed in Tasks 1-3 above.



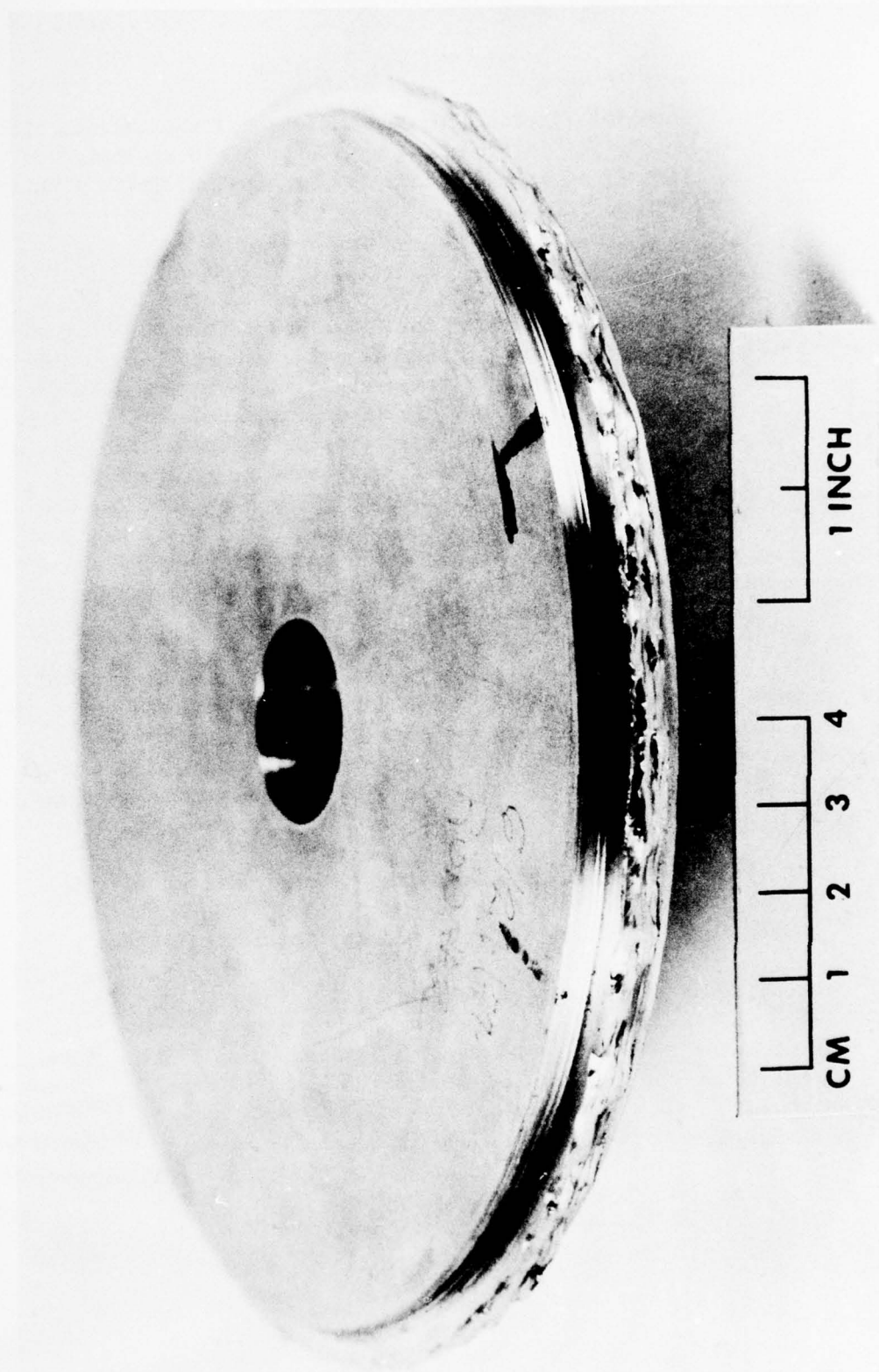
**0.2 INCH LAYERGLAZE BUILDUP**

(302 STAINLESS STEEL - AS DEPOSITED)



**0.2 INCH LAYERGLAZE BUILDUP**

(302 STAINLESS STEEL—AFTER MACHINING)



## B. Thermal Analysis

This task involved the modeling and analysis of the thermal history of a structure produced by the layerglazing approach. This analysis was performed by Mr. D. L. Williams, Advanced Systems Thermal Design, Pratt & Whitney Aircraft Government Products Division.

### Modeling and Analytical Approach

The melting of a thin foil of the PDS alloy onto a rotating substrate is modeled and thermally analyzed in the following manner. As modeled when the material builds up, the substrate temperature increases because the energy being applied on its outer circumference has to be conducted to its cooled inner surface. (This occurs in the present case because the beam size is assumed to be the full width of the disk.) A cyclic substrate temperature field exists because the material is heated locally and then is allowed to cool for one revolution.

The cycle is then repeated. A two-dimensional finite-element heat-balance model (Fig. 6-8) was used to calculate the transient temperature field. The inner circumference is kept at 200°F (93°C). The beam size was taken to be 0.030 x 1 in. (0.076 x 2.54 cm).

The heat conduction problem was approached using an analytical approximate method (Ref. 36) in order to avoid the complexities and cost of a numerical solution. The major assumption was to neglect the latent heat of melting. The agreement between the analytical finite-element heat-balance methods was shown by Greenwald (Ref. 36) to be excellent. Other assumptions made for the analytical method include:

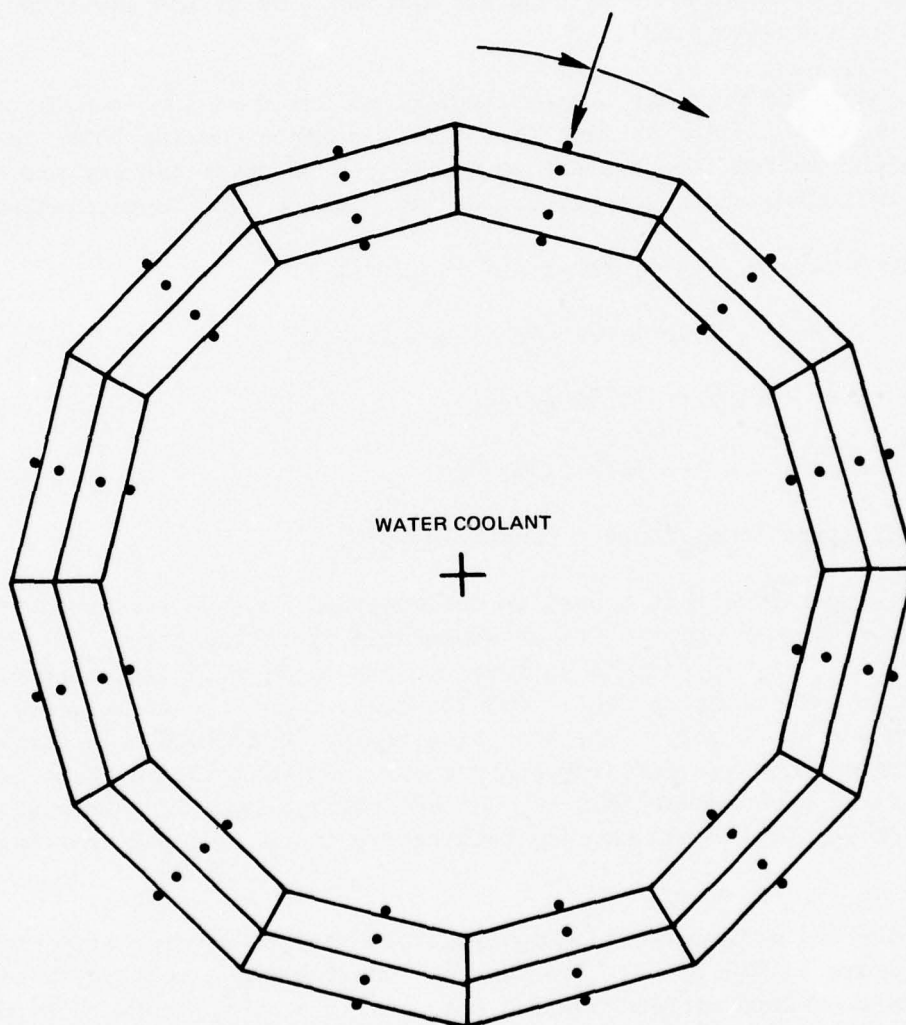
- The melt layer is a one-dimensional semi-infinite solid.
- Heat input is constant during the application of power.
- Cooling is by conduction only.
- The material is homogeneous with constant properties (equivalent to IN-100 at the melting temperature).
- Substrate surface temperature is constant.



**TWO-DIMENSIONAL FINITE-ELEMENT HEAT-BALANCE MODEL**

MATERIAL'S PHYSICAL PROPERTIES SAME AS IN-100

ID = 8 IN.      MOVING LINE  
OD = 10 IN.    HEAT SOURCE  
WIDTH = 1 IN.



77-11-159-6

## Results

The finite-element heat-balance model was used to calculate the temperature profile in the disk as a function of power density for a uniformly heated disk. This condition defines the limiting case of infinite disk speed and establishes maximum substrate temperatures. As shown in Fig. 6-9, radial conduction in this case limits power density to about  $10^5$  W/cm<sup>2</sup>. At a higher power density, the substrate surface temperature was also calculated as a function of dwell time at constant power density. The results shown in Fig. 6-10 indicate that the substrate surface temperature is independent of dwell time for dwell times less than 0.01 seconds (disk speeds greater than 5.73 RPM). At higher disk speeds, substrate surface temperature is constant and the same as the limiting case above (uniformly heated disk).

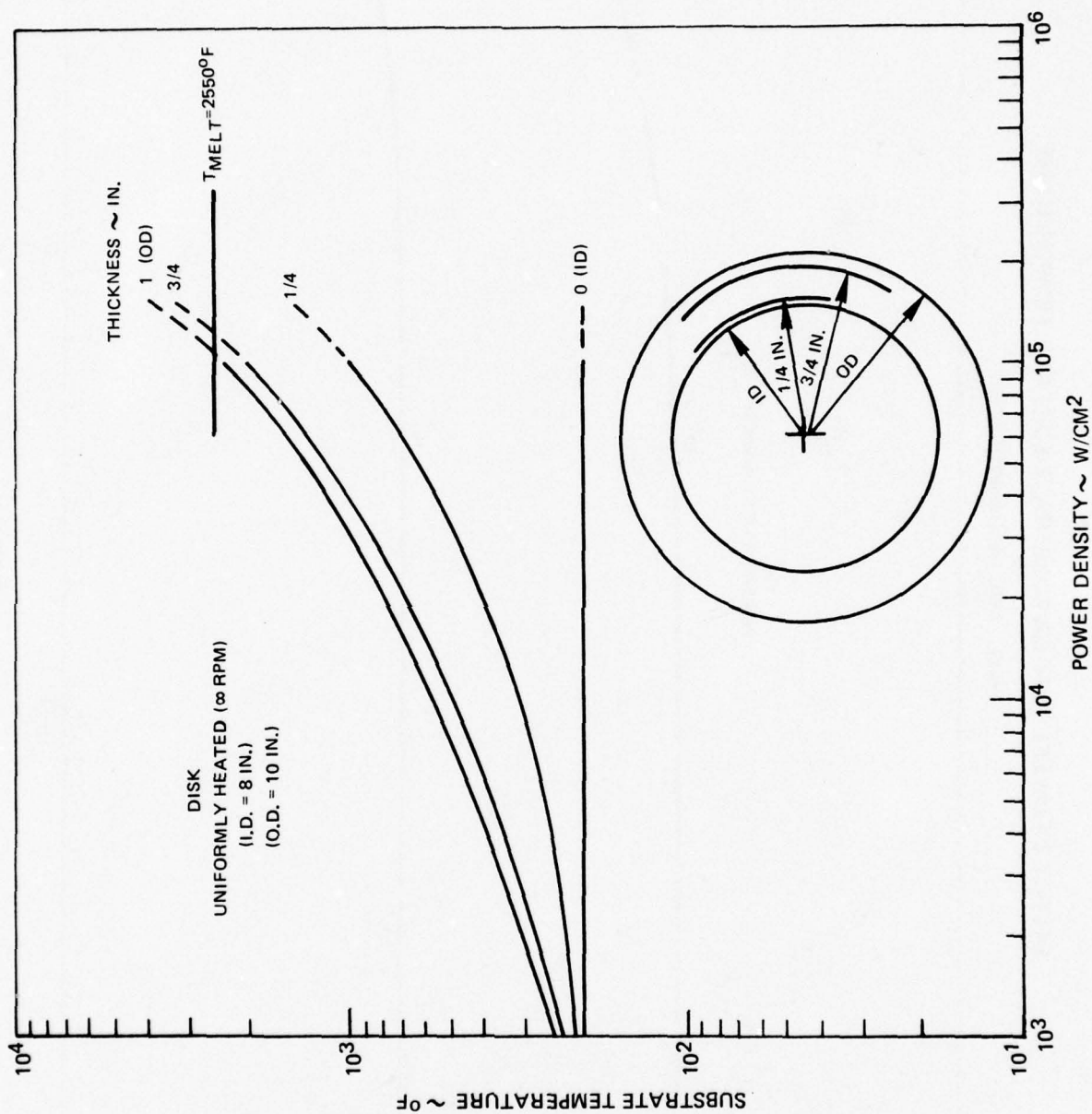
The information from the heat-balance model was used in the analytical heat conduction model to determine maps that define surface cooling rate, melt depth and the maximum surface temperature as a function of power density and dwell time. The following materials properties were assumed in these calculations:

- Conductivity = 24.4 BTU/hr-ft-°F (42.2 W/m·K)
- Specific Heat = 0.16 BTU/lb-°F (6,700 J/kg·K)
- Density = 489 lb/ft<sup>3</sup> (7.83 gm/cc)
- Melt temperature = 2550°F (1399°C)
- Vaporization temperature = 3992°F (2200°C).

The maximum temperature that occurs in the material must be less than the vaporization temperature in order to be an acceptable operating point. Operating maps (Figs. 6-11, 12, 13) define surface cooling rate, melt depth and surface temperature as a function of dwell time for power densities of  $10^4$ ,  $3.2 \times 10^4$  and  $10^5$  W/cm<sup>2</sup>, respectively. The operating region is defined by a surface temperature greater than the melt temperature but less than the vaporization temperature. For a given power density, surface cooling rate increases with decreasing dwell time. Both surface temperature and melt depth decrease with dwell time.

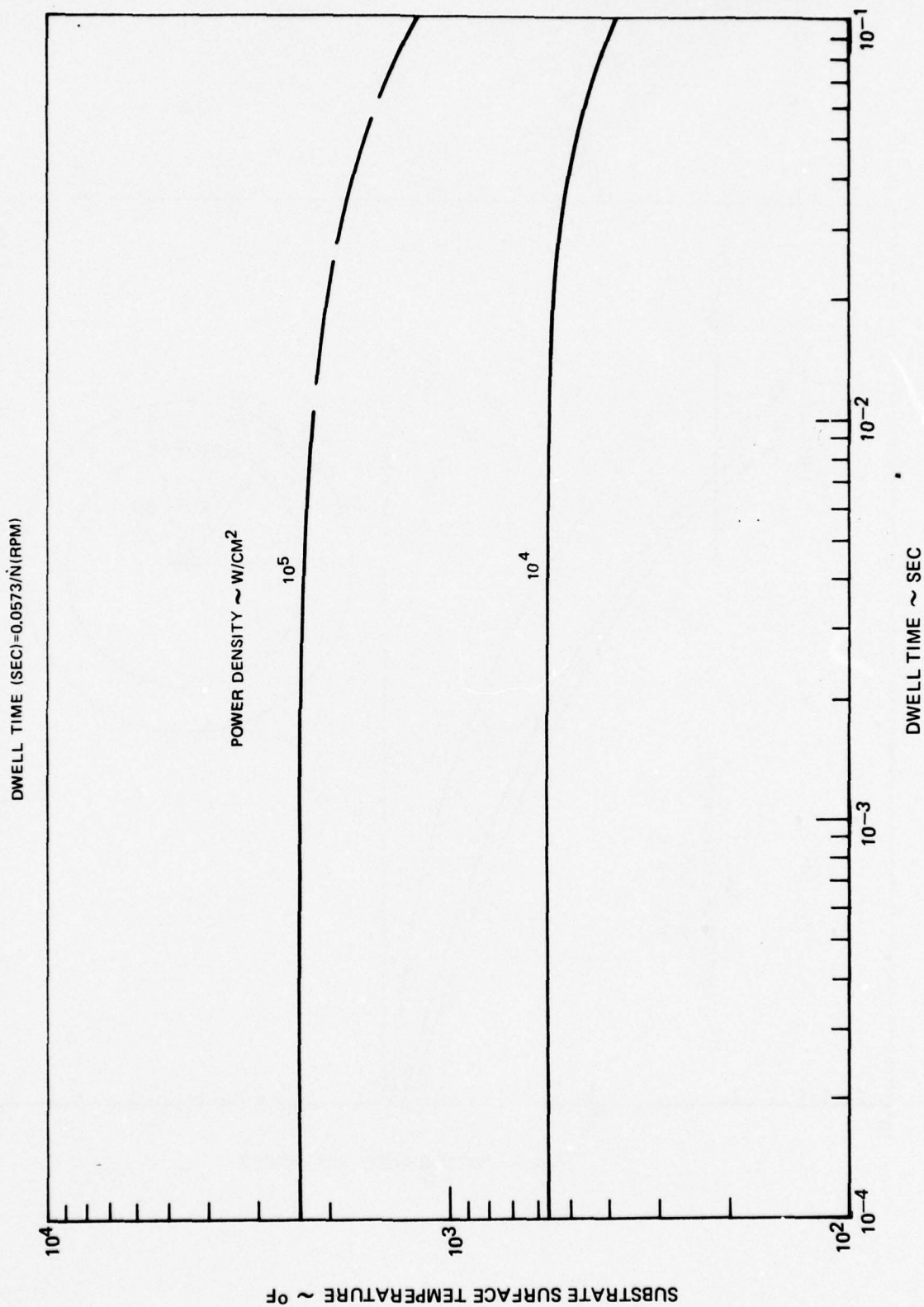
To obtain the maximum surface cooling rate conditions, the maps were cross-plotted as shown in Fig. 6-14. For the case considered, a melt depth of 0.001 in. will achieve a maximum surface cooling rate of  $1.2 \times 10^6$  °C/sec with a power density of  $3 \times 10^4$  W/cm<sup>2</sup> and a dwell time of 0.0021 seconds. Maximum surface cooling rate is a trade-off between power density, dwell time and substrate surface temperature. Surface temperature increases as power density increases for a constant melt depth or as melt depth increases for a constant power density as shown in Fig. 6-15.

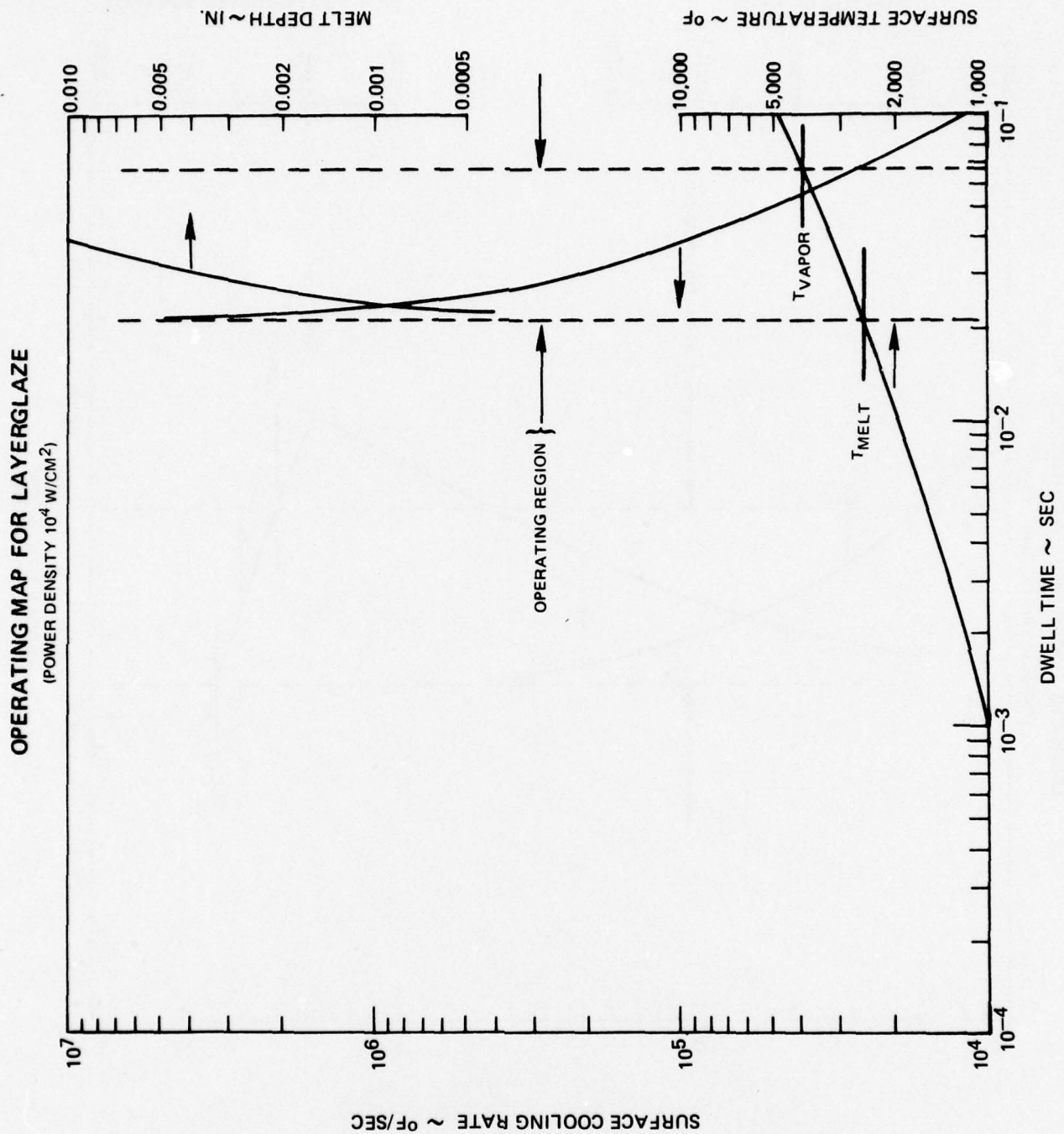
## EFFECT OF POWER DENSITY ON SUBSTRATE TEMPERATURE PROFILE

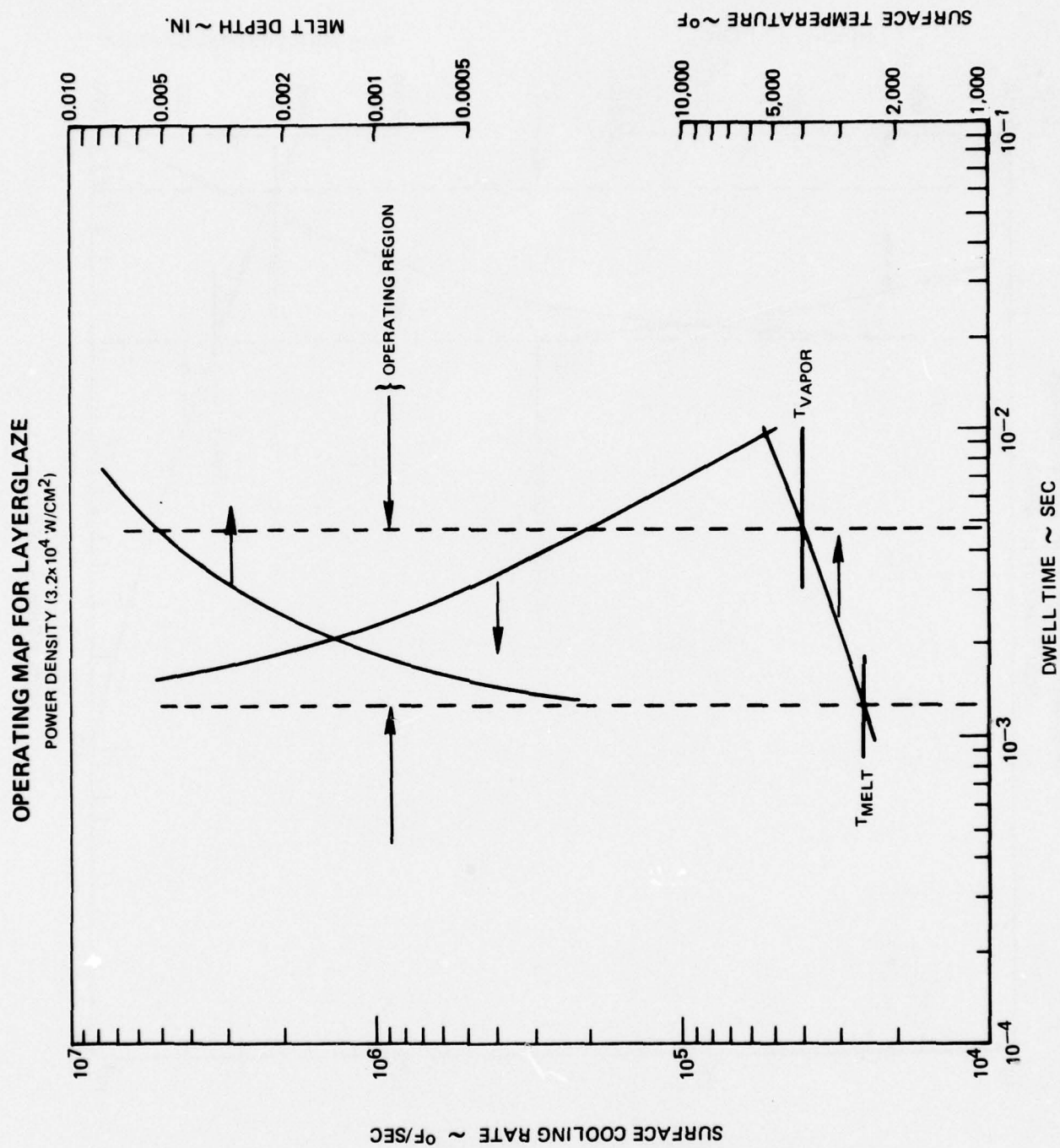




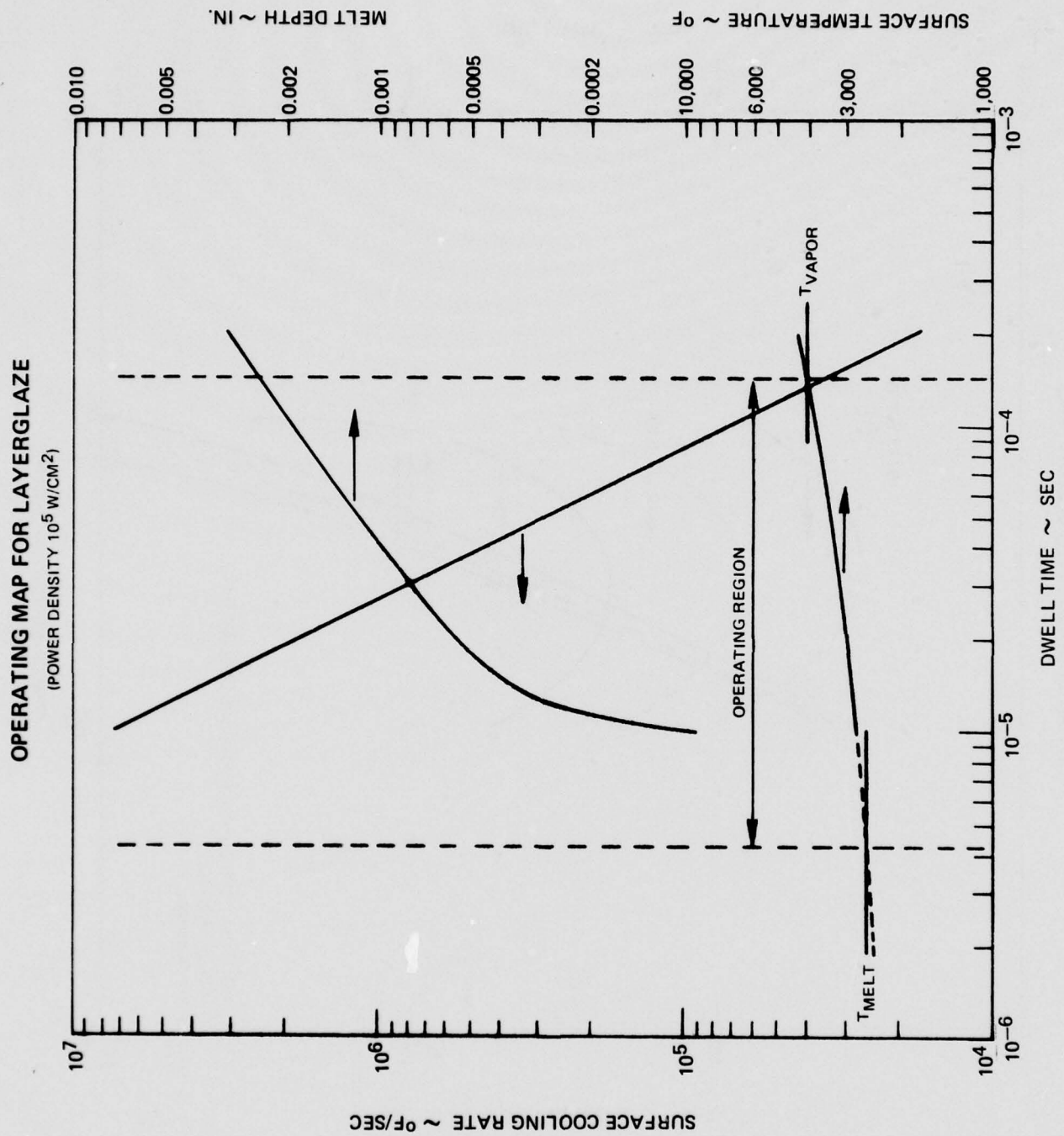
## EFFECT OF DWELL TIME ON SUBSTRATE SURFACE TEMPERATURE

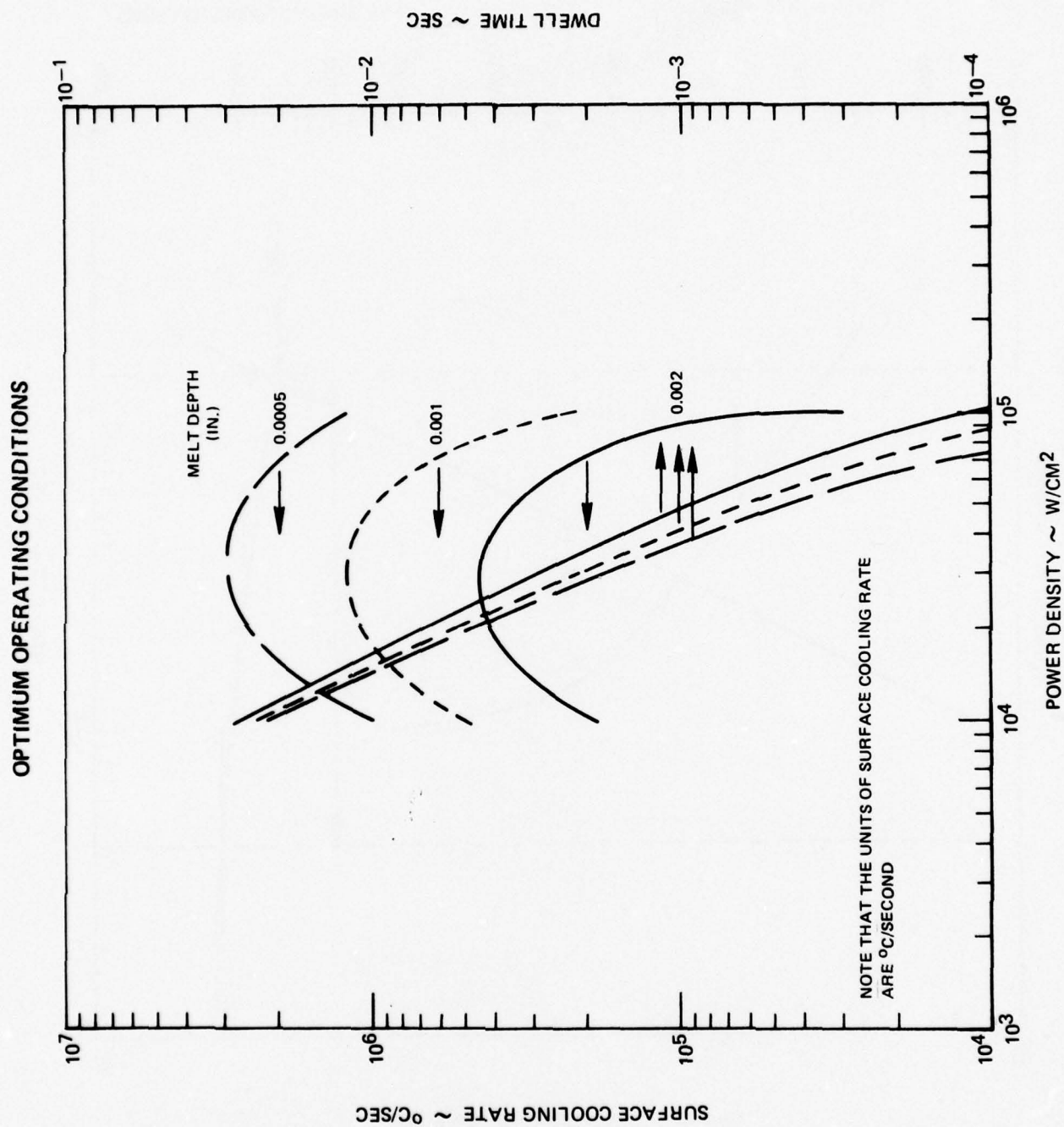




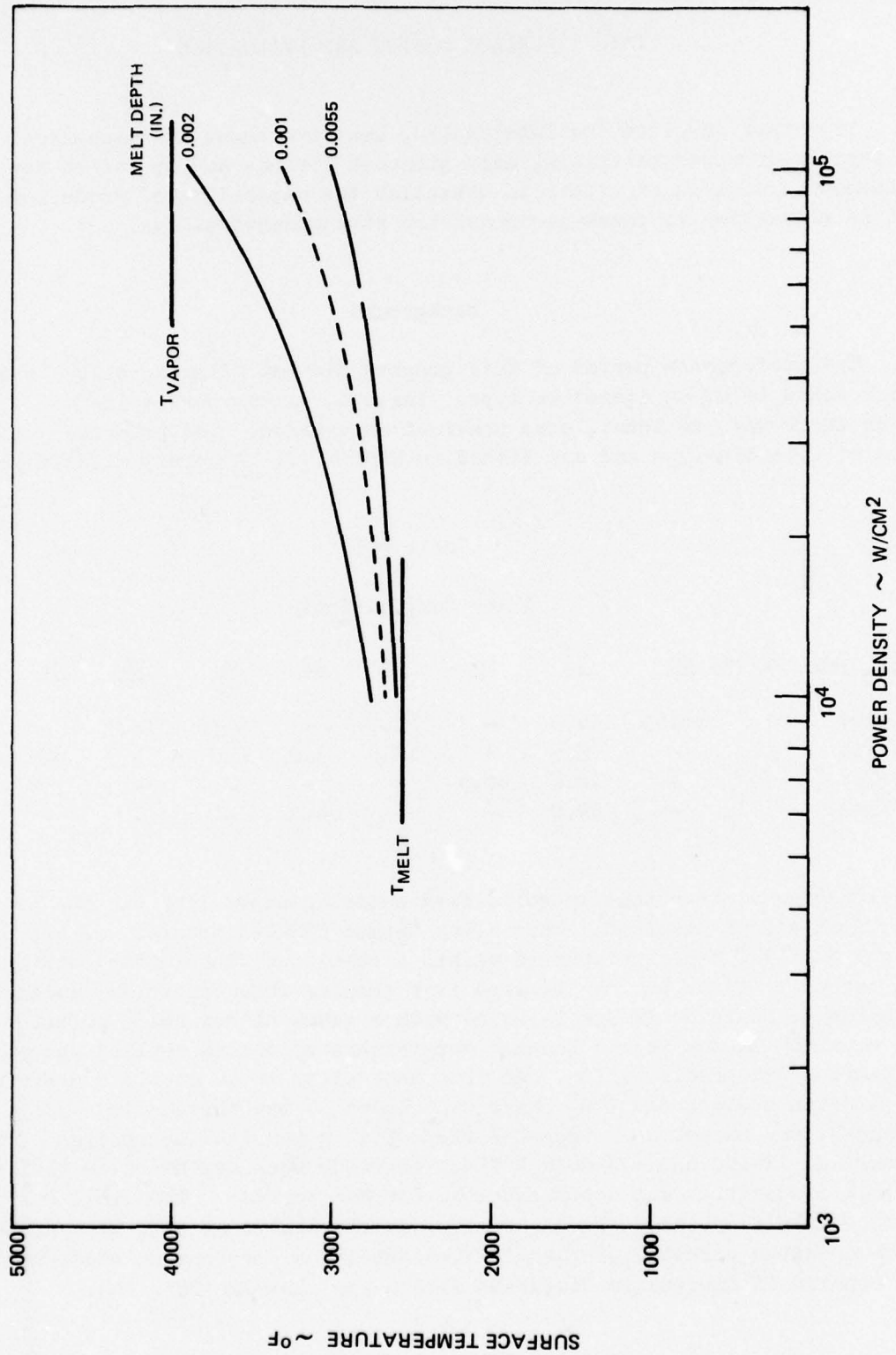








## SURFACE TEMPERATURE AS A FUNCTION OF POWER DENSITY AND MELT DEPTH





## TASK 7 - ALLOY DESIGN AND EVALUATION

This task involved the fabrication, heat treatment and mechanical testing of rapidly-quenched materials, melt-quenched ribbons and sputtered deposits of candidate alloys in an effort to establish the capability of producing the required properties in phase-decomposition strengthened alloys.

## Background

The performance period of this program did not allow an alloy investigation which would be of an iterative type. Instead, alloys were selected for study for which there was, at least, some previous experience. The principal alloys chosen were of eutectic-type and are listed in Table 7-I. A cobalt alloy which was

Table 7-I

## Alloy Compositions

<u>Alloy Type</u>	<u>w/o</u>	<u>Co</u>	<u>Ni</u>	<u>Fe</u>	<u>Cr</u>	<u>Al</u>	<u>C</u>	<u>Ta</u>	<u>Ti</u>	<u>B</u>	<u>Mo</u>
CoTaC		56.55	10.0	-	20.0	-	0.75	12.7	-	-	-
NiTiC		-	79.5	-	10.0	3.0	1.0	-	6.5	-	-
FeTiB		-	10.0	80.6	-	-	-	-	7.0	2.4	-
NiMoAl		-	59.0	-	-	4.0	-	-	-	-	37.0

developed as a directionally solidified eutectic superalloy was one of the four principal alloys examined. This alloy termed CoTaC-3 consists of approximately 10 vol % of TaC fibers dispersed within a cobalt solid solution matrix (Ref. 37). The second alloy to be investigated is a complex eutectic which consists of titanium monocarbide fibers (~5 v/o) with a gamma nickel solid solution matrix; the aluminum in the matrix becomes supersaturated during cooling which results in gamma prime precipitation. An iron base alloy which should contain under equilibrium a dispersed TiB<sub>2</sub> phase was chosen as the third alloy system. A pseudo-binary eutectic is reported (Ref. 38) in the Fe-TiB<sub>2</sub> section of the Fe-Ti-B ternary at 1340°C and 6.3 mole % TiB<sub>2</sub>; previous work demonstrated that an alloy of this composition was hyper-eutectic (excess boride). The final eutectic alloy examined was from the Ni-Mo-Al ternary system; alloys of this type are being studied in the directionally solidified condition for turbine blade applications and consist of fibrous Mo dispersed with a  $\gamma/\gamma'$  matrix (Ref. 39).

The alloy compositions selected for investigation were those of the nominal equilibrium eutectics. Two different considerations will eventually be involved in the selection of optimum compositions for applications in the rapidly solidified condition. On one hand, if the results from splat-quenched materials provide an indication, the strength potential of highly supersaturated alloys is great. In this case, a composition would be selected which upon rapid quenching would result in a metastable, single phase alloy which is hardened by phase decomposition; alloys which are hypo-eutectic might serve this purpose. In the second case, a fine-scale eutectic microstructure formed by melt quenching would be sought. The second phase particles would be larger in size, represent a higher volume percent of the alloy, and should possess a higher thermal stability. For alloys of this type, hyper-eutectic compositions would usually be required in order to obtain coupled growth at high cooling rates (Ref. 40).

### Experimental Procedure

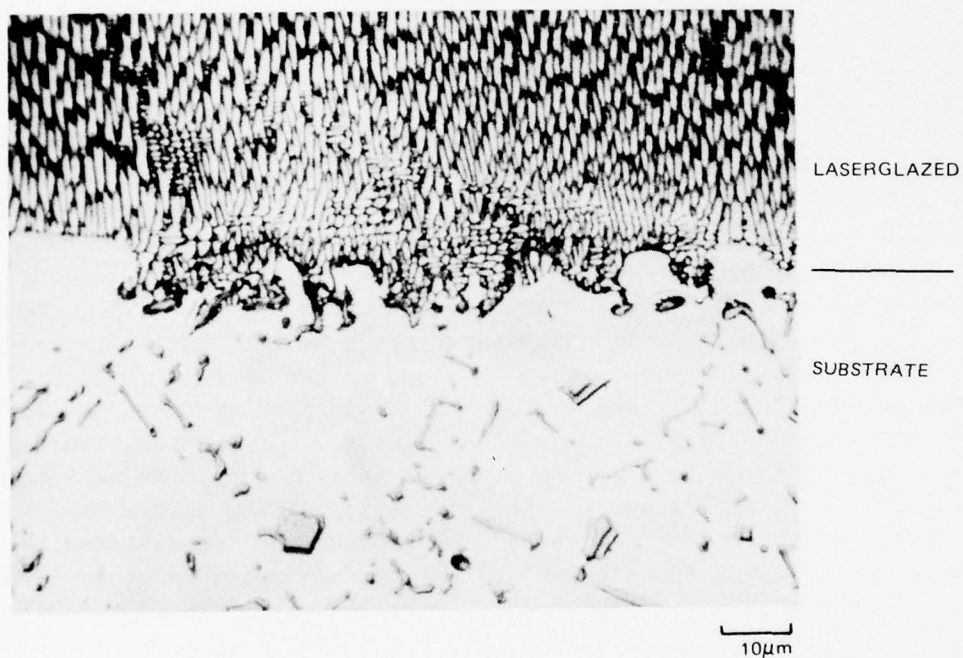
Cast samples of the alloys listed in Table 7-I were prepared by induction melting of the elements under inert gas and by pouring into copper chill molds. Four separate approaches were used to provide microstructures which represent the materials in a rapidly quenched state. The first was the LASERGLAZING approach wherein a thin, molten surface layer of the alloy is rapidly self-quenched. Cooling rates in the range of  $10^5$  to  $10^8$  °C/sec may be obtained by this process. The second procedure, which may produce cooling rates in the  $10^5$ - $10^6$  °C/sec range, is melt quench ribbon casting, as practiced by Allied Chemical in the making of glassy metals. The third approach involved the incremental laser melting and solidification of slab samples. Autogenous, overlapping deep welds were made in the alloys to provide structures quenched at an intermediate cooling rate ( $\sim 10^4$ - $10^5$  °C/sec). The preparation of the alloys as sputtered deposits (effective cooling rates  $\sim 10^{15}$  °C/sec) was accomplished by the Government Products Division of Pratt and Whitney Aircraft, and this technique served as the last approach to be evaluated.

### Results

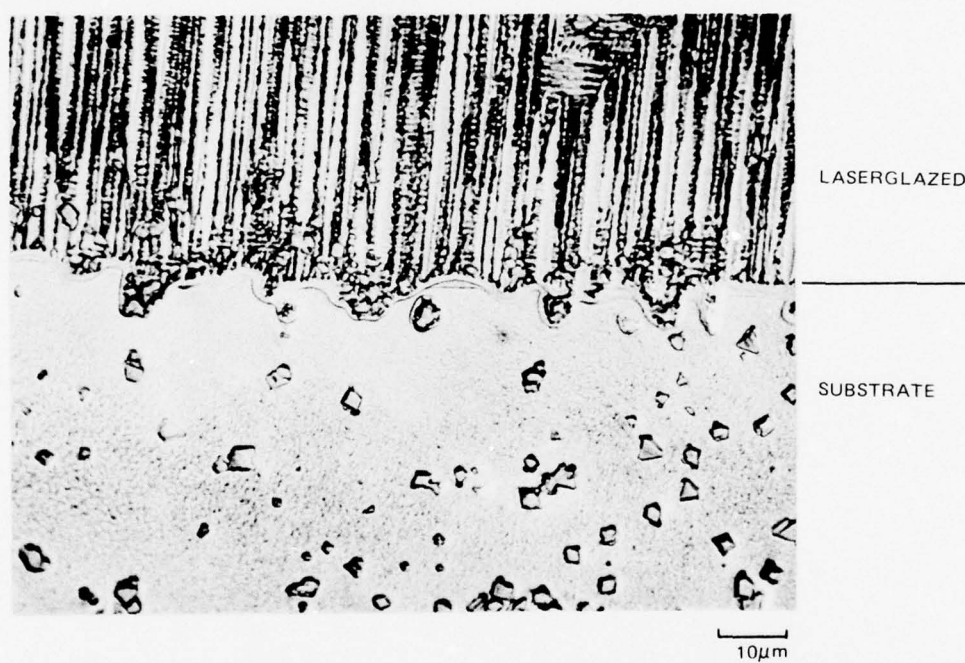
#### LASERGLAZED Structures

Numerous laser glazing passes were made on the CoTaC, NiTiC and FeTiB eutectics to produce rapidly quenched layers of thicknesses in the range 25 to 150  $\mu$ m. Representative microstructures from these alloys are displayed in Figs. 7-1, 7-2, and 7-3. When tested at a load of 50 grams, with a Vickers indenter (D.P.H.), the alloys showed microhardnesses up to 550, 450 and 800 kg/mm<sup>2</sup>, respectively. Assuming a correspondence between hardness and strength as has been observed in

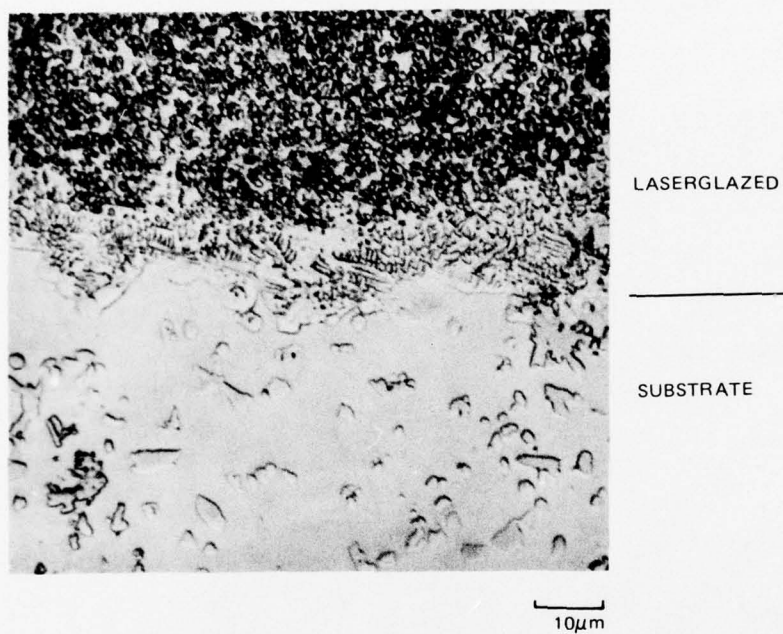
STRUCTURE OF LASERGLAZED CoTaC





STRUCTURE OF LASERGLAZED  $\text{NiTiC}$ 

STRUCTURE OF LASERGLAZED FeTiB



glassy metals, these hardnesses correspond to strengths of 1790 MPa (260 ksi) for the CoTaC alloy, 1470 MPa (210 ksi) for the NiTiC alloy and 2610 MPa (380 ksi) for the FeTiB alloy. The eutectic microstructures generally show a dendritic metal phase and some interdendritic eutectic which exhibits a higher volume percent of second phase when compared to the equilibrium structure; the eutectic reactions are displaced by the high freezing velocity. Undissolved primary, second-phase particles are also observed.

#### Melt-Quenched Ribbons

Despite a number of attempts by Allied Chemical with the CoTaC, NiTiC and FeTiB alloys, only the FeTiB alloy yielded an unoxidized, continuous ribbon product when processed in vacuum. Unoxidized and fragmented lengths of CoTaC were produced. These were suitable for hardness evaluation, but their nonuniformity did not permit tensile evaluation. The NiTiC alloy presented casting problems related to wetting which were not overcome during this initial attempt at ribbon fabrication.

Two different casting products each were examined for the CoTaC and FeTiB alloys. These are identified as samples 6 and 9 and samples 7 and 8, respectively. They were all prepared in vacuum; one chill block material was used for CoTaC (Number 6) and FeTiB (Number 7) and a different chill block material for CoTaC (Number 9) and FeTiB (Number 8). Improved wetting and a correspondingly higher cooling rate was experienced in the latter cases. The microhardnesses of these products when measured at 50 grams load were 588 and 583 kg/mm<sup>2</sup> (CoTaC samples 6 and 9, respectively) and 938 and 865 kg/mm<sup>2</sup> (FeTiB samples 7 and 8, respectively). (These hardnesses are the average of ten tests.) Using an estimate that the strength is one-third the hardness, we therefore predict the strength of these products to be 1920 MPa (278 ksi), 1900 MPa (276 ksi), 3060 MPa (444 ksi) and 2820 MPa (409 ksi), respectively.

Ribbons of the FeTiB alloy, nominally 0.005 x 0.150 cm (0.0127 x 0.381 in.) in cross section, were mounted on tray grips. Each fracture surface was photographed at 50X and fracture areas were determined from planimeter traces. The ultimate strength and approximate plastic strain at fracture exhibited by specimens with 2.5 cm (1 in.) gage lengths are listed in Table 7-II. These were obtained on the as-processed ribbons (samples 7 and 8) and on ribbons annealed in vacuum for 1 hr at 800 and 1000°C.

FeTiB specimens from sample 8 were examined by X-ray diffraction and after electrochemically thinning by transmission electron microscopy. The bright side of the as-received ribbon (side adjacent chill) showed a [100] texture normal to the ribbon surface. After aging some evidence of TiB<sub>2</sub> and Fe<sub>23</sub>B<sub>6</sub> was observed in the X-ray patterns. In transmission, as shown in Fig. 7-4, a dendritic form of b.c.c. iron (labeled B in the micrograph) was found in an amorphous matrix



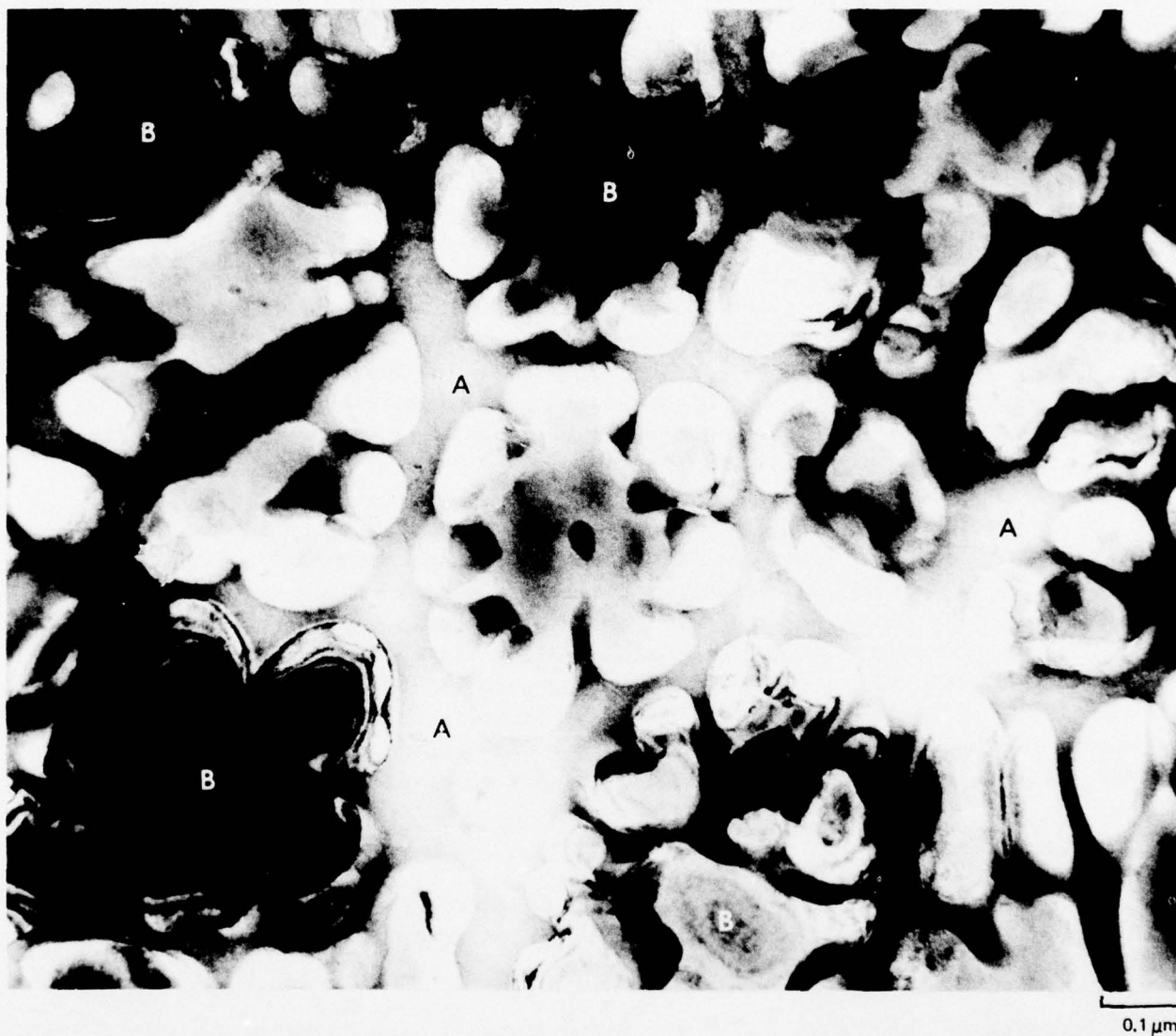
Table 7-II

Strength and Approximate Plastic Strain at  
Fracture for FeTiB Alloys

<u>Sample No.</u>	<u>Ultimate MPa</u>	<u>Strength (ksi)</u>	<u>~ Percent Plastic Strain at Fracture</u>	<u>Condition</u>
7-1	2010	(292)	0.2	As-processed
7-2	1805	(262)	0.3	
8-2	1840	(267)	0.05	
8-3	2985	(433)	0.5	
8-4	2225	(323)	0.2	
7-1	1930	(280)	4.1	800°C/1 hr anneal in vacuo
7-2	1765	(256)	2.7	
7-3	1665	(242)	2.3	
8-2	1910	(277)	1.9	
8-3	1695	(246)	1.1	
8-4	2065	(300)*	3.5	
7-1	1380	(200)*	3.7	1000°C/1 hr anneal in vacuo
7-2	1310	(190)*	2.1	
8-2	1445	(210)*	2.8	
8-3	1445	(210)*	3.8	
8-4	1515	(220)*	2.5	

\*Specimen necked, strength based on estimate of original area

## ELECTRON MICROGRAPH OF AS RECEIVED FeTiB ALLOY (SPEC.NO. 8)



(labeled A). After an 800°C anneal (Fig. 7-5), the structure displayed a relatively uniform distribution of small iron crystallites. Distinct second phase particles were not observed.

#### Incrementally Melted Alloys

In order to provide representative eutectic alloys in a rapidly quenched condition for mechanical property evaluation, overlapping deep-penetration laser welds were made in chill cast slabs. Compression coupons were cut from the weld metal in the form of square cross-section columns (~0.25 cm on a side and 0.50 cm in length) (0.10 x 0.20 in.). Yield strength was determined on these samples as a function of temperature at a strain rate of  $10^{-2}$  min<sup>-1</sup>. The alloys previously mentioned (CoTaC, NiTiC and FeTiB), and a Ni-37Mo-4Al alloy were evaluated. The Ni-Mo-Al displayed as shown in Fig. 7-6 a dendritic gamma structure and an interdendritic eutectic structure. In this case as with the other eutectics, the eutectic reaction was displaced at high freezing velocity so the alloy appears hypo-eutectic. Higher aluminum containing alloys were also processed, but they were found to be unweldable at this intermediate rate of quenching. The yield strengths of the various alloys are shown in Table 7-III. In all cases except that of the Ni-Mo-Al alloy, progressive yield strengths were measured; that is, yielding was accomplished at one temperature, the temperature was changed and the specimen was reyielded.

A comparison between the yield strength of the CoTaC alloy formed by incremental melting and the alloy hot isostatically pressed from powders are shown in Fig. 7-7. A micrograph of the deformed alloy is also included and shows slip bands decorated by precipitate particles. The specimen obviously appears hypo-eutectic. The strength potential of rapidly quenched alloys is best demonstrated by the Ni-Mo-Al alloy. This alloy is extremely strong even at 760°C. As presently constituted the alloy is too brittle; fracture occurs soon after yielding. By reducing the molybdenum content of the alloy and through other compositional modifications, a high strength and more ductile material may result.

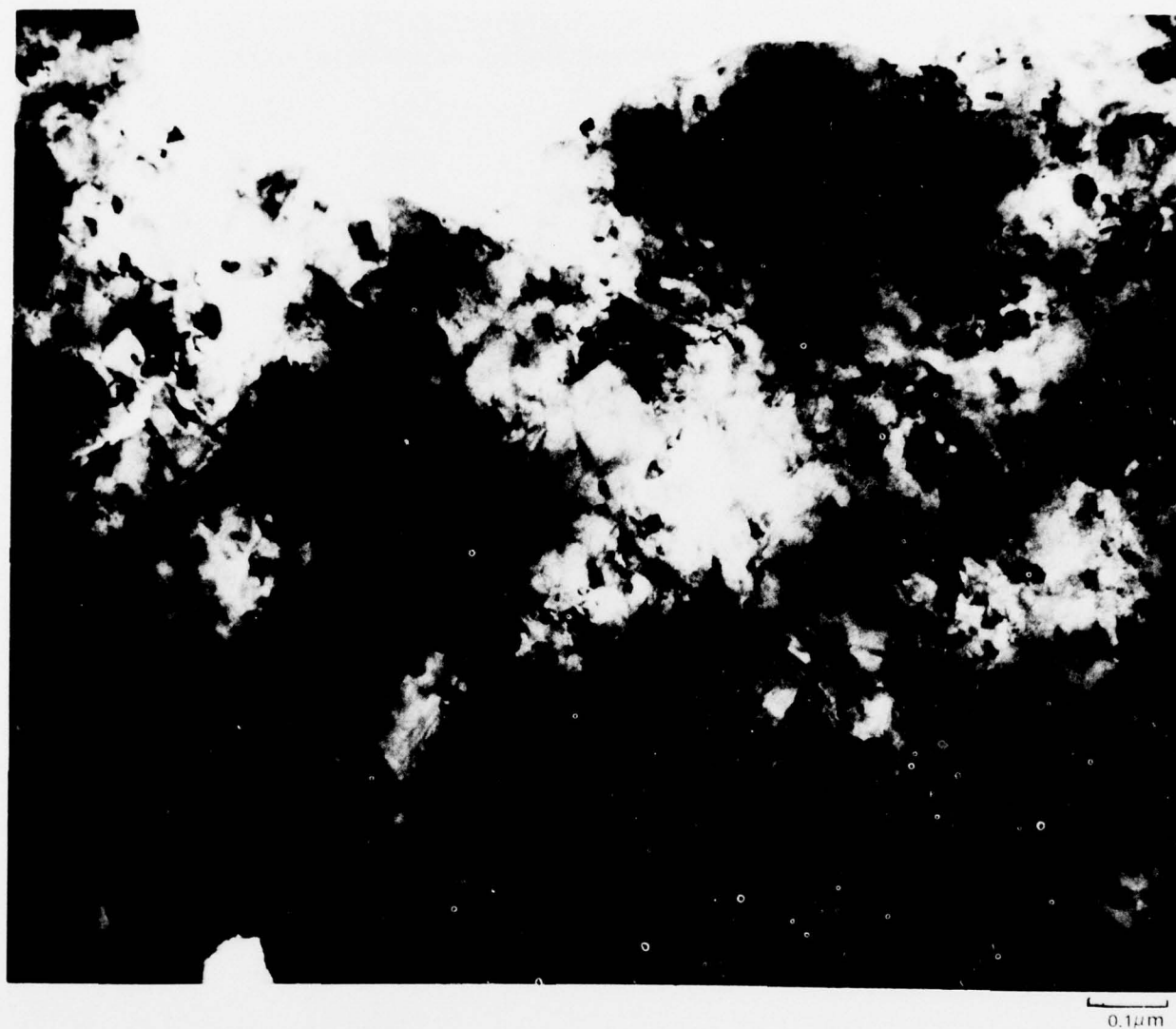
#### Sputtered Deposits

The experiments reported here were performed by Pratt and Whitney Aircraft Government Products Division. The responsible personnel were H. A. Beale, R. J. Hecht, P. R. Holiday, J. R. Mullaly and C. T. Torrey.

Deposits of the CoTaC, NiTiC and FeTiB alloys listed in Table 7-I were sputtered in a triode system onto water cooled substrates. Opposed sputtering targets were employed with the substrate mounted and rotated between the targets. Deposition rates were on the order of 7.6  $\mu$ m/hr (0.3 mils/hr); substrates were



TRANSMISSION ELECTRON MICROGRAPH OF FeTiB ALLOY AFTER 800°C  
THERMAL TREATMENT



0.1μm

STRUCTURE OF INCREMENTALLY MELTED Ni-Mo-Al EUTECTIC ALLOY

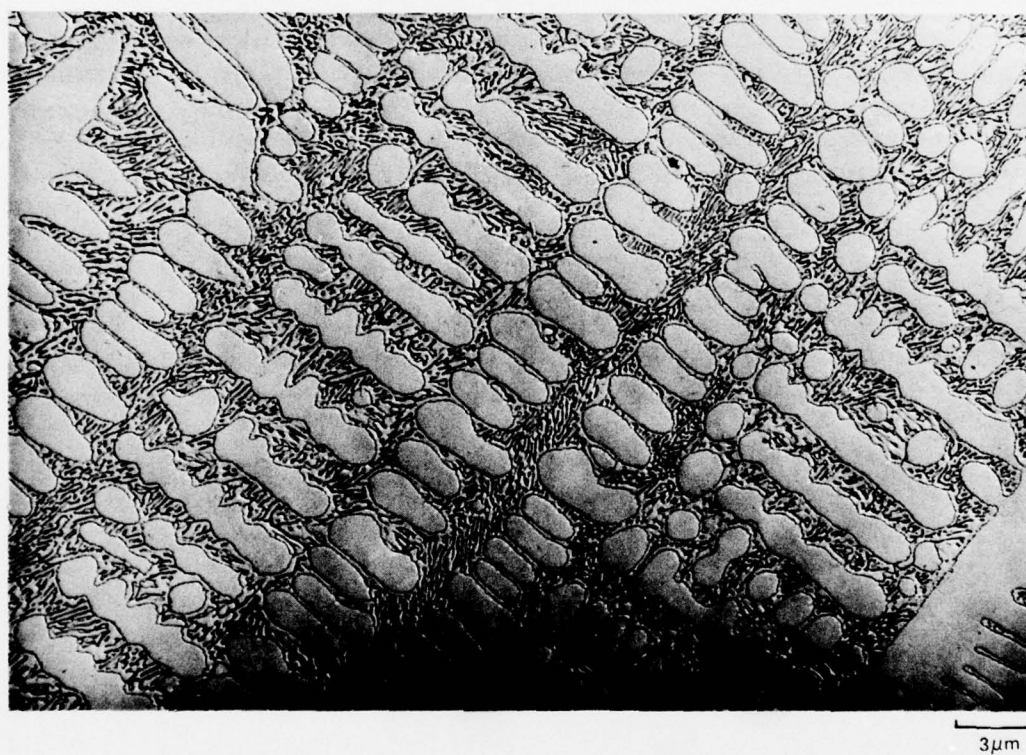


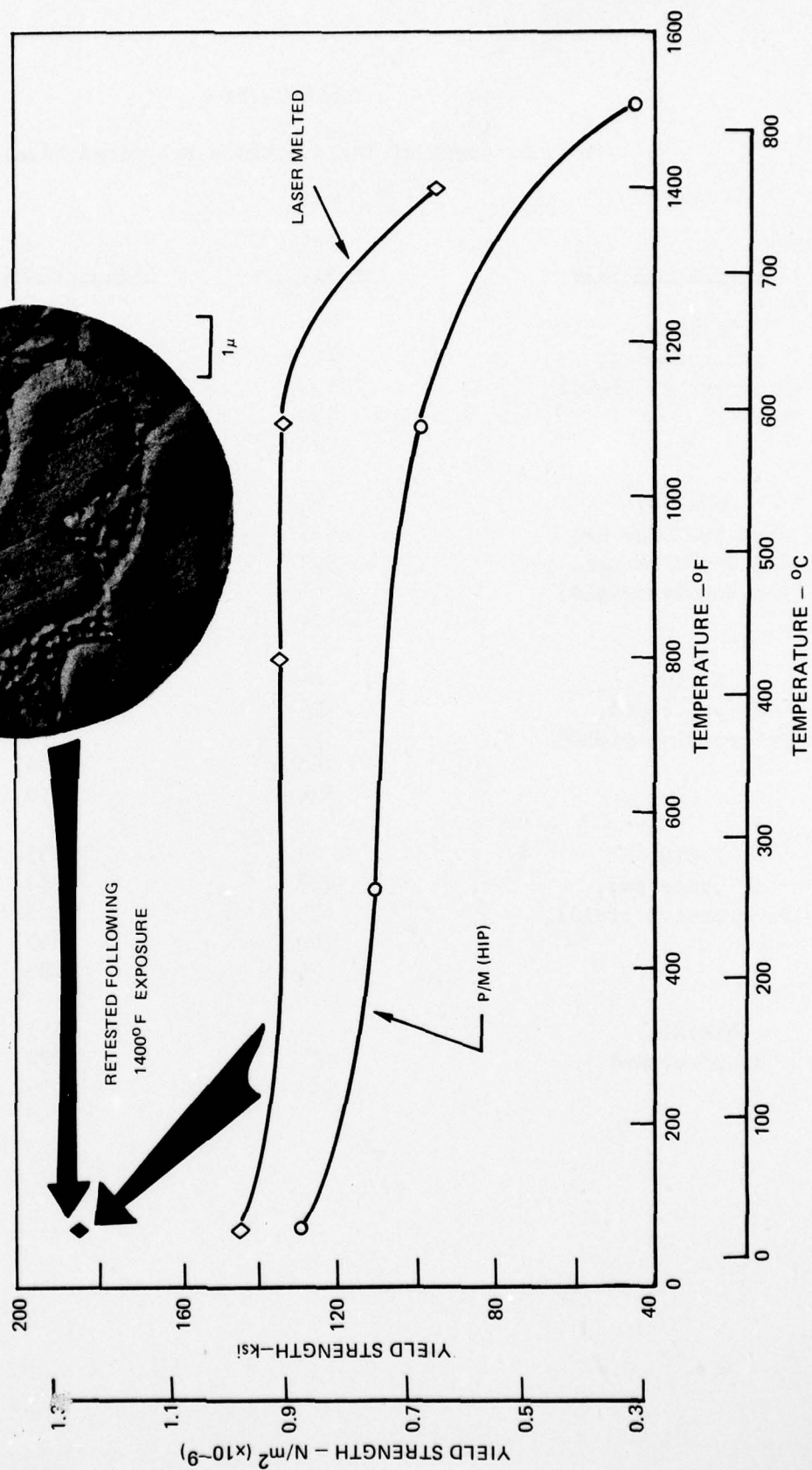
Table 7-III

## Yield Strength of Incrementally Processed Alloys

<u>Alloy, Comments</u>	<u>Test Temp, °C</u>	<u>0.2% Yield Strength MPa (ksi)</u>
CoTaC-3, As processed, (Progressive yield)	24	1005 (146)
	427	930 (135)
	593	930 (135)
	760	660 ( 96)
	24	1280 (186)
CoTaC-3, Aged 700°C/24 hrs and 900°C/24 hrs, (Progressive yield)	24	835 (121)
	427	785 (114)
	593	805 (117)
	760	475 ( 69)
	24	1000 (145)
NiTiC, As processed, (Progressive yield)	24	910 (132)
	427	925 (134)
	593	875 (127)
	760	690 (100)
	24	1110 (161)
FeTiB, As processed, (Progressive yield)	24	1235 (179)
	427	1290 (187)
	593	625 ( 91)
	760	205 ( 30)
	24	1125 (163)
NiMoAl, As processed	24	2355 (342)
	427	2220 (322)
	760	1755 (255)



## STRUCTURES AND PROPERTIES OF Co-TaC ALLOYS

(INCREMENTALLY LASER MELTED AND  
COOLED AT INTERMEDIATE RATES)

negatively biased at 15 volts in one case and unbiased in the second. Integrally cooled copper served as the substrate for the cobalt and nickel deposits, and aluminum was the substrate for the iron deposits. These substrates were chosen so that they could be removed from the deposits by chemical dissolution. Specimens were electrochemically thinned for examination by transmission electron microscopy. The effect of thermal treatments on structure and hardness were evaluated.

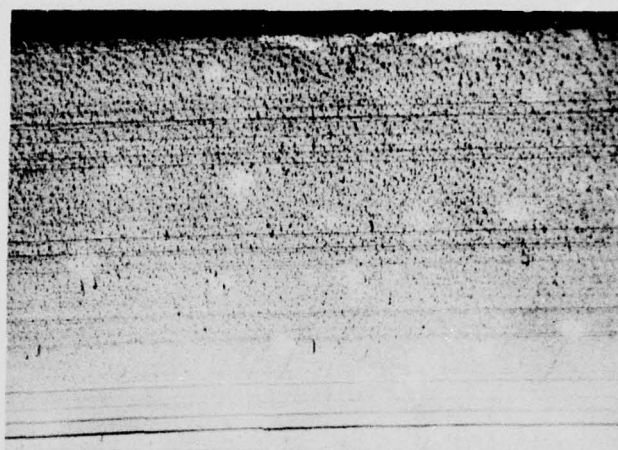
Examples of the sputtered microstructures of the Co, Ni and Fe base alloys are shown in Fig. 7-8. The structures of these alloys revealed by transmission electron microscopy in the as-deposited conditions are displayed in Figs. 7-9, -10 and -11. The attendant electron diffraction patterns show the following features. The pattern for the cobalt alloy is reasonably sharp and does not show rings attributable to a second phase, e.g. TaC. The nickel pattern is again reasonably sharp with no indication of a carbide second phase. The iron pattern is a diffuse ring pattern, positions of rings in general agreement with an alpha (bcc) iron; this alloy suggests the greatest glass-forming tendency. When heated in the electron microscope, the following changes were noted in the structures. In the cobalt alloy at 700°C, extra lines due to precipitation of apparently TaC are observed in electron diffraction. In the nickel alloy, recrystallization of the alloy is observed at 760°C as is the precipitation of TiC and perhaps Cr<sub>23</sub>C<sub>6</sub>. In the iron alloy at 650°C, some grain coarsening is observed as is the precipitation of what is probably Fe<sub>2</sub>B.

The Vickers hardnesses of the various deposits after annealing for 4 hrs in vacuum at various temperatures are shown in Figs. 7-12, -13, and -14. The cobalt alloy showed a gradual fall in room temperature hardness (from approximately 925 to 840 kg/mm<sup>2</sup>) as the thermal treatment increased from 370 to 704°C. The hardnesses of the nickel and cobalt alloys (which were deposited at 0 and -15 volt bias) were dependent on the sputtering conditions, but both showed a peak in hardness with annealing temperature. In the case of the nickel alloy, the peak occurred at approximately 540°C at an approximate hardness of 925 kg/mm<sup>2</sup>. In the case of the iron alloy, the hardness peaked at 540°C at a value of 1475 kg/mm<sup>2</sup>.

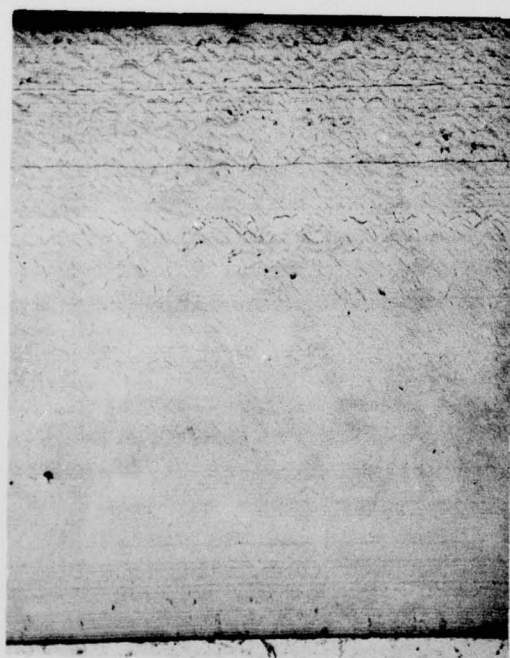
The effect of a nucleation and aging treatment on the hardness of thick deposits (Fig. 7-8) were determined as shown in Fig. 7-15. The heat treatment which consisted of 4 hrs at the nucleation temperature and 4 hrs at 649°C caused a peak in the room temperature hardness of the three alloys for a nucleation temperature of 538°C. The alloys after this treatment were not too dissimilar in hardness; the nickel alloy displayed a hardness of 795 K.H.N., the cobalt alloy a hardness of 780 K.H.N. and the iron alloy a hardness of 765 K.H.N.

## MICROSTRUCTURE OF SPUTTERED DEPOSITS

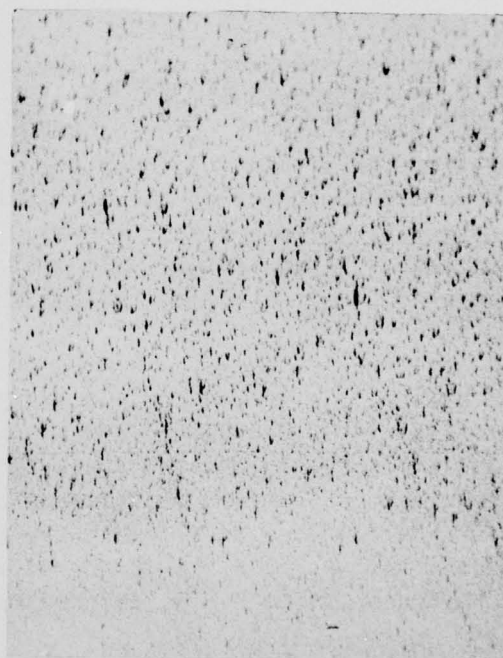
A. CoTaC, B. NiTiC, C. FeTiB



A.



B.



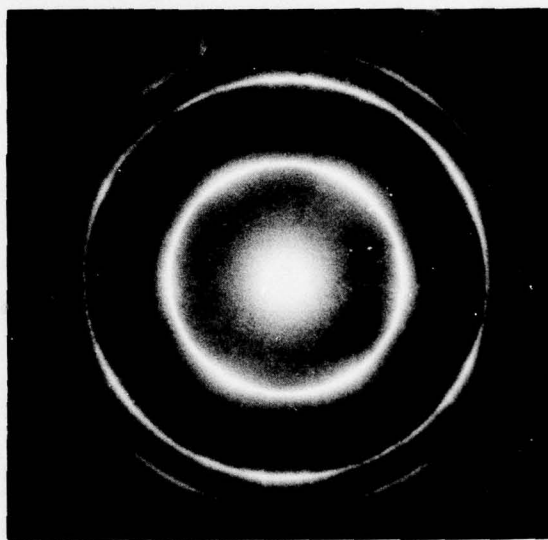
C.



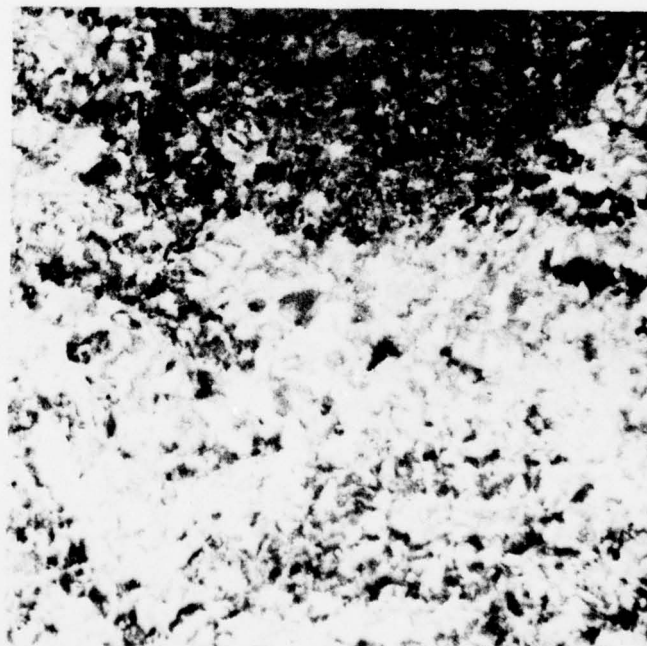
## STRUCTURE AND ELECTRON DIFFRACTION PATTERN FROM SPUTTERED CoTaC DEPOSIT



0.5 $\mu$ m



STRUCTURE AND ELECTRON DIFFRACTION PATTERN FROM SPUTTERED NiTiC DEPOSIT

0.5  $\mu\text{m}$

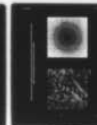
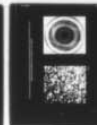
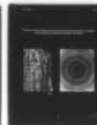
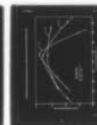
AD-A049 312

UNITED TECHNOLOGIES RESEARCH CENTER EAST HARTFORD CONN F/G 11/6  
ASSESSMENT OF ADVANCED LASER MATERIALS PROCESSING TECHNOLOGY.(U)  
NOV 77 E M BREINAN N00014-77-C-0418  
UTRC/R77-912887-3 NL

UNCLASSIFIED

2 OF 2

AD  
A049312



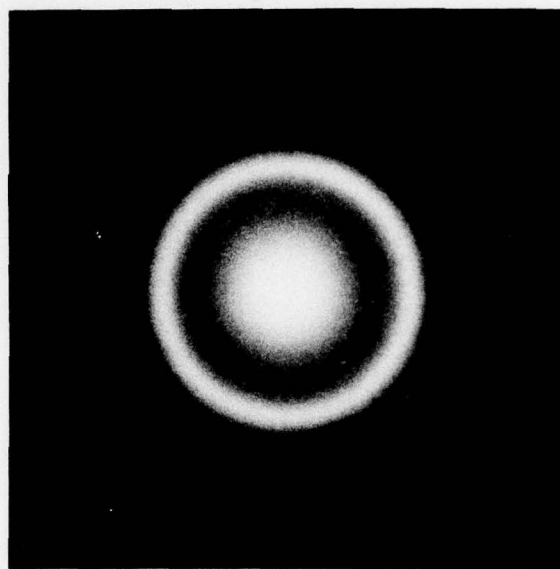
END  
DATE  
FILMED  
3 - 78  
DDC



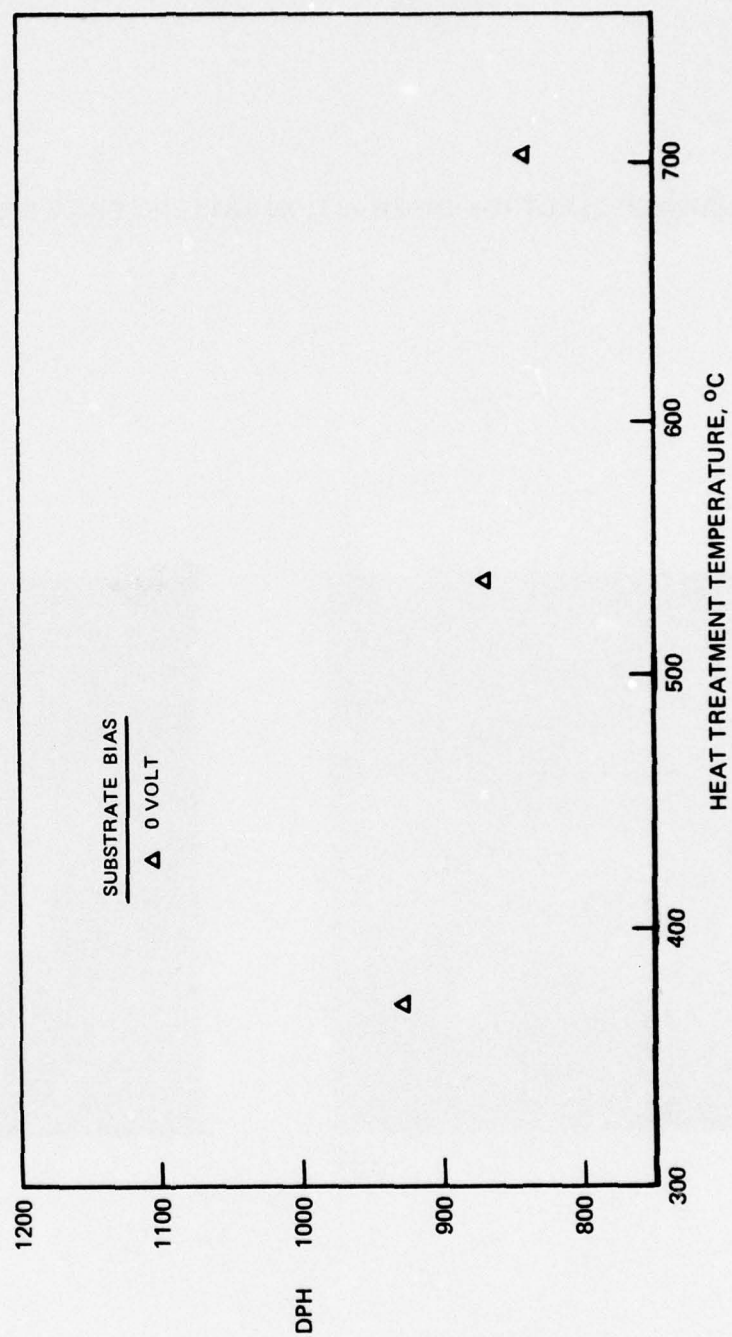
## STRUCTURE AND ELECTRON DIFFRACTION PATTERN FROM SPUTTERED FeTiB DEPOSIT



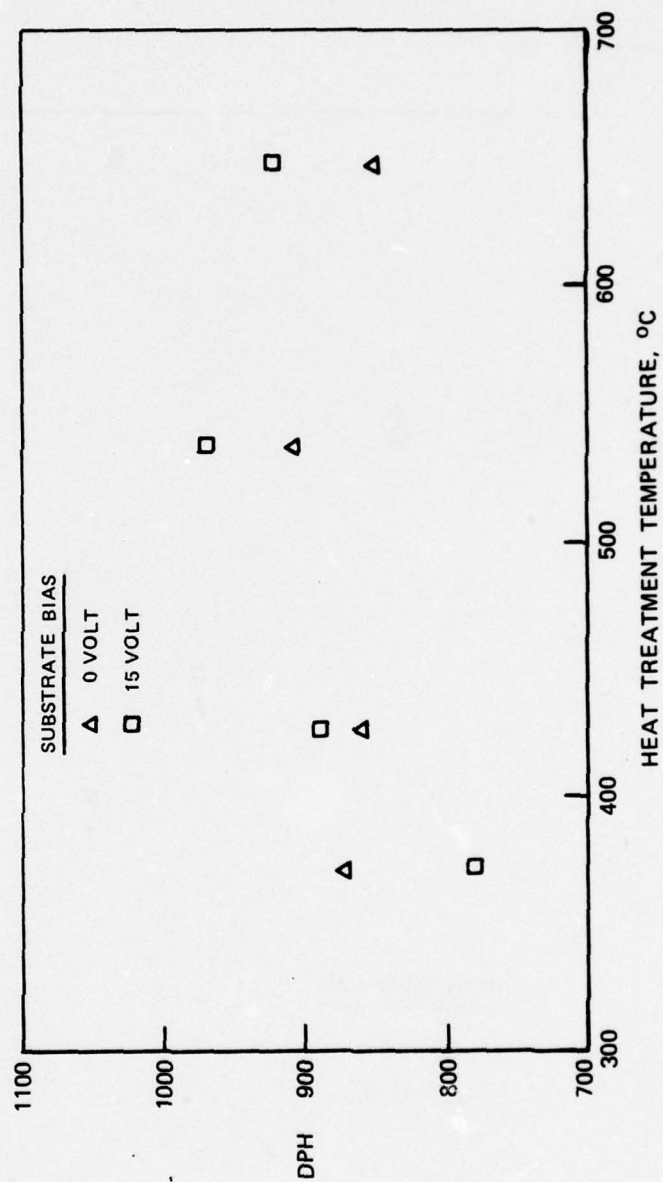
0.5  $\mu\text{m}$



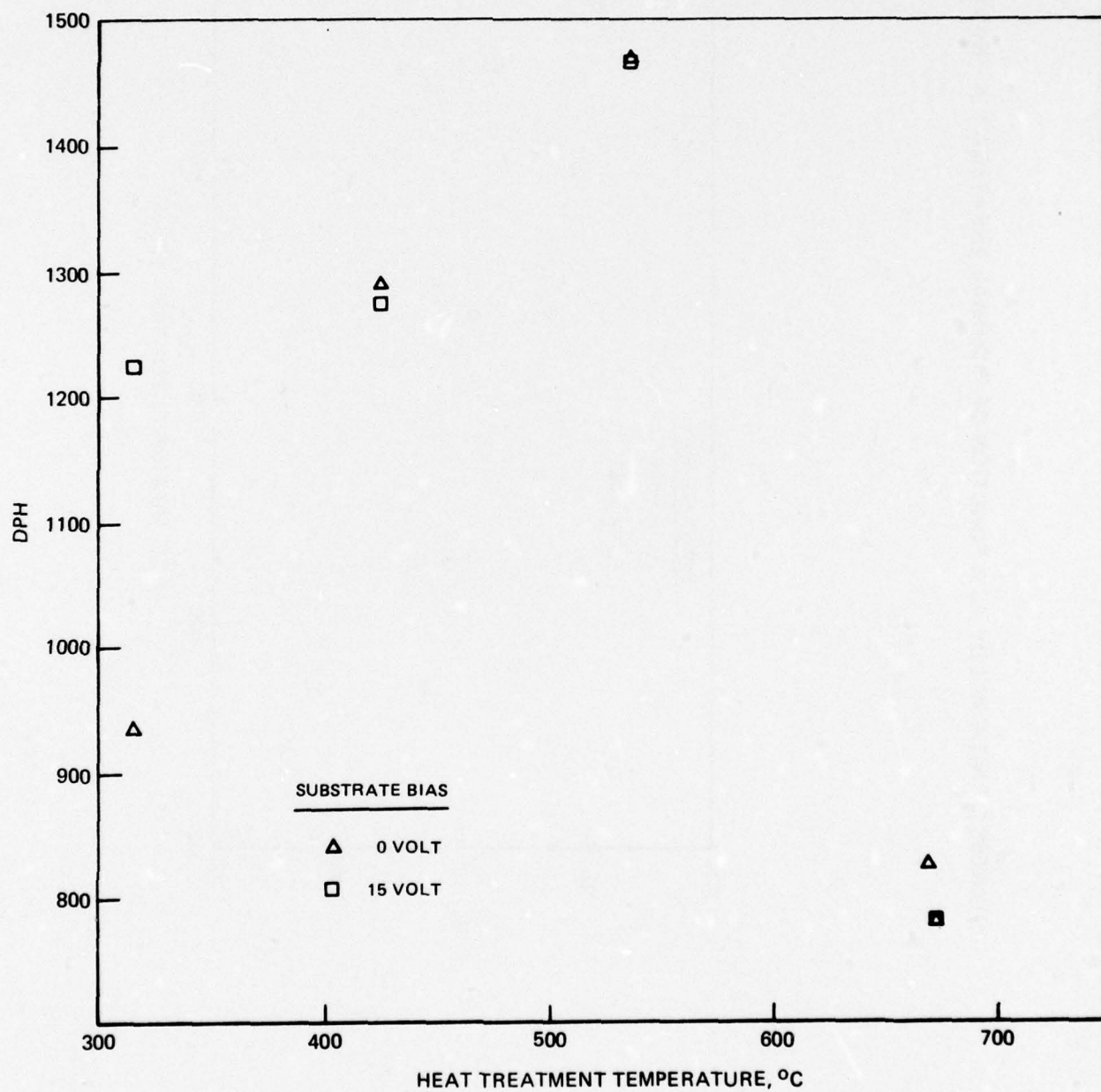
HARDNESS OF CoTaC ALLOY AS A FUNCTION OF THERMAL TREATMENT (4 HRS IN VACUUM)



HARDNESS OF NiTiC ALLOY AS A FUNCTION OF THERMAL TREATMENT (4 HRS IN VACUUM)

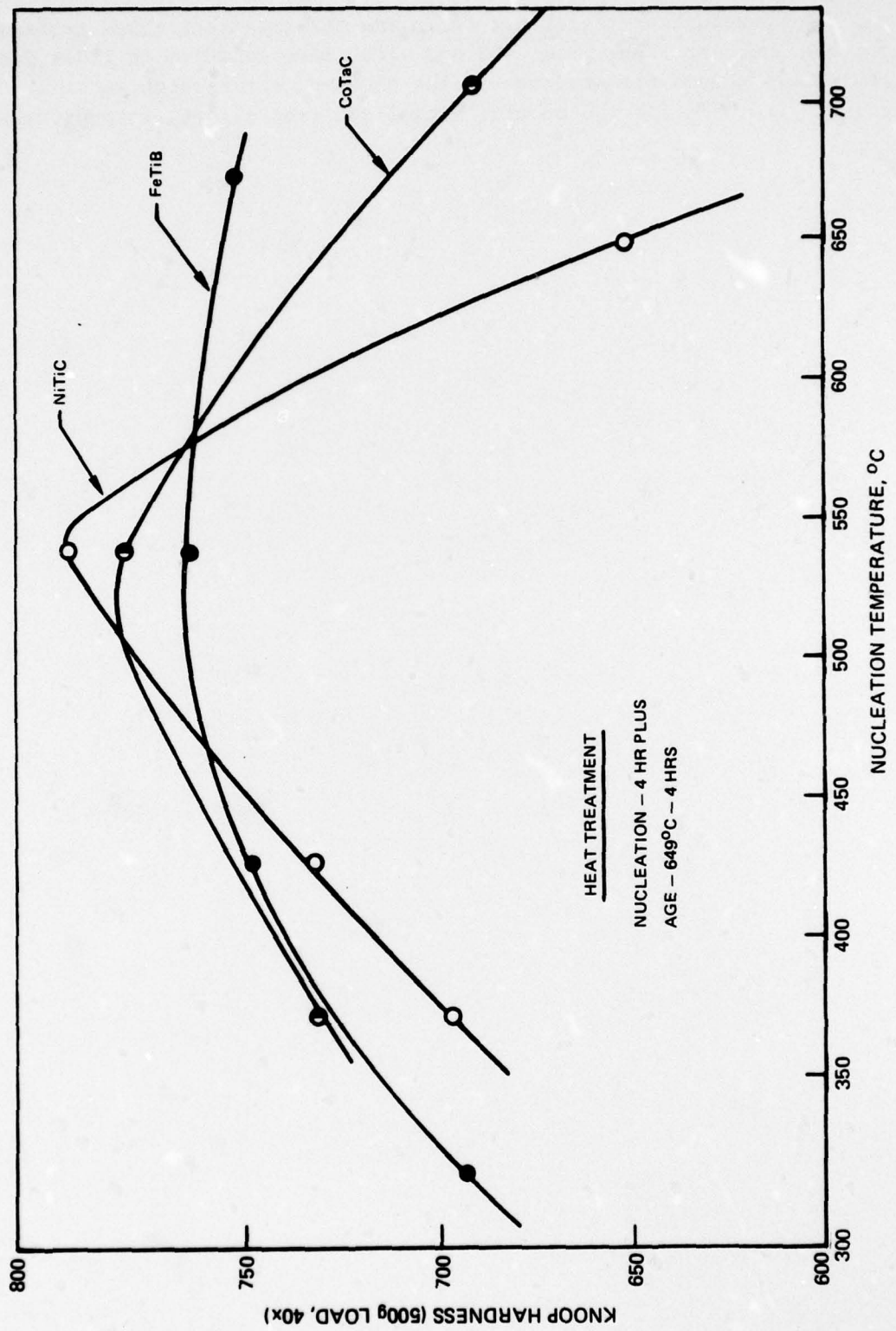


## HARDNESS OF FeTiB ALLOY AS A FUNCTION OF THERMAL TREATMENT (4 HRS IN VACUUM)



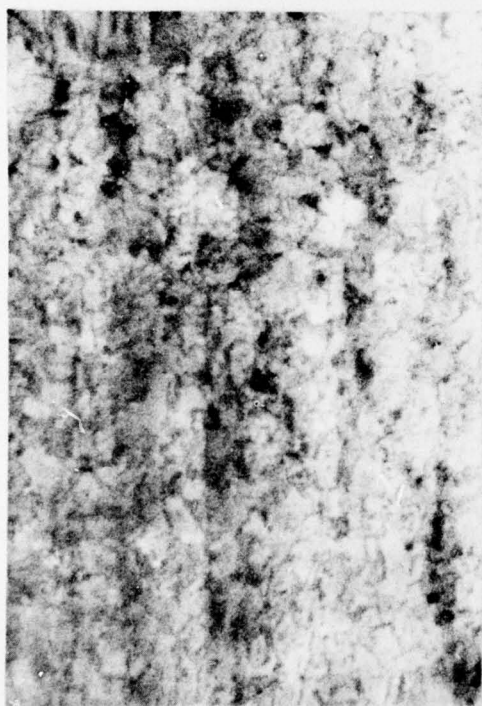


## HARDNESS OF SPUTTERED DEPOSITS AS A FUNCTION OF NUCLEATION TEMPERATURE

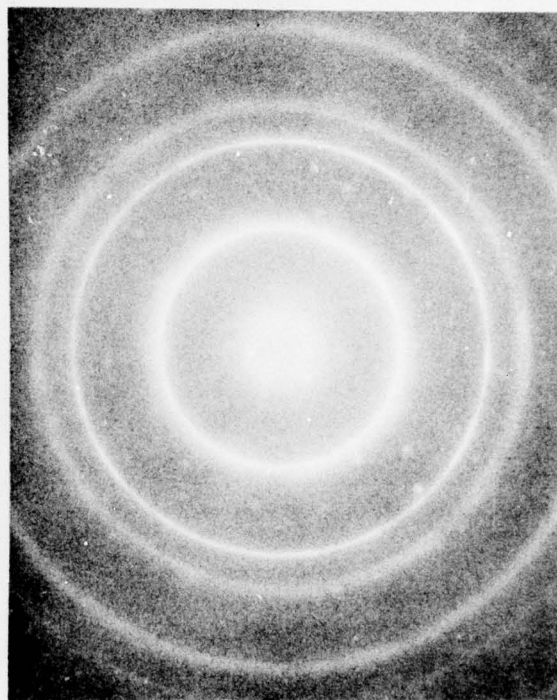


The structure of the alloys following the treatment which produced peak hardness are shown in Figs. 7-16, -17 and -18. Some evidence of lines due to the precipitate phases are observed in the electron diffraction patterns. These are TaC, TiC and TiB<sub>2</sub> for the cobalt, nickel and iron alloys, respectively.

STRUCTURE AND ELECTRON DIFFRACTION PATTERN FROM SPUTTERED CoTaC DEPOSIT  
AFTER 538°C/4 HR AND 649°C/4 HR THERMAL TREATMENT

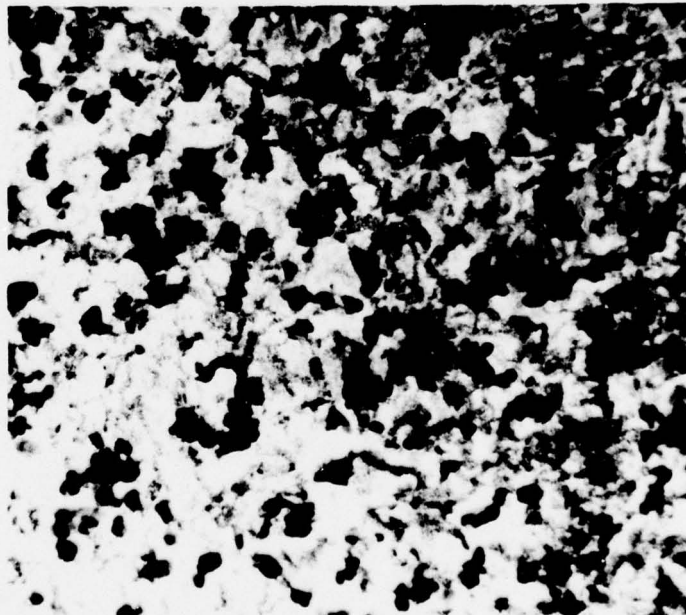
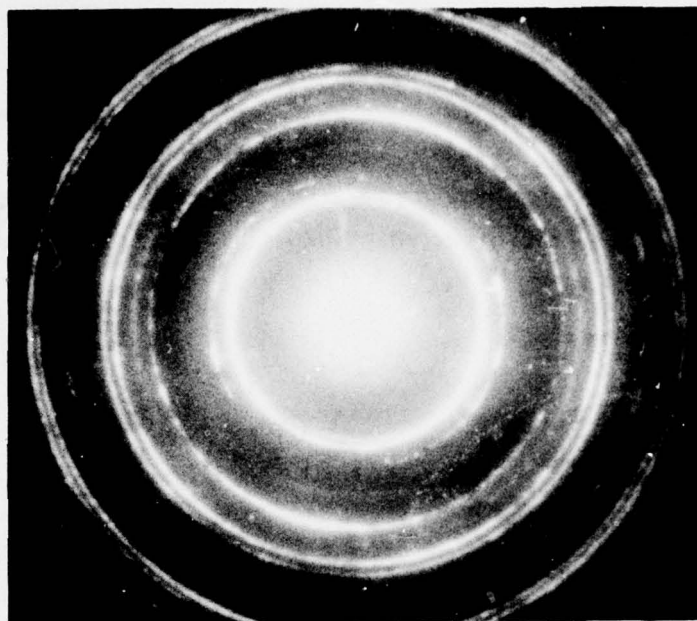


0.5 μm





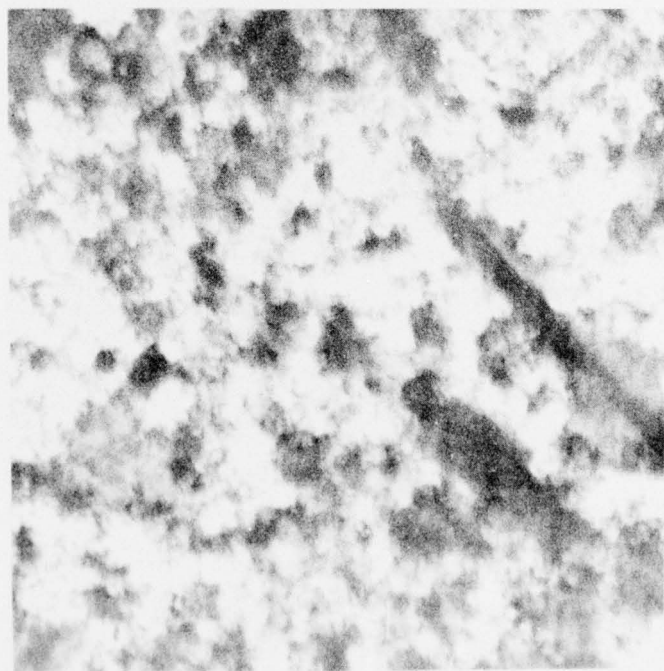
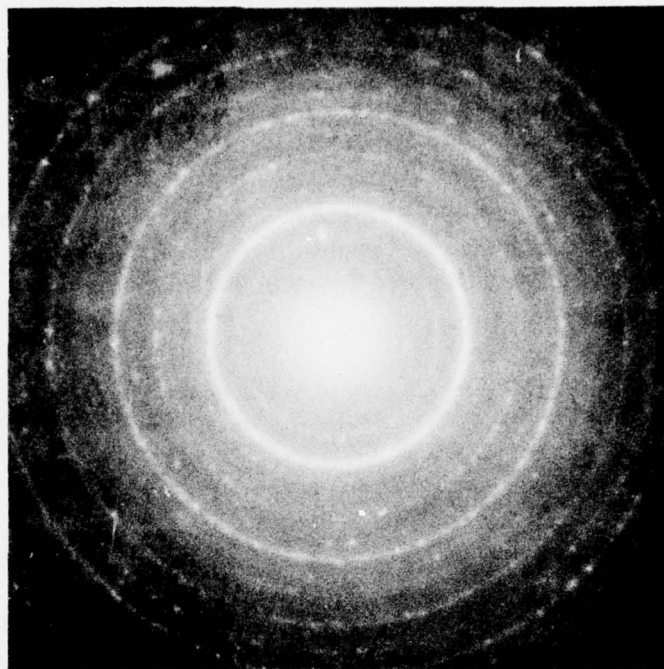
STRUCTURE AND ELECTRON DIFFRACTION PATTERN FROM SPUTTERED NiTiC DEPOSIT AFTER  
538°C/4 HR AND 649°C/4 HR THERMAL TREATMENT



0.5 μm



STRUCTURE AND ELECTRON DIFFRACTION PATTERN FROM SPUTTERED FeTiB DEPOSIT AFTER  
538°C/4 HR AND 649°C/4 HR THERMAL TREATMENT



0.15 μm

# REFERENCES

1. Breinan, E. M., C. M. Banas, & M. A. Greenfield, Laser Welding-The Present State of the Art. Reported to the Annual Assembly of the IIW Tel Aviv, Israel July 6-12, 1975, IIW Document #LV-181-75.
2. Breinan, E. M., and C. M. Banas: Evaluation of Basic Laser Welding Capabilities, Technical Report on Office of Naval Research Contract N00014-74-C-0423.. United Technologies Research Center Report R75-911989-4, November 1975.
3. Breinan, E. M., Banas, C. M., McCarthy G. P. and B. A. Jacob: Evaluation of Basic Laser Welding Capabilities Technical Report on Office of Naval Research Contract N00014-74-C-0423. United Technologies Research Center Report R77-911989-10, March 1977.
4. Breinan, E. M., Laser Welding, 1976 McGraw Hill Yearbook of Science & Technology, Mc-Graw Hill Book Co., New York, NY pp. 233-237 (1976).
5. Breinan, E. M., Laser Beam Welding, 1976 American Welding Society Handbook, Vol. 1, 7th Edition, American Welding Society, Miami, FL pp. 21-22 (1976).
6. Breinan, E. M. & C. M. Banas, High Power Laser Welding, Proceedings, 50th Anniversary Meeting of the Japan Welding Society, Osaka Japan, August 25-27, 1975 pp. 631-636.
7. Breinan, E. M. & C. M. Banas, Fusion Zone Purification During Welding With High Power CO<sub>2</sub> Lasers, Proceedings, 50th Anniversary Meeting of the Japan Welding Society, Osaka, Japan. Aug. 25-27, 1975 pp. 137-142.
8. Breinan, E. M. & C. M. Banas, Preliminary Evaluation of Laser Welding of X-80 Arctic Pipeline Steel, Welding Research Council Bulletin #201, Welding Research Council, New York, NY, December 1974.
9. CO<sub>2</sub> Laser Welding Joins the Parade, Welding Engineer, Aug. 1970 pp. 42-44.
10. Yessik, M. & D. J. Schmatz, Laser Processing at Ford, Metal Progress, May 1975 pp. 61-66.
11. Locke, E. V., E. D. Hoag & R. A. Hella, Deep Penetration Welding with High Power CO<sub>2</sub> Lasers, IEEE Journal of Quantum Electronics, Vol. QE-8, No. 2, Feb. 1972.
12. Banas, C. M., Laser Welding Developments, Proceedings of the CEEB International

Conference on Welding Research Related to Power Plant, Southampton, England, Sept. 17-21, 1972.

13. Ball, W. C. & C. M. Banas, Welding with a High Power CO<sub>2</sub> Laser, SAE Paper #740863, Oct. 1974.
14. Staff Report, State of the Art in Continuous Nd-YAG Welding, Metal Progress, Nov. 1970.
15. Barber, R. H., Laser Welding Applications, SME Paper No. AD74-405, 1974.
16. British Welding Institute Works with 2 kW, CO<sub>2</sub> System, Lasersphere, Vol. 3, No. 1, Jan. 15, 1973, p. 3.
17. Locke, E. V. & F. D. Seamon, Materials Processing With a Multikilowatt CO<sub>2</sub> Laser, Paper Presented at the SAE National Aerospace Engineering & Manufacturing Conference, San Diego, Cal. Oct. 13, 1974.
18. Yessik, M. & D. J. Schmatz, Laser Processing in the Automotive Industry, SME Paper MR74-962, 1974.
19. Adams, M. J., CO<sub>2</sub> Laser Welding of Aero-Engine Materials, Report No. 3335/3/73, British Welding Institute, Cambridge, England, 1973.
20. Gagliano, F. P., Interaction of Laser Radiation With Metals to Produce Welds, SME Paper MR74-954, 1974.
21. Baardsen, E. L., D. J. Schmatz & R. E. Bisaro, High Speed Welding of Sheet Steel with a CO<sub>2</sub> Laser, Welding Journal, April 1973.
22. Webster J-W, Welding at High Speed with the CO<sub>2</sub> Laser, Metal Progress, Nov. 1970.
23. Sullivan, A. B. J. & P. T. Houldcroft, Gas Jet Laser Cutting, British Welding Journal, Aug. 1967.
24. Miller, S. Ray Jr. Laser Die Making Machines in Production, SME Paper MR74-966, 1974.
25. Belforte, D. A., CO<sub>2</sub> Laser Cuts Metal-and Costs, Electro-Optical Systems Design, May 1975.
26. Wick, D. W., Lasercutting-Current Applications, Future Potentials, SME Paper MR74-965, 1974.
27. Breinan, E. M., Laser Beam Cutting, 1976 American Welding Society Welding



Handbook, Vol. 1, 7th Edition, American Welding Society, Miami, Florida, pp. 30-31, (1976).

28. Hanson, W. E., Applications for Industrial Lasercutter Systems, SME Paper #MR76-874, 1976.
29. Breinan, E. M., Banas, C. M. & J. P. Carstens, Transformation Hardening of Cast Irons Using High Power CO<sub>2</sub> Lasers, ASM Conference on Laser Surface Treatment for Automotive Applications, Detroit Michigan, Feb. 17, 1976.
30. Engel, S. L., Basics of Laser Heat Treating, SME Paper #MR76-857, SEM 1976.
31. Breinan, E. M., Kear, B. H., Banas, C. M. & L. E. Greenwald, Surface Treatment of Superalloys by Laser Skin Melting, Superalloys, Metallurgy & Manufacture Proceedings, Third International Symposium, Claitors Publishing Co., Baton Rouge, La. p. 345 (1976).
32. Breinan, E. M., Kear, B. H. & C. M. Banas, Processing Materials With Lasers, Physics Today, p. 44, Nov. 1976.
33. Breinan, E. M., Kear, B. H., Banas, C. M. & L. E. Greenwald, Laser Glazing-A New Process for Production and Control of Rapidly Chilled Metallurgical Microstructures SME Paper #MR76-867, SME, Dearborn, MI 1976.
34. Walsh, J. M. Whittles, J. C., Kear, B. H. & E. M. Breinan, Suppression of  $\gamma'$  in Laser Melted Nickel Base Alloy, Proceedings 8th International Conference on X-ray Optics and Microanalysis and 35th Electron Microscopy Society of America, Boston, MA Aug. 1977.
35. Kear, B. H. & E. M. Breinan, Laser Glazing, A New Process for Production and Control of Rapidly Chilled Metallurgical Microstructures, Proceedings Sheffield International Conference on Solidification & Casting, Ranmoor House, Sheffield University, July 1977.
36. Greenwald, L. E., Analytical Study of Heat Transfer Properties at the Melt Interface of a Rapidly Cooling Solid, UTRC Report R77-111321-1, June 1977.
37. Trottier, J. P., T. Khan, J. F. Stohr, M. Rabinovitch and H. Bibring, Improvement in the Stress-Rupture Strength of Directionally Solidified CoTaC-Type Composites Through Carbide Precipitation, Cobalt No. 3, pp 54-61 (1974).



38. Shurin, A. K. and V. E. Panarin, Phase Equilibria and Structure of Alloys Fe-TiB<sub>2</sub>, Fe-ZrB<sub>2</sub>, and Fe-HfB<sub>2</sub>, Russian Met., Vol. 5, pp. 192-195 (1974).
39. Lemkey, F. D. and D. D. Pearson, Creep Rupture, Stability and Fatigue Evaluation of D.S. Gamma Prime/Gamma-Alpha Eutectic Superalloy, First Quarterly Report, N62269-77-C-0055, June 28, 1977.
40. Jackson, K. A., The Dendrite-Eutectic Transition in Sn-Pb Alloys, Trans. AIME, Vol. 242, pp. 1275-1279 (1968).

BASIC DISTRIBUTION LIST

October 1976

Technical and Summary Reports		
<u>Organization</u>	<u>No. of Copies</u>	<u>Organization</u>
Defense Documentation Center Cameron Station Alexandria, Virginia 22314	(12)	Naval Construction Battalion Civil Engineering Laboratory Port Hueneme, California 93043 Attn: Materials Division (1)
Office of Naval Research Department of the Navy		Naval Electronics Laboratory Center San Diego, California 92152
Attn: Code 471 (1)		Attn: Electron Materials (1)
Code 102 (1)		Sciences Division (1)
Code 470 (1)		
Commanding Officer Office of Naval Research Branch Office 495 Summer Street Boston, Massachusetts 02210	(1)	Naval Missile Center Materials Consultant Code 3312-1 Point Mugu, California 93041 (1)
Commanding Officer Office of Naval Research Branch Office 536 South Clark Street Chicago, Illinois 60605	(1)	Commanding Officer Naval Surface Weapons Center White Oak Laboratory Silver Spring, Maryland 20910 Attn: Library (1)
Office of Naval Research San Francisco Area Office 760 Market Street, Room 447 San Francisco, California 94102 Attn: Dr. P. A. Miller (1)	(1)	David W. Taylor Naval Ship R&D Center Materials Department Annapolis, Maryland 21402 (1)
Naval Research Laboratory Washington, D.C. 20390		Naval Undersea Center San Diego, California 92132 Attn: Library (1)
Attn: Code 6000 (1)		Naval Underwater System Center Newport, Rhode Island 02840 Attn: Library (1)
Code 6100 (1)		
Code 6300 (1)		Naval Weapons Center China Lake, California 93555 Attn: Library (1)
Code 6400 (1)		
Code 2627 (1)		
Naval Air Development Center Code 302 Warminster, Pennsylvania 18974 Attn: Mr. F. S. Williams (1)	(1)	Naval Postgraduate School Monterey, California 93940 Attn: Mechanical Engineering Dept. (1)
Naval Air Propulsion Test Center Trenton, New Jersey 08628		Naval Air Systems Command Washington, D.C. 20360
Attn: Library (1)	(1)	Attn: Code 52031 (1)
		Code 52032 (1)
		Code 320 (1)

## BASIC DISTRIBUTION LIST (Cont'd)

October 1976

<u>Organization</u>	<u>No. of Copies</u>	<u>Organization</u>	<u>No. of Copies</u>
Naval Sea System Command Washington, D.C. 20362 Attn: Code 035	(1)	NASA Headquarters Washington, D.C. 20546 Attn: Code RRM	(1)
Naval Facilities Engineering Command Alexandria, Virginia 22331 Attn: Code 03	(1)	NASA Lewis Research Center 21000 Brookpark Road Cleveland, Ohio 44135 Attn: Library	(1)
Scientific Advisor Commandant of the Marine Corps Washington, D.C. 20380 Attn: Code AX	(1)	National Bureau of Standards Washington, D.C. 20234  Attn: Metallurgy Division Inorganic Materials Division	(1) (1)
Naval Ship Engineering Center Department of the Navy CTR BG #2 3700 East-West Highway Prince Georges Plaza Hyattsville, Maryland 20782 Attn: Engineering Materials and Services Office, Code 6101	(1)	Defense Metals and Ceramics Information Center Battelle Memorial Institute 505 King Avenue Columbus, Ohio 43201	(1)
Army Research Office Box CM, Duke Station Durham, North Carolina 27706 Attn: Metallurgy & Ceramics Div.	(1)	Director Ordnance Research Laboratory P.O. Box 30 State College, Pennsylvania 16801	(1)
Army Materials and Mechanics Research Center Watertown, Massachusetts 02172 Attn: Res. Programs Office (AMXMR-P)	(1)	Director Applied Physics Laboratory University of Washington 1013 Northeast Fortieth Street Seattle, Washington 98105	(1)
Air Force Office of Scientific Research Bldg. 410 Bolling Air Force Base Washington, D.C. 20332 Attn: Chemical Science Directorate Electronics and Solid State Sciences Directorate	(1) (1)	Metals and Ceramics Division Oak Ridge National Laboratory P.O. Box X Oak Ridge, Tennessee 37380	(1)
Air Force Materials Lab (LA) Wright-Patterson AFB Dayton, Ohio 45433	(1)	Los Alamos Scientific Laboratory P.O. Box 1663 Los Alamos, New Mexico 87544 Attn: Report Librarian	(1)
		Argonne National Laboratory Metallurgy Division P.O. Box 229 Lemont, Illinois 60439	(1)



## BASIC DISTRIBUTION LIST (Cont'd)

October 1976

<u>Organization</u>	<u>No. of Copies</u>	<u>Organization</u>	<u>No. of Copies</u>
Brookhaven National Laboratory Technical Information Division Upton, Long Island New York 11973 Attn: Research Library	(1)		
Library Building 50 Room 134 Lawrence Radiation Laboratory Berkeley, California	(1)		



M  
July 1977

# SUPPLEMENTARY DISTRIBUTION LIST

## Technical and Summary Reports

Professor G. S. Ansell  
Rensselaer Polytechnic Institute  
Dept. of Metallurgical Engineering  
Troy, NY 12181

Professor Dieter G. Ast  
Cornell University  
Department of Materials Science  
and Engineering  
College of Engineering, Bard Hall  
Ithaca, NY 14853

Professor H. K. Birnbaum  
University of Illinois  
Department of Metallurgy  
Urbana, IL 61801

Dr. E. M. Breinan  
United Technologies  
Research Center  
East Hartford, CT 06108

Professor H. D. Brody  
University of Pittsburgh  
School of Engineering  
Pittsburgh, PA 15213

Dr. Arthur E. Clark  
Naval Surface Weapons Center  
Solid State Division  
White Oak Laboratory  
Silver Spring, MD 20910

Professor J. B. Cohen  
Northwestern University  
Dept. of Material Sciences  
Evanston, IL 60201

Professor M. Cohen  
Massachusetts Institute of Technology  
Department of Metallurgy  
Cambridge, MA 02139

Dr. Ronald B. Diegle  
505 King Avenue  
Columbus, OH 43201

Mr. G. A. DiPietro  
Advanced Vacuum Systems  
30 Faulkner Street  
Ayer, MA 01432

Professor Thomas W. Eagar  
Massachusetts Institute of Technology  
Department of Materials Science  
and Engineering  
Cambridge, MA 02139

Professor B. C. Giessen  
Northeastern University  
Department of Chemistry  
Boston, MA 02115

Dr. G. T. Hahn  
Battelle Memorial Institute  
Department of Metallurgy  
505 King Avenue  
Columbus, OH 43201

Dr. David G. Howden  
Battelle Memorial Institute  
Columbus Laboratories  
505 King Avenue  
Columbus, OH 43201

Professor C. E. Jackson  
Ohio State University  
Dept. of Welding Engineering  
190 West 19th Avenue  
Columbus, OH 43210

Dr. Lyman A. Johnson  
General Electric Company  
P.O. Box 8  
Schenectady, NY 12301

Dr. C. S. Kortovich  
TRW, Inc.  
23555 Euclid Avenue  
Cleveland, OH 44117

Professor D. A. Koss  
Michigan Technological University  
College of Engineering  
Houghton, MI 49931

M  
July 1977

SUPPLEMENTARY DISTRIBUTION LIST (Cont'd)

Professor E. Laughlin  
Carnegie-Mellon University  
Schenley Park  
Pittsburgh, PA 15213

Professor A. Lawley  
Drexel University  
Dept. of Metallurgical Engineering  
Philadelphia, PA 19104

Dr. John Mahoney  
Phrasor Technology  
110 South Euclid Avenue  
Pasadena, CA 91101

Dr. H. Margolin  
Polytechnic Institute of New York  
333 Jay Street  
Brooklyn, NY 11201

Professor K. Masabuchi  
Massachusetts Institute of Technology  
Department of Ocean Engineering  
Cambridge, MA 02139

Dr. H. I. McHenry  
National Bureau of Standards  
Institute for Basic Standards  
Boulder, CO 80302

Professor J. W. Morris, Jr.  
University of California  
College of Engineering  
Berkeley, CA 94720

Professor Ono  
University of California  
Materials Department  
Los Angeles, CA 90024

Dr. M. Pakstys  
General Dynamics  
Electric Boat Division  
Eastern Point Road  
Groton, CT 06340

Dr. Neil E. Paton  
Rockwell International  
Science Center  
1049 Camino Dos Rios  
P.O. Box 1085  
Thousand Oaks, CA 91360

Professor R. M. Pelloux  
Massachusetts Institute of Technology  
Department of Materials  
Science and Engineering  
Cambridge, MA 02139

Mr. A. Pollack  
David W. Taylor Naval Ship  
Research and Development Center  
Annapolis Laboratory  
Annapolis, MD 21402

Dr. Karl M. Prewé  
United Technologies Laboratories  
United Technologies Corporation  
East Hartford, CT 06108

Professor David Roylance  
Massachusetts Institute of Technology  
77 Massachusetts Avenue  
Cambridge, MA 02139

Professor W. F. Savage  
Rensselaer Polytechnic Institute  
School of Engineering  
Troy, NY 12181

Dr. C. Shaw  
Rockwell International Science Center  
1049 Camino Dos Rios  
P.O. Box 1085  
Thousand Oaks, CA 91360

Professor O. D. Sherby  
Stanford University  
Materials Sciences Division  
Stanford, CA 94300

M  
July 1977

SUPPLEMENTARY DISTRIBUTION LIST (Cont'd)

Dr. R. P. Simpson  
Westinghouse Electric Corporation  
Research and Development Center  
Pittsburgh, PA 15235

Dr. W. A. Spitzig  
U.S. Steel Corporation  
Research Laboratory  
Monroeville, PA 15146

Dr. E. A. Starke, Jr.  
Georgia Institute of Technology  
School of Chemical Engineering  
Atlanta, GA 30332

Professor N. S. Stoloff  
Rensselaer Polytechnic Institute  
School of Engineering  
Troy, NY 12181

Dr. E. R. Thompson  
United Technologies Research Center  
United Technologies Corporation  
East Hartford, CT 06108

Professor David Turnbull  
Harvard University  
Division of Engineering and  
Applied Physics  
Cambridge, MA 02139

Professor W. E. Wallace  
University of Pittsburgh  
Pittsburgh, PA 15260

Dr. F. E. Wawner  
University of Virginia  
School of Engineering and  
Applied Science  
Charlottesville, VA 22901

Dr. C. R. Whitsett  
McDonnell Douglas Research  
McDonnell Douglas Corporation  
St. Louis, MO 63166

Dr. J. C. Williams  
Carnegie-Mellon University  
Department of Metallurgy and  
Materials Sciences  
Schenley Park  
Pittsburgh, PA 15213

Professor H. G. F. Wilsdorf  
University of Virginia  
Charlottesville, VA 22903

Dr. M. A. Wright  
University of Tennessee  
Space Institute  
Tullahoma, TN 37388